



INELASTIC SCATTERING MATRIX  
ELEMENTS FOR THE COLLISION  
 $B(^2P_{1/2}) + H_2(j) \rightarrow B(^2P_{3/2}) + H_2(j')$

THESIS

Thomas A. Niday, Second Lieutenant, USAF

AFIT/GAP/ENP/99M-06

**DISTRIBUTION STATEMENT A**  
Approved for Public Release  
Distribution Unlimited

DEPARTMENT OF THE AIR FORCE  
AIR UNIVERSITY

**AIR FORCE INSTITUTE OF TECHNOLOGY**

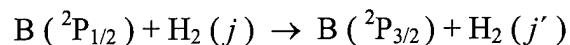
19990402 009

AFIT/GAP/ENP/99M-06

The views expressed in this thesis are those of the author and do not reflect the official policy or position of the Department of Defense or the U.S. Government.

INELASTIC SCATTERING MATRIX

ELEMENTS FOR THE COLLISION



THESIS

Presented to the Faculty of the Graduate School of Engineering

of the Air Force Institute of Technology

Air University

Air Education and Training Command

In Partial Fulfillment of the Requirements for the

Degree of Master of Science in Engineering Physics

Thomas A. Niday, B.S.

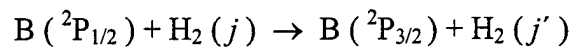
Second Lieutenant, USAF

March 1999

Approved for public release; distribution unlimited

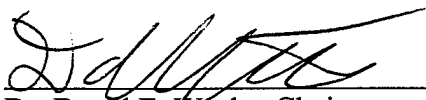
INELASTIC SCATTERING MATRIX

ELEMENTS FOR THE COLLISION

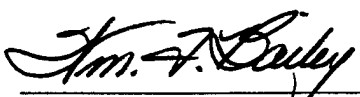


Thomas A. Niday, B.S.  
Second Lieutenant, USAF

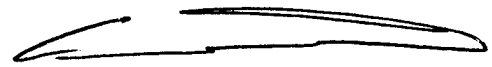
Approved:

  
\_\_\_\_\_  
Dr. David E. Weeks, Chairman

2 Mar 99  
date

  
\_\_\_\_\_  
Dr. William F. Bailey

2 Mar 99  
date

  
\_\_\_\_\_  
Lt. Col. Glen P. Perram, USAF

8 Mar 99  
date

### **Acknowledgments**

I would like to thank my advisor, Dr. David Weeks, for his support and valuable discussions. I also am indebted to Dr. Millard H. Alexander for providing us with the potential energy surfaces for this study. I would also like to acknowledge support from the Air Force Office of Scientific Research and computational support from the Aeronautical Systems Center Major Shared Resource Center.

## Table of Contents

	Page
Acknowledgments.....	iii
List of Figures.....	vi
List of Tables .....	viii
Abstract.....	ix
I. Introduction .....	1
Motivation .....	1
Problem Statement.....	3
Approach .....	3
II. Background .....	6
S-Matrix Elements.....	6
The Channel Packet Method.....	7
Atomic Units.....	11
Adiabatic and Diabatic Potential Surfaces .....	11
III. Representation of the Hamiltonian .....	15
Overview .....	15
Space-Fixed Coordinate Systems .....	16
Body-Fixed Coordinate Systems .....	18
The Hamiltonian .....	20
Restriction to Two Internal Degrees of Freedom .....	21
Choice of Basis .....	22
Representation of Each Term of the Hamiltonian .....	25
Potential Expansion Coefficients.....	31
IV. Implementation .....	35
Numerical Representation of Wave Packets .....	35
Gaussian Wave Packets .....	36
Propagation of the Wave Function .....	37
Absorbing Boundary Conditions .....	39
Implementation of the Channel Packet Method .....	41
Accuracy of Wave Packet Propagation .....	42
Accuracy of Computation of S-Matrix Elements .....	45

Validation of S-matrix Elements .....	46
Graphical Visualization .....	47
V. Results and Discussion.....	51
Truncation of Basis.....	51
<i>Para</i> Basis Sets.....	52
The “One-Dimensional” Problem .....	57
Application of Channel Packet Method to “1D” Problem .....	60
Application to Larger Basis Sets .....	73
Conclusion.....	81
Appendix.....	83
Bibliography .....	95
Vita.....	101

## List of Figures

	Page
Figure 1. Space-fixed coordinates.....	17
Figure 2. Space-fixed center of mass coordinates .....	18
Figure 3. Body-fixed coordinate system I.....	19
Figure 4. Body-fixed coordinate system II .....	20
Figure 5. Coupling case "1A".....	23
Figure 6. Block schematic of the Hamiltonian matrix .....	55
Figure 7. Diagonal elements of potential matrix in diabatic representation .....	56
Figure 8. First row of potential matrix in diabatic representation .....	56
Figure 9. Adiabatic potential surfaces .....	57
Figure 10. Diabatic (solid) and adiabatic (dashed) potential surfaces for ( 0 ) basis.....	59
Figure 11. Propagation of reactant Møller state in ( 0 ) basis.....	68
Figure 12. Correlation function $C_{3/2,1/2}(t)$ .....	69
Figure 13. Fourier transform of $C_{3/2,1/2}(t)$ .....	70
Figure 14. Expansion coefficients $\eta$ of initial reactant and product wave packets .....	70
Figure 15. Probability $P^{3/2, 1/2}$ of transition .....	71
Figure 16. Probability of reflection $P^{1/2,1/2}$ in the uncoupled case .....	73
Figure 17. Correlation function $C_{3/2, 1/2}(t)$ in the ( 0, 2 ) and ( 0, 2, 4 ) bases .....	75
Figure 18. Probabilities of transition $P^{3/2, 1/2}$ for the ( 0, 2 ) and ( 0, 2, 4 ) bases.....	78
Figure 19. Sum over final transition probabilities for all bases .....	80
Figure 20. Expansion coefficients $\eta$ of initial wave packets (product has $j = 2$ ) .....	81



Figure 21. Probabilities of transition from the ground state in the ( 0 ) basis .....	83
Figure 22. Probabilities of transition from the ground state in the ( 0, 2 ) basis .....	87
Figure 23. Probabilities of transition from the ground state in the ( 0, 2, 4 ) basis .....	94

## List of Tables

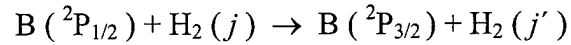
	Page
Table 1. Parameters in the Hamiltonian.....	22
Table 2. Angular Momentum Quantum Numbers .....	24
Table 3. Rotational levels of H <sub>2</sub> .....	34
Table 4. Size of <i>para</i> bases with $J = 1/2$ .....	54
Table 5. Channel Packet Parameters.....	61

**Abstract**

Initial efforts to characterize the scattering dynamics of  $B + H_2$  focus on computing scattering matrix elements for the fine structure transition  $B (^2P_{1/2}) \rightarrow B (^2P_{3/2})$  in collisions with  $H_2$ , allowing for rotational excitation. Using a new application of the time dependent Channel Packet Method (CPM), reactant and product wave packets are prepared in the asymptotic limit on the  $B (^2P_{1/2})$  and  $B (^2P_{3/2})$  surfaces. They are propagated using the split operator method together with a unitary transformation between the diabatic and adiabatic representations. Scattering matrix elements are computed from the Fourier transform of the correlation function between the evolving wave packets. These computations directly support the Air Force Office of Scientific Research (AFOSR) Molecular Dynamics program and the Air Force Research Laboratory (AFRL) High Energy Density Matter (HEDM) program. In particular, the CPM is well suited to handle non-adiabatic molecular reaction dynamics on multiple potential energy surfaces, as encountered in the dynamics of a wide variety of molecular systems, including  $B + H_2$ . Further motivation for investigating the specific dynamics of  $B + H_2$  stems from the potential application of solid molecular hydrogen, doped with boron atoms, as a high energy rocket propellant.

## INELASTIC SCATTERING MATRIX

### ELEMENTS FOR THE COLLISION



### I. Introduction

#### Motivation

The Air Force High Energy Density Matter (HEDM) program investigates the development of improved propulsion and explosive systems. A principal goal in propulsion is to improve the specific impulse ( $I_{sp}$ ) of the propellant. Efforts to synthesize a novel, high performance rocket propellant using boron atoms trapped in a matrix of solid molecular hydrogen [1] have recently generated a great deal of interest. Theoretical calculations have shown that if one could achieve doping of 5% molar atomic concentration of boron, the specific impulse would show a 21% improvement over standard liquid oxygen – liquid hydrogen propellants [1]. Thus there is great interest in the trapping of boron and other atomic species in solid molecular hydrogen matrices. As of 1994, however, only weak B atom molar concentrations (0.01%) could be achieved [1]. Hence the spectroscopy and reactive dynamics of systems of boron and hydrogen are of great interest. The particular scattering event we study, motivated by this interest, is the collision  $\text{B} ({}^2\text{P}_{1/2}) + \text{H}_2 (j) \rightarrow \text{B} ({}^2\text{P}_{3/2}) + \text{H}_2 (j')$ . This collision is not reactive, but it is inelastic due to the possibility of the fine structure transition  $\text{B} ({}^2\text{P}_{1/2}) \rightarrow \text{B} ({}^2\text{P}_{3/2})$  and the possibility of the rotational transition  $\text{H}_2 (j) \rightarrow \text{H}_2 (j')$ .

The dynamics of a collision between a single boron atom B and a hydrogen molecule  $H_2$  are completely described by matrix elements of the scattering operator (S-matrix elements). The absolute values squared of S-matrix elements yield the probability of transition or reaction from a given initial state to a given final state. Together with the distribution of reactant states, S-matrix elements can be used to compute cross sections and reaction rate constants. These quantities are expected to contribute to large-scale synthesis efforts of boron in hydrogen matrices.

Several authors have treated analogous systems of atoms making fine structure transitions during collisions with diatomic molecules or noble gases. Chu and Dalgarno [2] studied fine structure transitions in collisions of  $C^+ (^2P)$  and  $H_2$ , where the complex was assumed to be collinear and the hydrogen molecule was constrained to its ground rotational state. Flower and Launay [3,4] extended the study of  $C^+ + H_2$ , lifting the collinearity restriction, and considering the possibility of simultaneous rotational excitation of the  $H_2$  molecule. Also related are several studies of fine structure transitions between alkali atoms and inert-gas atoms including  $Na (^2P_j) + He$  [5], and  $Na (^2P_j) + Ar$  [6]. Rebentrost and Lester [7-10] carried out a study of the  $F (^2P) + H_2$  system, including the construction of the potential energy surfaces, transformation to an approximate diabatic basis, and a time independent calculation of scattering matrix elements and cross sections for the fine structure transition, including rotational excitation of the hydrogen molecule. In this system, the spin-orbit splitting of fluorine ( $404\text{ cm}^{-1}$ ) [9,10] roughly corresponds to the energy required to make a  $j = 0 \rightarrow j = 2$  rotational transition, so there was a near resonant effect that enhanced that cross section.

## Problem Statement

To make a propellant that achieves the theoretical improvement in specific impulse described above, one must be able to achieve higher concentrations of B atoms trapped in the H<sub>2</sub> matrix. To do this, an understanding of the dynamics of B atoms in the H<sub>2</sub> matrix is important. A first step in studying these dynamics is to study the dynamics of a single B + H<sub>2</sub> collision, characterized by scattering matrix (S-matrix) elements. We compute S-matrix elements as a function of energy for the fine structure transition  $B(^2P_{1/2}) \rightarrow B(^2P_{3/2})$  during collisions with H<sub>2</sub>, while allowing for the possibility of rotational, but not vibrational, excitation of the hydrogen molecule.

## Approach

S-matrix elements can be computed by a variety of methods. We will use the time-dependent Channel Packet Method (CPM). Time dependent methods give S-matrix elements as a function of energy, for one set of quantum numbers that identify specific initial and final states. The time dependent Channel Packet Method uses propagation of wave packets that explore the interaction potential to derive S-matrix elements as a function of energy for the specific initial and final states. Previous calculations for similar reactions have used time independent methods such as close-coupled methods [11-13].

To compute S-matrix elements one must know the interaction potential. The potential energy surfaces governing the dynamics of the  $B + H_2$  interaction have been computed by Alexander [14]. They display a strong barrier to formation [14] of the  $BH_2$  molecule, and at low energies, the formation of a van der Waals complex,  $B \cdots H_2$ , is possible [15]. The interaction of B and  $H_2$  is complicated by the fact that the ground state of B ( $2s^2 2p^2 P$ ) is sixfold degenerate, if spin-orbit coupling is neglected. This degeneracy means that the interaction takes place on multiple coupled potential energy surfaces, rather than a single potential energy surface, adding to the computational difficulty. The interaction dynamics are described by three potential energy surfaces (independent of spin) corresponding to the three  $2p$  states of the boron atom as it interacts with the hydrogen molecule. The six total surfaces describing the interaction of B ( $^2P_j$ ) with  $H_2$  are only separated by a constant spin-orbit splitting term in the limit of infinite separation of the boron and hydrogen, but they are split at shorter range by the interaction.

Section II gives a brief background on the theory of S-matrix elements, the use of the channel packet method, and the concept of adiabatic and diabatic potential energy surfaces to model the interaction. In Section III, we identify the coordinate systems and the scattering Hamiltonian. The Hamiltonian is then represented in a complete basis. We then make simplifying approximations by neglecting the vibrational degree of freedom of the hydrogen molecule, limiting the highest rotational state accessible to the hydrogen, and using the “Centrifugal Sudden” approximation. Section IV describes the implementation of the channel packet method, and discusses specific numerical issues,

including wave packets, the numerical fidelity of the calculation, and methods to validate the calculated S-matrix elements. Section V presents the results of the scattering calculations. Results are first discussed for the simplest case: where the hydrogen is restricted to its ground ( $j = 0$ ) rotational state. S-matrix elements where rotational excitation is allowed are then presented.



## II. Background

### S-Matrix Elements

A scattering problem can be characterized by the scattering operator  $\hat{S}$ , which gives the asymptotic ( $t \rightarrow +\infty$ ) product state  $|\Psi_{product}\rangle$  in terms of the asymptotic ( $t \rightarrow -\infty$ ) reactant state  $|\Psi_{reactant}\rangle$  by

$$|\Psi_{product}\rangle = \hat{S} |\Psi_{reactant}\rangle \quad (1)$$

Knowledge of  $\hat{S}$  gives one all information of experimental interest [16], since many reactions typically take place on very short time scales and the intermediate states are not experimentally observable. Matrix elements of the scattering operator can be used to obtain the probability of a final state given the initial state:

$$P_{fi} = \left| \langle \Psi_{final} | \hat{S} | \Psi_{initial} \rangle \right|^2 \quad (2)$$

We desire scattering matrix (S-matrix) elements where the initial and final states are asymptotic momentum eigenstates, labeled by the reactant and product momenta  $k_\gamma$  and channel quantum numbers  $\gamma$ .

$$S_{\pm k_\gamma, \pm k_\gamma}^{\gamma' \gamma} = \langle k' \gamma' | \hat{S} | k \gamma \rangle \quad (3)$$

The amplitude squared  $|S|^2$  of the S-matrix elements gives the probability that the transition will take place. From S-matrix elements, one can compute scattering cross sections and the corresponding rate constants.

### The Channel Packet Method

The time dependent channel packet method (CPM) [17,18] is based on the Møller operator formulation of scattering theory [16]. The Møller operators are defined by:

$$\hat{\Omega}_\pm^\gamma = \lim_{t \rightarrow \mp\infty} \exp\left(\frac{i\hat{H}t}{\hbar}\right) \exp\left(\frac{-i\hat{H}_0^\gamma t}{\hbar}\right) \quad (4)$$

where  $\hat{H}$  is the Hamiltonian, and  $\hat{H}_0^\gamma$  is the asymptotic channel Hamiltonian labeled by the quantum numbers contained in  $\gamma$ . The Møller operators have the property that  $\hat{S} = \hat{\Omega}_-^\dagger \hat{\Omega}_+$ . The Møller operators can be used to define Møller states in terms of initial reactant and product states, defined arbitrarily at  $t = 0$ :

$$|\Psi_\pm^\gamma\rangle \equiv \hat{\Omega}_\pm^\gamma |\Psi_{in, out}^\gamma\rangle \quad (5)$$

The initial reactant (product) states  $|\Psi_{in,out}^{\gamma}\rangle$  are typically chosen to be Gaussian wave packets entering (leaving) the interaction region, so that they possess momentum components that will give S-matrix elements (Eq. ( 3 ) ) that are of interest. Once the Møller states are constructed, the correlation function  $C_{\gamma\gamma}(t)$  is then computed as one of the Møller states is evolved under the full Hamiltonian:

$$C_{\gamma\gamma}(t) = \langle \Psi_{-}^{\gamma} | \exp(\frac{-i\hat{H}t}{\hbar}) | \Psi_{+}^{\gamma} \rangle \quad (6)$$

The Fourier transform of the correlation function, appropriately normalized, will give the S-matrix elements as a function of energy [19]:

$$S_{\pm k_{\gamma}, \pm k_{\gamma}}^{\gamma\gamma} = \frac{\hbar(2\pi)^{-1} (|k'_{\gamma}| |k_{\gamma}|)^{1/2}}{(\mu_{\gamma}, \mu_{\gamma})^{1/2} \eta_{-}^{*}(\pm k'_{\gamma}) \eta_{+}(\pm k_{\gamma})} \int_{-\infty}^{\infty} dt \exp(\frac{iEt}{\hbar}) C_{\gamma\gamma}(t) \quad (7)$$

In Eq. ( 7 )  $E$  is the total energy,  $\gamma$  labels each reaction channel,  $\mu_{\gamma'}$  and  $\mu_{\gamma}$  are reduced masses, and  $\eta_{-}$  and  $\eta_{+}$  are momentum space expansion coefficients used to define the initial reactant and product wave packets. The initial wave packets must be prepared to have either all negative or all positive momentum components for the above formula to be applicable. A more general formula [17] is required when this is not the case.

Typically it is most convenient to prepare the initial wave packets as described above. However, one difficulty with the channel packet method occurs for low energy, where the initial packets do not possess significantly large momentum components. At these low

energies, the numerical result becomes invalid, because one is dividing a small number (the Fourier transform of the correlation function) by another small number (the expansion coefficients). The use of wave packets with both positive and negative momentum components may help with this situation, but it complicates the evaluation of the S-matrix.

To apply the channel packet method to a scattering problem, one must define initial reactant and product wave packets that contain momentum components that correspond to energies for which the S-matrix elements are desired. In our multiple surface problem, the initial reactant packet can be defined on one surface and the initial product packet on the other surface, so that the transition probability between the surfaces, which represent different initial and final sets of quantum numbers, can be found. Next, the reactant and product Møller states are numerically computed by the action of the Møller operators. The Møller operators first propagate the reactants (products) backward (forward) in time, away from the interaction region, under the asymptotic channel Hamiltonian  $\hat{H}_0'$ . This can be done analytically if the initial states are chosen to be Gaussian wave packets, which is often the case, for simplicity. The analytic propagation is to a time  $\tau$  that is large enough so that the wave packet is then (numerically) in the asymptotic limit, where the full Hamiltonian  $\hat{H}$  is equivalent to the asymptotic Hamiltonian  $\hat{H}_0'$ . Then, the wave packet is numerically propagated in the opposite direction of time under the action of the full Hamiltonian  $\hat{H}$ , back to  $t = 0$ , where it is then the Møller state.

Once the Møller states are created, the next step is to compute the correlation function between them while one of them, say the reactant Møller state, is evolved backward and forward in time under the action of the full Hamiltonian. This is done with the same numerical propagation method used for the computation of the Møller states. A time range  $[\tau_-, \tau_+]$  is chosen to approximate the true range  $(-\infty, \infty)$  by stopping the evaluation of the correlation function when it decays to numerical insignificance, when the evolving reactant Møller state has finally completely exited the interaction region.

After the full correlation function is computed, it can then be used in Eq. ( 7 ) to compute the S-matrix elements. To evaluate the S-matrix elements as a function of the total energy of the system we require the implicit dependence of the expansion coefficients  $\eta(k)$  on energy, given by

$$k_\gamma(E) = \left[ \frac{2\mu_\gamma}{\hbar} (E - E_\gamma) \right]^{1/2} \quad (8)$$

where  $E_\gamma$  is the asymptotic energy of the channel labeled by  $\gamma$ , for example the rotational and electronic fine-structure energies in our problem.

Previously, the CPM has been used in scattering problems involving rovibronic transitions on a single electronic surface, including computation of state to state S-matrix elements for the collinear  $\text{H} + \text{H}_2(\nu) \leftrightarrow \text{H} + \text{H}_2(\nu')$  reaction [19-21]. Another two dimensional calculation computes S-matrix elements for  $\text{OC} + \text{OH} (\nu=0) \leftrightarrow$

OCO ( $\nu=0$ ) + H [22]. In a three-dimensional calculation, Dai and Zhang [23] have used the CPM to compute S-matrix elements for the H + O<sub>2</sub> reaction. The CPM has also been used to develop approximate methods for computing S-matrix elements, including a semiclassical method [24] and a method adapted to work with a time-dependent self consistent field approach [20].

### Atomic Units

Atomic units [25] are convenient for atomic and molecular calculations. One atomic unit of mass is the mass of the electron, one atomic unit of energy is twice the ionization energy of the hydrogen atom, one atomic unit of distance is the Bohr radius  $a_0$ , and one atomic unit of time is the time for an electron in the first classical Bohr orbit to travel one atomic unit of distance. The atomic unit of angular momentum is  $\hbar$ , which conveniently allows  $\hbar$  to be omitted from equations presented in atomic units.

### Adiabatic and Diabatic Potential Surfaces

To solve a scattering problem one needs a reliable description of the potential energy surfaces that describe the interaction between the scattering partners. A basic approximation required to even discuss the concept of a potential energy surface is the Born-Oppenheimer approximation [26], which allows one to use potential energy

surfaces to describe the nuclear motion under certain assumptions. In this approximation, the nuclear position operators are demoted to parameters and the electronic Schrödinger equation is solved for the electronic wavefunctions and energy levels, as functions of the nuclear positions. The electronic energy levels as a function of nuclear position form adiabatic potential energy surfaces and define an adiabatic basis.

Using this approximation involves neglecting terms that take the form of matrix elements of the nuclear momentum operators in the full Hamiltonian between the electronic eigenstates. This means that the nuclear kinetic energy operator in the full Hamiltonian is not diagonal in the adiabatic representation. The approximation is good when the energy levels are well separated compared to the energy of the nuclear motion. This can be a good approximation for interactions with closed-shell atoms, in which the electronic energy levels are well separated, on the order of eV. However, for interactions with open-shell atoms such as B ( $^2P$ ), the  $^2P_j$  level is nearly sixfold degenerate, since the energies for the  $^2P_{1/2}$  (twofold degenerate) and  $^2P_{3/2}$  (fourfold degenerate) levels are close (the spin-orbit splitting constant  $\xi$  for B is  $10.7 \text{ cm}^{-1}$ ) [14,27]. Thus the off-diagonal matrix elements of the nuclear kinetic energy operator cannot be ignored. They can be treated approximately by transforming to a diabatic representation [26,28-32], where the nuclear kinetic energy is diagonal but the potential energy is no longer diagonal. The transformation to the diabatic representation can be derived by solving a differential equation involving the above mentioned matrix elements [28].

The determination of the potential energy surfaces for molecular interactions is a challenging problem. One may use *ab initio* methods to solve the electronic Schrödinger equation at various nuclear locations, obtaining the electronic eigenvalues and wavefunctions. Examples of these calculations are self-consistent field methods and configuration-interaction methods [11], which are both used to solve the Hartree-Fock equations. However, certain regions of the surfaces may be known experimentally to better accuracy than is available theoretically, so another approach is to use experimental data to construct analytic models for which the potential matches the experimental values at the known locations.

To construct the (approximate) diabatic representation, one must know the electronic wavefunctions, which implies that one has already calculated the adiabatic energy levels. Thus in an *ab initio* treatment of the potential surfaces for a problem such as ours, it is essential for a representation of the diabatic potentials to be given with the adiabatic potentials, or one would have to redo the entire potential surface calculation just to obtain the transformation from the adiabatic to diabatic basis. Without the transformation, there is not enough information to model the interaction fully.

The Hamiltonian matrix in the diabatic representation will be obtained in Section III. The potential energy, including the angular effective potentials, is not diagonal in the diabatic representation. The diabatic potential matrix  $V_D(R)$  is diagonalized to obtain the adiabatic representation, which is used in the wave packet propagation. The unitary transformation  $U(R)$  that accomplishes this diagonalization is



obtained by placing the eigenvectors of the matrix in columns of a new matrix, and can be used to transform the wavefunction between the adiabatic and diabatic representations:

$$\begin{aligned}
 V_D \Psi_D(R) &= U U^\dagger V_D U U^\dagger \Psi_D(R) \\
 &\equiv U V_A U^\dagger \Psi_D(R) \\
 &\equiv U V_A \Psi_A(R)
 \end{aligned} \tag{9}$$

where  $\Psi_D(R)$  and  $\Psi_A(R)$  are the diabatic and adiabatic nuclear wavefunctions (column vectors) and  $V_A(R)$  is the diagonal adiabatic potential matrix. Hence the potential energy  $V_D$  (or any power of  $V_D$ , and hence any function of  $V_D$ ) acting on the nuclear wavefunction in the diabatic representation  $\Psi_D(R)$  can be evaluated with Eq. (9) by applying the Hermitian conjugate of the unitary transformation  $U(R)$  to the state, applying the diagonal adiabatic potential energy  $V_A(R)$  operator and then transforming back with  $U(R)$ . The benefit of this transformation approach is that during the wave packet propagation, the Hamiltonian is exponentiated, which is straightforward for a diagonal operator. The unitary transformation that diagonalizes the diabatic potential energy matrix will be a function of the nuclear coordinates. However, any unitary transformations that are not functions of the nuclear coordinates may be applied to a diabatic representation and it will remain diabatic (the nuclear kinetic energy will still be approximately diagonal) [26].

### **III. Representation of the Hamiltonian**

#### **Overview**

To treat the scattering problem, we must identify a coordinate system, the Hamiltonian, and a basis with which the Hamiltonian is represented. Much of the general procedure for atom-atom, atom-diatom and atom-molecule collisions is developed in several papers and books [11,33-47]. We outline the key steps here as applied to the  $B + H_2$  scattering problem. Most approaches are designed to work with time-independent methods; however, some authors [45-50] discuss the approach as it applies to time dependent methods. The method we use is similar to the “close-coupled wave packet” (CCWP) method [45-47], because the wavefunction is represented as a function of  $R$ , while the angular variables are replaced by their conjugate momenta, described by coupled equations.

A difficulty stems from the consideration of angular momenta that must be added together to obtain the total angular momentum. These include the rotational angular momentum of the  $H_2$  diatom, the orbital angular momentum of the  $B \cdots H_2$  pair, and the open-shell electronic angular momentum of the boron. Other angular momenta that are neglected are electronic angular momentum of  $H_2$  (it is assumed to be in a  $^1\Sigma$  state) and nuclear spin of the boron. There are numerous angular momentum coupling schemes

(Hund's cases) which, while equivalent if treated fully, are intended to provide alternative approximate approaches [33,51].

### Space-Fixed Coordinate Systems

We are primarily concerned with identifying the location of the nuclei. Since there are three atoms, there are nine degrees of freedom, requiring nine coordinates. In general treatments, the three atoms are typically labeled A, B, and C, where for our problem A labels the boron, and BC labels the hydrogen molecule. The first coordinate system that may be considered is a space fixed laboratory coordinate system, shown in Figure 1, in which the nine coordinates are the three Cartesian coordinates of the three atoms. The Hamiltonian can be transformed to a space fixed center of mass (SF) coordinate system, shown in Figure 2, by separating out the coordinates  $\vec{R}_{CM} = (X_{cm}, Y_{cm}, Z_{cm})$  describing the center of mass motion of the system. The other six coordinates are  $\vec{R}$ , the vector between the A atom and the center of mass of BC, and  $\vec{r}$ , the vector between the B and C atoms.

It is desirable to use a set of internal coordinates to describe the system. The potential energy surfaces are found by solving the Schrödinger equation in a system in which the electronic coordinates are measured relative to the nuclear coordinates - a body-fixed (BF) coordinate system. The internal coordinates that are used are often called Jacobi scattering coordinates. Let A label the boron, and BC label the hydrogen

molecule, as is typical. Then the (A, BC) Jacobi coordinates are  $R$ , the distance from the center of mass of the BC diatom to the A atom;  $r$ , the distance between B and C, and  $\theta$ , the angle between the H<sub>2</sub> bond and the line connecting the B atom to the H<sub>2</sub> center of mass. One can also use the (B, AC) or (C, AB) Jacobi coordinates; the three possible sets of Jacobi coordinates label three possible arrangement channels. For our problem, which is nonreactive, the system stays in the (A, BC) channel, making those coordinates the most convenient. If we use the (A, BC) internal coordinates, together with the three coordinates that describe the center of mass motion of the system, we still need three more coordinates to describe the orientation of the ABC system in space. These are found by transforming to a body-fixed (BF) coordinate system. There are two common ways to do this:

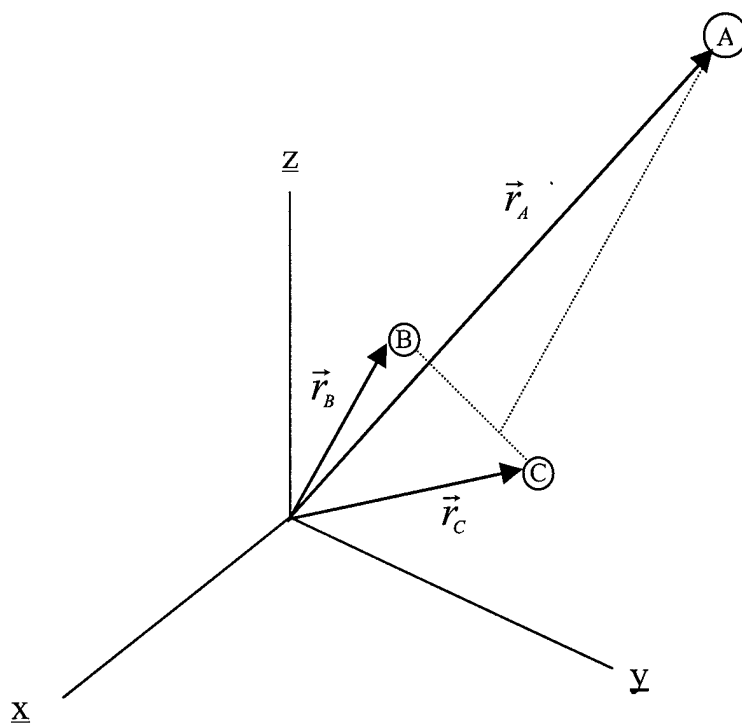


Figure 1. Space-fixed coordinates

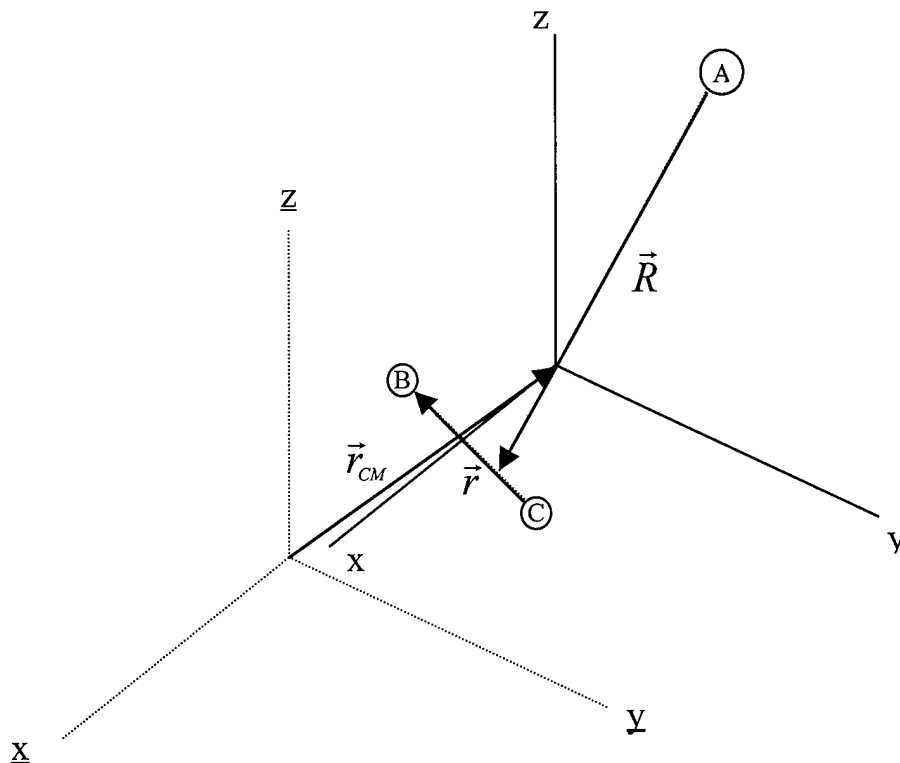


Figure 2. Space-fixed center of mass coordinates

### Body-Fixed Coordinate Systems

The space fixed center of mass coordinate system can be transformed to a quasi-body fixed coordinate system defined as follows: Locate the body-fixed  $z$ -axis to point from the center of mass of the  $H_2$  molecule to the B atom, then locate the body-fixed  $y$ -axis in the space-fixed  $xy$ -plane. The transformation from SF to BF coordinates can be described by Euler angles  $(\alpha \beta 0)$ , where  $\alpha$  and  $\beta$  are the azimuthal and polar angles of the B +  $H_2$  rotor with respect to the SF frame. The internal coordinate  $\theta$  is the polar angle of the  $H_2$  diatom with respect to the BF frame, and  $\phi$  is the azimuthal coordinate of the  $H_2$

with respect to the BF frame. The complete set of body-fixed coordinates is thus  $X_{cm}$ ,  $Y_{cm}$ ,  $Z_{cm}$ ,  $\alpha$ ,  $\beta$ ,  $R$ ,  $r$ ,  $\theta$ , and  $\phi$ . These coordinates are illustrated in Figure 3, and will be used later to define a representation for the Hamiltonian.

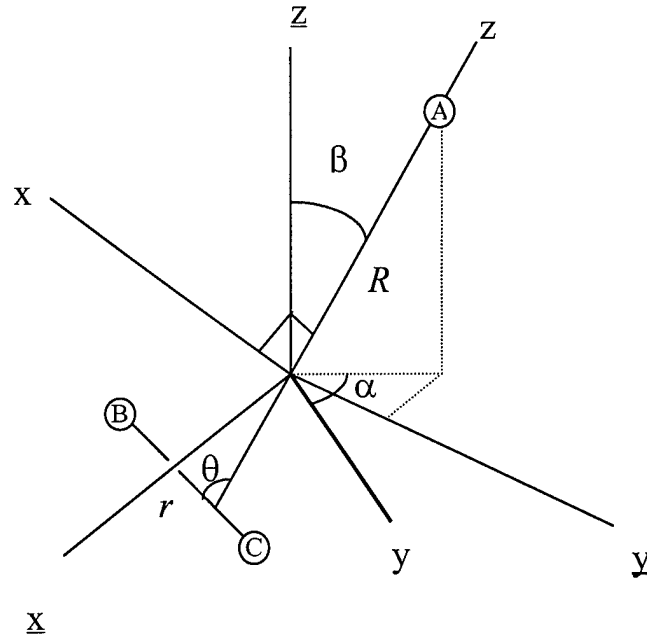


Figure 3. Body-fixed coordinate system I

For completeness, another body-fixed coordinate system can be defined in a similar fashion. Locate the BF z-axis in the same fashion as above. Then locate the BF x axis in the plane of the ABC system, perpendicular to the BF z-axis. The transformation in this case is described by Euler angles  $(\alpha \beta \gamma)$ . The complete set of body-fixed coordinates is thus  $X_{cm}$ ,  $Y_{cm}$ ,  $Z_{cm}$ ,  $\alpha$ ,  $\beta$ ,  $\gamma$ ,  $R$ ,  $r$ , and  $\theta$ , and is illustrated in Figure 4. However, these coordinates will not be considered further in this work.

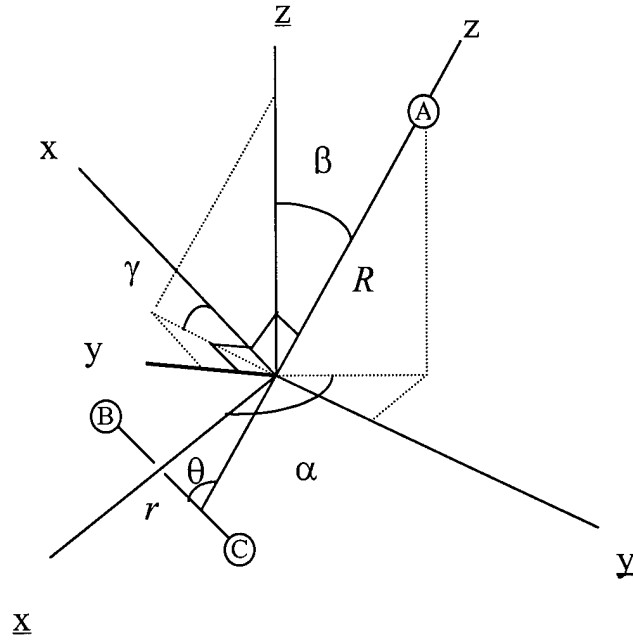


Figure 4. Body-fixed coordinate system II

### The Hamiltonian

The (A,BC) Hamiltonian for the nuclear motion is [52-54]

$$\hat{H} = \frac{\hat{p}_R^2}{2\mu_{A,BC}} + \frac{\hat{p}_r^2}{2\mu_{BC}} + \frac{\hat{j}^2}{2\mu_{BC}r^2} + \frac{\hat{L}^2}{2\mu_{A,BC}R^2} + \hat{V}_{el} + \hat{V}_{so} \quad (10)$$

where

$$\mu_{A,BC} = \frac{m_A(m_B + m_C)}{m_A + m_B + m_C}$$

$$\mu_{BC} = \frac{m_B m_C}{m_B + m_C} \quad (11)$$

In Eq. ( 10 )  $\hat{p}_R$  and  $\hat{p}_r$  are the momentum operators for motion of A relative to BC and the vibrational motion of BC.  $\hat{j}$  is the orbital angular momentum operator (BF or SF) for the BC molecule, and  $\hat{L}$  is the orbital angular momentum operator for A and the BC pair.  $\hat{V}_{el}$  and  $\hat{V}_{so}$  are the electrostatic and spin-orbit potential operators.

### Restriction to Two Internal Degrees of Freedom

To restrict the problem to two internal degrees of freedom, the BC bond length  $r$  will be held fixed at  $r_{eq}$ . Thus the  $\hat{p}_r^2$  term is zero, and the potential will be evaluated at the fixed length  $r_{eq}$ , which, for  $H_2$ , is taken to be 1.402 atomic units, as computed by Alexander [14]. This approximation amounts to neglecting the vibrational degree of freedom of the hydrogen molecule, which can be a good approximation at low energies, since the threshold for the  $\nu = 0 \rightarrow \nu = 1$  vibrational transition for  $H_2$  occurs at an energy of 0.0199 atomic units, which is larger than the highest energies for which we obtain S-matrix elements (see Section V). The hydrogen molecule is further assumed to be in a  $^1\Sigma$  state, so that it contributes zero electronic angular momentum. Table 1 lists some of the constant parameters in the Hamiltonian.



Table 1. Parameters in the Hamiltonian

<u>Name</u>	<u>Meaning</u>	<u>Value (atomic units)</u>
$m_H$	Mass of hydrogen	1837.15
$m_B$	Mass of boron 11	20208.7
$\mu_{BC}$	Reduced mass of H <sub>2</sub>	918.58
$\mu_{A,BC}$	Reduced mass of B...H <sub>2</sub> pair	3109.03
$\xi$	Spin-orbit constant of boron	$4.876 \times 10^{-5}$
$r_{eq}$	Fixed H <sub>2</sub> bond length	1.402

### Choice of Basis

Once the Hamiltonian is identified in operator form, it must be represented in a basis to be considered numerically. A good basis is identified by Dubernet and Hutson in a paper that outlines several possibilities [33]. We use their “Case 1A” angular basis set, which is named for Hund’s coupling case “A”. The Case 1A coupling diagram is shown in Figure 5 (from Ref. [33]). This coupling scheme in which  $j_a$ ,  $j$  and  $J$  project separately onto the BF z-axis provides a simple framework to neglect (if numerically justified) some of the coupling terms between these angular momenta which arise from the angular kinetic energy terms in the Hamiltonian, but not the potential energy. This is done later

in Section V, through the centrifugal sudden approximation. With some notational changes, the full basis is

$$\left| \begin{matrix} J & j & l & s & j_a & R \\ M & k & & & \omega & \end{matrix} \right\rangle \quad (12)$$

In this basis  $J$  is the total angular momentum quantum number and  $M$  its projection on the space-fixed  $z$ -axis.  $j$  and  $k$  are the diatom orbital angular momentum and its projection on the body-fixed  $z$ -axis.  $l$  and  $s$  are the orbital and spin angular momenta of the boron atom and take the values 1 and 1/2 for the  $2p$  orbital.  $j_a$  and  $\omega$  are the boron atom total angular momentum and projection on the body-fixed  $z$ -axis.  $R$  is the Jacobi coordinate described above, and  $r$  is omitted due to the constraint to two degrees of freedom. Since  $j$  and  $j_a$  are present in the basis, terms

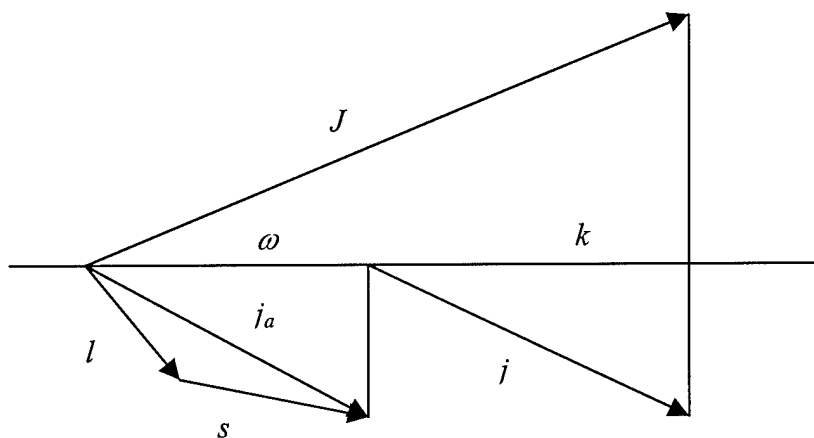


Figure 5. Coupling case "1A"

Table 2. Angular Momentum Quantum Numbers

<u>Quantum Number</u>	<u>Meaning</u>
$J$	Total angular momentum (conserved)
$M$	Projection of $J$ on SF z-axis (conserved)
$P$	Projection of $J$ on BF z-axis; equal to $k + \omega$
$j$	Diatom ( $H_2$ ) angular momentum
$k$	Projection of $j$ on BF z-axis
$L$	Orbital angular momentum of B + $H_2$ pair
$l$	Electronic orbital angular momentum of B (unpaired)
$s$	Spin angular momentum of B (unpaired)
$j_a$	Total B atom electronic angular momentum
$\omega$	Projection of $j_a$ on BF z-axis

Using the coordinate system where the BF x-axis is in the SF  $xy$ -plane (BF coordinate system I), this basis represented in angular coordinates is [33]

$$\begin{aligned}
 & \left\langle \alpha \beta \theta \phi ; l s \begin{smallmatrix} j_a \\ \omega \end{smallmatrix} R' \left| \begin{smallmatrix} J & j \\ M & k \end{smallmatrix} l s \begin{smallmatrix} j_a \\ \omega \end{smallmatrix} R \right\rangle \right. \\
 & \quad = \left( \frac{2J+1}{4\pi} \right)^{1/2} \mathcal{D}_{M(k+\omega)}^{J*}(\alpha, \beta, 0) Y_{jk}(\theta, \phi) \delta(R - R')
 \end{aligned} \tag{13}$$

where  $k + \omega$  is the projection of  $J$  onto the BF z-axis ( $L$  can have no projection on the BF z-axis), and is called  $P$  in Ref. [33]. The rotation matrix element multiplied by the prefactor is the rotor wave function for the A-BC system that describes its orientation with respect to the SF axes with the angles  $\alpha$  and  $\beta$ . The spherical harmonic is the wavefunction for the BC diatom, which describes its orientation with respect to the BF axes, with angles  $\theta$  and  $\phi$ .

### Representation of Each Term of the Hamiltonian

Using the above basis, we evaluate matrix elements of the Hamiltonian. For notational convenience, we omit  $J$ ,  $M$ ,  $l$ ,  $s$ , and  $R$  from the basis vectors, since  $J$  and  $M$  are conserved by the Hamiltonian; also we only consider  $^2P_j$  states of boron, so  $l$  and  $s$  are conserved by our Hamiltonian (though this is only approximate).  $R$  is implicitly assumed to be present. Matrix elements of the Hamiltonian are

$$H_{jj'kk'}^{j_a j_a' \omega \omega'} = \left\langle \begin{array}{c} j \ j_a \\ k \ \omega \end{array} \right| \hat{H} \left| \begin{array}{c} j' \ j_a' \\ k' \ \omega' \end{array} \right\rangle \quad (14)$$

Matrix elements for each term in the Hamiltonian can be considered separately. For the radial kinetic energy term, the matrix elements are

$$\left\langle \begin{matrix} j & j_a \\ k & \omega \end{matrix} \right| \frac{\hat{p}_R^2}{2\mu_{A,BC}} \left| \begin{matrix} j' & j'_a \\ k' & \omega' \end{matrix} \right\rangle = -\frac{\hbar^2}{2\mu_{A,BC}} \frac{1}{R} \frac{\partial^2}{\partial R^2} R \delta_{xx'} \quad (15)$$

$$\delta_{xx'} \equiv \delta_{JJ'MM'II's's'} \delta_{jj'kk'} \delta_{j_a j'_a \omega \omega'} \delta(R - R')$$

where the  $\delta_{xx'}$  shorthand indicates that the term is diagonal in all the angular quantum numbers (Though a delta function in  $R$  is present, the kinetic energy is of course not diagonal in  $R$ , due to the derivative). The angular kinetic energy of the BC diatom is also diagonal:

$$\left\langle \begin{matrix} j & j_a \\ k & \omega \end{matrix} \right| \frac{\hat{j}^2}{2\mu_{BC} r_{eq}^2} \left| \begin{matrix} j' & j'_a \\ k' & \omega' \end{matrix} \right\rangle = \frac{\hbar^2 j(j+1)}{2\mu_{BC} r_{eq}^2} \delta_{xx'} \equiv b j(j+1) \delta_{xx'} \quad (16)$$

where the above equation also defines the rotational constant  $b$  of the  $H_2$  rotor. However, the  $\hat{L}^2$  term, the “tumbling” energy of rotation of the BC diatom and the A atom together, is not diagonal and poses some difficulty. This term must be evaluated by using the fact that  $\hat{L}^2 = (\hat{J} - \hat{j} - \hat{j}_a)^2$  :

$$\begin{aligned} \hat{L}^2 &= \hat{J}^2 + \hat{j}^2 + \hat{j}_a^2 - 2\hat{J} \cdot \hat{j} - 2\hat{J} \cdot \hat{j}_a + 2\hat{j} \cdot \hat{j}_a \\ &= \hat{J}^2 + \hat{j}^2 + \hat{j}_a^2 - \hat{J}^+ \hat{j}_- - \hat{J}^- \hat{j}_+ - 2\hat{J}_z \hat{j}_z \\ &\quad - \hat{J}^+ \hat{j}_{a-} - \hat{J}^- \hat{j}_{a+} - 2\hat{J}_z \hat{j}_{a_z} \\ &\quad + \hat{j}_+ \hat{j}_{a-} + \hat{j}_- \hat{j}_{a+} + 2\hat{j}_z \hat{j}_{a_z} \end{aligned} \quad (17)$$

The diagonal portion is thus

$$\begin{aligned} \left\langle j j_a \left| \frac{\hat{L}^2}{2\mu_{A,BC} R^2} \right| j' j'_a \right\rangle = \\ \frac{\hbar^2}{2\mu_{A,BC} R^2} \left( J(J+1) + j(j+1) + j_a(j_a+1) - 2(k+\omega)^2 + 2k\omega \right) \delta_{xx}, \end{aligned} \quad (18)$$

while there are off-diagonal terms in  $k$ ,  $\omega$ , and  $P = k + \omega$ , arising from the raising and lowering operators. The actions of the terms in Eq. (17) that involve raising and lowering operators on the basis functions are

$$\begin{aligned} \hat{J}^\pm \hat{J}_\mp \left| j j_a \right\rangle &= \hbar^2 (J(J+1) - P(P \mp 1))^{1/2} (j(j+1) - k(k \mp 1))^{1/2} \left| j j_a \right\rangle \\ \hat{J}^\pm \hat{J}_{a\mp} \left| j j_a \right\rangle &= \hbar^2 (J(J+1) - P(P \mp 1))^{1/2} (j(j+1) - \omega(\omega \mp 1))^{1/2} \left| j j_a \right\rangle \\ \hat{J}_\pm \hat{J}_{a\mp} \left| j j_a \right\rangle &= \hbar^2 (j(j+1) - k(k \pm 1))^{1/2} (j(j+1) - \omega(\omega \mp 1))^{1/2} \left| j j_a \right\rangle \end{aligned} \quad (19)$$

The raising and lowering operators  $\hat{J}_\pm$  and  $\hat{J}_{a\pm}$  behave in the usual manner, but the operators  $\hat{J}^\pm$  behave differently, since the body-fixed operators must be used for  $\hat{J}$ , denoted by the raised  $\pm$  signs. The actions of the body-fixed raising and lowering operators are interchanged [55] so that  $\hat{J}^+$  is a lowering operator and  $\hat{J}^-$  is a raising operator, and both affect the quantum number  $P$  of the state. Hence in the three terms considered above, the action of the two operators is first to apply a raising (or lowering) operator to raise (lower)  $k$  or  $\omega$ . In the first two, the body-fixed raising (lowering)

operators then raise (lower)  $P$  to match the fact that  $k$  or  $\omega$  has been raised (lowered) - for a ket to be valid,  $P$  must equal  $k + \omega$ . In the last case in Eq. ( 19 ), the other of  $k$  or  $\omega$  is lowered (raised).

Thus the kinetic energy term, through the contribution of the  $\hat{L}^2$  term, is not diagonal in the total body-fixed projection  $P = k + \omega$ . However, the overall magnitude of the  $\hat{L}^2$  term is usually small for our problem, for low values of  $J$ , due to the small magnitude of the rotational “constant”  $B(R) \equiv \hbar^2 / ( 2 \mu_{A,BC} R^2 )$  relative to the potential energy (see section V). Later the terms off-diagonal in  $P$  will be neglected, but the third portion of Eq. ( 19 ), which is diagonal in  $P$  but not in  $k$  and  $\omega$ , will be kept.

Next we require the matrix elements of the potential in this basis. First consider the electrostatic potential  $\hat{V}_{el}$ . Dubernet and Hutson expand the potential as follows:

$$\hat{V}_{el}(\hat{R}, \hat{\theta}, \hat{\phi}, \hat{\theta}_a, \hat{\phi}_a) = \sum_{\lambda_r \lambda_a \mu} V_{\lambda_r \lambda_a \mu}(\hat{R}) C_{\lambda_r \mu}(\hat{\theta}, \hat{\phi}) C_{\lambda_a - \mu}(\hat{\theta}_a, \hat{\phi}_a) \quad (20)$$

where  $C_{lm}$  is a renormalized spherical harmonic [56],  $\theta_a$  and  $\phi_a$  are electronic coordinates of the boron  $2p$  orbital with respect to the BF  $z$ -axis, and the sum over  $\mu$  ranges from  $-\min(\lambda_r, \lambda_a)$  to  $+\min(\lambda_r, \lambda_a)$ . The coefficients  $V_{\lambda_r \lambda_a \mu}(R)$  are obtained from the calculation of the potential energy surfaces. Since the potential energy for the electrons is calculated in the body frame, the potential is actually a function of  $\phi - \phi_a$  rather than  $\phi$

and  $\phi_a$  separately. This is the reason that the same  $\mu$  appears in the two spherical harmonics [33]. For the interaction of a closed-shell molecule with an atom in a  $P$  state, only terms with  $\lambda_a = 0$  or 2 are present [33].

The matrix elements of the electrostatic potential, in the above expansion, are

$$\begin{aligned} \left\langle \begin{matrix} j & j_a \\ k & \omega \end{matrix} \right| \hat{V}_{el} \left| \begin{matrix} j' & j'_a \\ k' & \omega' \end{matrix} \right\rangle = \\ \sum_{\lambda_r \lambda_a \mu} V_{\lambda_r \lambda_a \mu}(R) \left\langle \begin{matrix} j \\ k \end{matrix} \right| C_{\lambda_r \mu}(\hat{\theta}, \hat{\phi}) \left| \begin{matrix} j' \\ k' \end{matrix} \right\rangle \left\langle \begin{matrix} j_a \\ \omega \end{matrix} \right| C_{\lambda_a \mu}(\hat{\theta}_a, \hat{\phi}_a) \left| \begin{matrix} j'_a \\ \omega' \end{matrix} \right\rangle \delta_{JJ' MM'} \delta_{ll' ss'} \delta(R - R') \end{aligned} \quad (21)$$

where

$$\begin{aligned} \left\langle \begin{matrix} j \\ k \end{matrix} \right| C_{\lambda_r \mu}(\hat{\theta}, \hat{\phi}) \left| \begin{matrix} j' \\ k' \end{matrix} \right\rangle &= (-1)^k [(2j+1)(2j'+1)]^{1/2} \\ &\times \begin{pmatrix} j & \lambda_r & j' \\ -k & \mu & k' \end{pmatrix} \begin{pmatrix} j & \lambda_r & j' \\ 0 & 0 & 0 \end{pmatrix} \end{aligned} \quad (22)$$

and

$$\begin{aligned} \left\langle \begin{matrix} j_a \\ \omega \end{matrix} \right| C_{\lambda_a \mu}(\hat{\theta}_a, \hat{\phi}_a) \left| \begin{matrix} j'_a \\ \omega' \end{matrix} \right\rangle &= (-1)^{\omega-s} (2l+1) [(2j_a+1)(2j'_a+1)]^{1/2} \\ &\times \begin{Bmatrix} j_a & \lambda_a & j'_a \\ l & s & l \end{Bmatrix} \begin{pmatrix} j'_a & \lambda_a & j_a \\ \omega' & -\mu & -\omega \end{pmatrix} \begin{pmatrix} l & \lambda_a & l \\ 0 & 0 & 0 \end{pmatrix} \end{aligned} \quad (23)$$



were computed using the Wigner–Eckhart Theorem and Racah algebra formalism by Dubernet and Hutson [33]. The symbols in large parentheses (:::) and braces {...} are 3-j and 6-j symbols [56]. Since a 3-j symbol is zero unless the lower row sums to zero, the first 3-j symbols in Eqs.-( 22 ) and ( 23 ) require

$$\begin{aligned} -k + \mu + k' &= 0 \\ \omega' - \mu - \omega &= 0 \end{aligned} \quad (24)$$

which implies

$$k + \omega = k' + \omega' \quad (25)$$

This reveals that the electrostatic potential is diagonal in the total body-frame projection quantum number  $P = k + \omega$ . Additionally, the expansion coefficients,  $V_{\lambda_r \lambda_a \mu}(R)$ , discussed later, will be nonzero only for even values of  $\lambda_r$ . This is a consequence of symmetry arising from the fact that  $H_2$  is a *homonuclear* molecule [14]. The 3-j symbols have the property

$$\begin{pmatrix} a & b & c \\ 0 & 0 & 0 \end{pmatrix} = 0 \quad (26)$$

if  $a + b + c$  is odd [56]. Together with the fact only even values of  $\lambda_r$  are present, this means that the second 3-j symbol in Eq. ( 22 ) implies that the transitions will take place separately within the sets of even and odd diatom rotational quantum numbers  $j$ .

The final term in the Hamiltonian is the spin-orbit term  $\hat{V}_{ls}$ . The usual form of this term,  $\xi(R) \hat{l} \cdot \hat{s}$ , requires the dependence of the spin-orbit coupling on the distance  $R$ . It is a common assumption (the “pure-precession” approximation [14]), which we make, to neglect the  $R$  dependence of this term, assuming that the interaction does not perturb the atomic orbitals significantly. The spin-orbit term is diagonal in our basis with matrix elements

$$\begin{aligned}
 \left\langle \begin{matrix} j & j_a \\ k & \omega \end{matrix} \right| \hat{V}_{so} \left| \begin{matrix} j' & j'_a \\ k' & \omega' \end{matrix} \right\rangle &= \frac{\xi}{2} (j_a(j_a + 1) - l(l + 1) - s(s + 1)) \delta_{xx}, \\
 &= \frac{\xi}{2} \left( j_a(j_a + 1) - \frac{11}{4} \right) \delta_{xx}, \\
 &= \begin{matrix} +\xi/2 & j_a = 3/2 \\ -\xi & j_a = 1/2 \end{matrix}
 \end{aligned} \tag{27}$$

where the value of  $\xi$  for boron is  $10.7 \text{ cm}^{-1}$ , or  $4.876 \times 10^{-5}$  atomic units [14,27].

### Potential Expansion Coefficients

One still needs the specific form of the potential energy expansion coefficients  $V_{\lambda_r \lambda_a \mu}(R)$  to compute the potential matrix elements. These coefficients have been determined by *ab initio* calculations. Three adiabatic potential surfaces describing the  $\text{B} + \text{H}_2$  interaction have been computed as functions of  $R$  and  $\theta$  by M. Alexander [14] using multireference, configuration-interaction calculations. In these calculations, the  $\text{H}_2$

bond length was held fixed at 1.402 atomic units as discussed earlier. The surfaces correspond to the three degenerate atomic  $2p$  orbitals, where spin has been neglected. From the adiabatic surfaces, diabatic potentials  $V_{xx}$ ,  $V_{yy}$ ,  $V_{zz}$  and  $V_{xz}$  have also been computed by Alexander as functions of  $R$  and  $\theta$  using an approximate transformation approach, developed by Rebentrost and Lester in their study of the similar  $F + H_2$  interaction [8,14]. The  $V_{xx}$ ,  $V_{yy}$ , and  $V_{zz}$  diabatic surfaces nominally correspond to the three orientations of the Cartesian  $p_x$ ,  $p_y$ , and  $p_z$  orbitals [14]. The off-diagonal coupling  $V_{xz}$  corresponds to an interaction between the two  $p$  orbitals in the triatomic plane. The 2D surfaces may be obtained from HIBRIDON™ [57,58]. This code has been graciously provided to us by Alexander.

In Ref. [14], Alexander expands the  $\theta$  dependence of the potential energy surfaces using reduced rotation matrix elements  $d_{m0}^l(\theta)$ , where  $l$  and  $m$  are arbitrary indices. Since the third index is zero, these are equivalent to spherical harmonics [56]:

$$d_{m0}^l(\theta) = \left( \frac{2\pi}{2l+1} \right)^{1/2} Y_{lm}(\theta, \phi) e^{-im\phi} \quad (28)$$

By defining  $V_s$  and  $V_d$  to be one-half the sum and difference of the  $V_{xx}$  and  $V_{yy}$  potential energy surfaces, so that

$$\begin{aligned} V_{xx} &= (V_s - V_d) \\ V_{yy} &= (V_s + V_d) \end{aligned} \quad (29)$$

the angular expansion was made by Alexander as follows:

$$\begin{aligned}
V_{zz}(R, \theta) &= \sum_{l=0} V_l^{zz}(R) d_{00}^l(\theta) \\
V_s(R, \theta) &= \sum_{l=0} V_l^s(R) d_{00}^l(\theta) \\
V_d(R, \theta) &= \sum_{l=2} V_l^d(R) d_{20}^l(\theta) \\
V_{xz}(R, \theta) &= \sum_{l=1} V_l^{xz}(R) d_{10}^l(\theta)
\end{aligned} \tag{30}$$

The  $R$ -dependent expansion coefficients  $V_l^{zz}(R)$ ,  $V^s(R)$ ,  $V_l^d(R)$ , and  $V_l^{xz}(R)$  are described in Ref. [14] and are available in the HIBRIDON™ code. For an interaction with a homonuclear molecule such as  $H_2$ , the odd- $l$  expansion coefficients vanish due to symmetry [14]. The above expansion coefficients are connected to the BF expansion coefficients  $V_{\lambda_r \lambda_a \mu}(R)$  that we need for Eq. ( 21 ) by the formulas given in Ref. [15] :

$$\begin{aligned}
V_{\lambda_r 00}(R) &= [2V_{\lambda_r}^s(R) + V_{\lambda_r}^{zz}(R)]/3 \\
V_{\lambda_r 20}(R) &= 5[-V_{\lambda_r}^s(R) + V_{\lambda_r}^{zz}(R)]/3 \\
V_{\lambda_r 21}(R) &= 5 V_{\lambda_r}^{zz}(R)/\sqrt{6} \\
V_{\lambda_r 22}(R) &= 5 V_{\lambda_r}^{zz}(R)/\sqrt{6}
\end{aligned} \tag{31}$$

Note that  $V_{\lambda_r \lambda_a \mu}(R) = V_{\lambda_r \lambda_a -\mu}(R)$  [33]. Since the odd- $l$  coefficients in Eq. ( 30 ) are zero, the BF expansion coefficients in Eq. ( 31 ) are thus zero for odd values of  $\lambda_r$ ; this satisfies the requirement for the conclusion earlier that the  $H_2$  rotational transitions will take place separately within the sets of odd and even  $j$  quantum numbers.

Since  $J$  and  $M$  are conserved, we first choose a block of the Hamiltonian matrix labeled by  $J$  and  $M$ . An approximation must be made later to truncate the (infinite) matrix by only including basis vectors up to a maximum value  $j_{\max}$  of the diatom rotational quantum number  $j$ . This may or may not be justifiable by the energetic accessibility of the higher  $j$  rotational states of the diatom, the energies of which are listed in Table 3. If the wave packet energies are lower than the cutoff needed to make a transition to a higher  $j$ , energy conservation forbids that state from being accessible.

Table 3. Rotational levels of  $H_2$

$j$	<u>Energy (atomic units)</u>
0	0
1	0.00055
2	0.00166
3	0.00332
4	0.00554
5	0.00831
6	0.01163
$j$	$2.769 \times 10^{-4} \times j(j+1)$

#### IV. Implementation

##### Numerical Representation of Wave Packets

To numerically represent a wavefunction, so that it can be propagated in the application of the channel packet method, we use a uniform spatial grid of discrete points at which the value of the wavefunction is tabulated. The spatial grid must be large enough in extent to support the entire wavefunction, which is possible because the wavefunction is chosen to be a wave packet finite in extent. The discretization of a wavefunction on a grid of  $N$  points is thus given by  $N$  numbers:

$$\langle x_{discrete} | \Psi \rangle = \Psi(x) = \begin{Bmatrix} \Psi_1(x_1) \\ \Psi_2(x_2) \\ \vdots \\ \Psi_N(x_N) \end{Bmatrix} \quad (32)$$

In a radial or Cartesian direction, the Fourier transform grid method that is used imposes requirements on the grid. The periodic boundary conditions assumed by the Fourier transform must be satisfied by the wave packet approaching zero at the grid boundaries, which must be monitored during the calculation. The same must be true of the momentum representation, which imposes a requirement on the grid spacing in the coordinate representation. The maximum momentum representable on a coordinate grid

with spacing  $\Delta x$  is given by the Nyquist value  $1 / (2 \Delta x)$ . Additionally, a true fast Fourier transform, scaling as  $O(N \log N)$  instead of  $O(N^2)$  is only available if the number of grid points  $N$  is a power of two; if more coordinate space is required to support the wavefunction, the number of grid points must be doubled, or the spacing  $\Delta x$  increased (which reduces the maximum representable momentum).

### Gaussian Wave Packets

A one-dimensional Gaussian wave packet, at  $t = 0$  with initial average position  $x_0$ , initial average momentum  $k_0$ , and initial position uncertainty  $\Delta x$  is defined in Merzbacher [59]:

$$\Psi(x, t = 0) = \frac{1}{(2\pi \Delta x^2)^{1/4}} \exp \left[ -\frac{(x - x_0)^2}{4 \Delta x^2} + i k_0 x \right] \quad (33)$$

To analytically evolve this wave packet to time  $t = \tau$ , we use the formula

$$\Psi(x, t = \tau) = \frac{\zeta^{-1/2}}{(2\pi \Delta x^2)^{1/4}} \exp \left[ \zeta^{-1} \left( -\frac{(x - x_0)^2}{4 \Delta x^2} + i k_0 x - \frac{i k_0^2 \tau}{2m} \right) \right] \quad (34)$$

$$\zeta = 1 + \frac{i \tau}{2m \Delta x^2}$$

The initial states used in the channel packet method are defined to be Gaussian wave packets. This allows Eq. ( 34 ) to be used to analytically propagate the wave packet where the potential is zero or a constant value (i.e. during the creation of a Møller state).

### Propagation of the Wave Function

The key element in a time dependent technique is a method of propagating the wave function. Several schemes exist and have been reviewed in the literature [60]; we use the split operator method [60]. This technique is based on the split operator approximation to the time evolution operator  $\hat{U}(t) = \exp(-i\hat{H}t/\hbar)$ . If the Hamiltonian for the nuclei is  $\hat{H} = \hat{T} + \hat{V}$ , where  $\hat{T}$  is the kinetic energy part, and  $\hat{V}$  is the potential energy part, one can write

$$|\Psi(t + \Delta t)\rangle = \left( \exp(-\frac{i\hat{V}\Delta t}{2\hbar}) \exp(-\frac{i\hat{T}\Delta t}{\hbar}) \exp(-\frac{i\hat{V}\Delta t}{2\hbar}) + O(\Delta t^3) \right) |\Psi(t)\rangle \quad (35)$$

The term  $O(\Delta t)^3$  arises from nonzero commutators involving  $\hat{T}$  and  $\hat{V}$ , and is neglected by using a sufficiently small time step  $\Delta t$ . By splitting the operator into separate exponentials of the kinetic and potential energy, these parts can be evaluated in representations in which they are diagonal. The potential energy  $\hat{V}$ , and thus its exponential, is diagonal in the coordinate representation and the adiabatic basis. The



kinetic energy  $\hat{T}$ , and its exponential, are diagonal in the momentum representation and the diabatic basis.

A Fourier transform connects the coordinate and momentum representations, and a unitary matrix transformation connects the adiabatic and diabatic bases. An application of this method has been demonstrated by Alvarellos and Metiu [61]. We have used their example wave packet propagation to test the code. The bulk of computational time is spent performing the Fourier and matrix transformations, so it is crucial to use a fast Fourier transform, which requires that the radial grid size be a power of two. The unitary matrix transformation is precomputed by one-time diagonalization of the potential matrix at all values of  $R$ . Its application becomes more time-consuming, and it requires increased amounts of storage, as the basis size increases. The application of the transform requires a matrix-vector multiplication, but not a diagonalization, at each value of  $R$ , so it scales both in time and storage requirements as  $O(M^2 \times N)$ , where  $M$  is the basis size and  $N$  is the number of radial grid points.

In our case, the radial kinetic energy operator becomes  $-\frac{\hbar^2}{2\mu_{A,BC}} \frac{1}{R} \frac{\partial^2}{\partial R^2} R$  in the coordinate representation and it is most convenient to store the “reduced” wavefunction  $R \Psi(R)$ . This reduces the action of the derivative to  $-\frac{\hbar^2}{2\mu_{A,BC}} \frac{\partial^2}{\partial R^2}$ , which is evaluated by transforming to the momentum representation with a Fourier transform. When wavefunctions are integrated to obtain the correlation function (Eq. (6) in the channel packet method), we must remember the volume element:

$$C_{\gamma'\gamma}(t) = \int_0^{\infty} \psi_{-}^{\gamma'}(R) \exp(-iHt/\hbar) \psi_{+}^{\gamma}(R) R^2 dR \quad (36)$$

Since the wavefunction is stored as  $R^{-1} \Psi(R)$ , the  $R^2$  in the integration is already accounted for. Hence the same computer code (representation of the wave packet and numerical integration) can be used for spherical coordinates and Cartesian coordinates, but the interpretation is different.

### Absorbing Boundary Conditions

Several issues can arise during the correlation function calculation. The grids used to calculate the Møller states may be different from the one used to calculate the correlation function. An example of this stems from the fact that absorbing boundary conditions (ABC) can be used to significantly speed up the calculation of the correlation function, by allowing the coordinate grid size to be reduced. If the evolving Møller state spreads significantly and reaches the grid boundary before it has ceased to overlap the fixed Møller state, it will reflect off the edge of the grid due to the periodic boundary condition nature of the Fourier transform propagation method, unless the grid is made extremely large to accomodate the full wave function. To avoid this, ABC can be placed on the edge of the grid. The ABC take the form of an imaginary part of the potential energy added to each adiabatic (diagonal) potential surface:

$$\hat{V} = \hat{V}_I + i\hat{V}_{ABC} \quad (37)$$

where  $\hat{V}_I$  is the interaction potential and  $\hat{V}_{ABC}$  is the absorbing potential [18]. When exponentiated in the time evolution operator, the ABC term attenuates the wavefunction at each time step (if  $\hat{V}_{ABC}$  has the correct sign, i.e. negative for a positive time step  $\Delta t$ ). Thus if ABC that do not overlap the fixed Møller state are placed at the grid boundaries, they will not affect the value of the correlation function, and the grid size can be significantly reduced. For a good example of the application of ABC to a two dimensional problem, see Calfas and Weeks, who applied it to the test case of  $H + H_2$  [18,62]. The absorbing boundary conditions are not perfect; they always cause some reflection. This is minimized by proper choice of the parameters used to define  $\hat{V}_{ABC}$ . We follow [18] and use

$$V_{ABC}(R) = A \exp\left[\frac{(R - R_{max})^2}{B}\right] \quad (38)$$

where  $A$  and  $B$  are adjustable parameters, and  $R_{max}$  is the value of  $R$  at the grid boundary.  $A$  is chosen to have the smallest value that completely attenuates the evolving wave packet, while at the same time  $B$  is chosen to have the largest value that keeps the ABC separate from the initial state and the interaction region. These choices are made to make the ABC as smooth and gradual as possible, to minimize reflection. For this problem, a suitable choice was found by trial and error to be  $A = 0.0015$  atomic units, and  $B = 30.0$  atomic units.

## Implementation of the Channel Packet Method

A general implementation requires three separate propagation stages:

- I. Preparation of the reactant Møller state
- II. Preparation of the product Møller state
- III. Evaluation of the correlation function

In stage I (stage II), the initial reactant (product) states are propagated backward (forward) in time under the asymptotic Hamiltonian to a time  $t$  sufficient to exit the interaction region. They are then numerically propagated forward (backward) in time under the full Hamiltonian, back to  $t = 0$ , and saved to disk as the Møller states.

In stage III, the reactant and product Møller states are loaded into memory, and the reactant state is propagated backward and forward in time until the correlation function decays to zero.

The specific problem in this thesis has been approached using explicit propagation of only one spatial variable,  $R$ , since the problem was reduced to a one-dimensional propagation on many surfaces in Section III. In this case, we can justify (with regard to computing time) a simplification of the above procedure. By preparing the Møller states in the asymptotic limit, the Møller states are equal to the initial states, and stages I and II do not need to be performed (if they were, the resulting Møller states

would be identical to the initial states.) Hence only stage III needs to be performed, and the Møller states are simply defined as the initial reactant and product wave packets.

Additionally, in the computation of S-matrix elements for transitions from the same reactant state to all possible product states, the reactant wave packet propagation is identical. Thus, the correlation functions between the evolving reactant Møller state and all the desired product Møller states are computed during one propagation of the reactant Møller state. After the propagation, each correlation function is used in Eq. ( 7 ) to compute the corresponding S-matrix elements.

#### Accuracy of Wave Packet Propagation

There are several parameters that affect the numerical accuracy of a wave packet propagation. These include the time step  $\Delta t$ , the coordinate grid spacing  $\Delta x$ , and the coordinate grid size, controlled by the grid spacing and the number of grid points  $N_x$ . The formal error in Eq. ( 35 ) for the split-operator method is  $O(\Delta t^3)$ . The numerical properties of the split-operator method have been treated [60]. A key positive point is that the split operator method is unitary, and thus norm-preserving (the integral of  $|\Psi|^2$  stays constant). The time step  $\Delta t$  must be chosen small enough so that the product of the potential or kinetic energy and  $\Delta t$  is also small. An insufficiently small time step can result in dramatically obvious errors in the wave packet propagation. The fundamental method, however, to check the time step, is to compare a wave packet propagation with

time step  $\Delta t$  to one with a reduced time step, say  $\Delta t/2$ , and evaluate the convergence of the propagated wavefunction with respect to the reduced time step.

The nature of the Fourier transform propagation method imposes several conditions on the spatial grid parameters  $N_x$  and  $\Delta x$ . First, the Fourier transform requires periodic boundary conditions. If a wave packet approaches one end of the grid, it will continue by wrapping around to the other side, if there is no potential to stop it. To satisfy the periodic boundary conditions but still represent the true, non-periodic, physical system, the wavefunction must smoothly approach zero at the grid boundaries. For our problem of a wave packet traveling on a potential surface where the only coordinate is the radial coordinate  $R$ , the potential is steeply repulsive at the small  $R$  edge of the grid, and the wave packet is defined for energies that cannot (classically) penetrate the barrier, so it effectively decays to zero on that edge. However, if the wave packet begins to approach the large  $R$  grid boundary, it will incorrectly reflect from the boundary, due to the steep wall at the small  $R$  edge and the periodic boundary conditions. Thus during the evaluation of the correlation function, when part of the wave packet reaches the edge long before other portions have exited the interaction region, absorbing boundary conditions are used to prevent the wavefunction from reaching the grid boundary. However, the absorbing boundary conditions can also introduce error through unintended reflections, which are minimized by the proper choice of  $\hat{V}_{ABC}$  above.

The other significant issue arising from the nature of the Fourier transform is the analogous requirement that the momentum grid satisfy similar conditions above. The

momentum grid is defined by the choice of coordinate grid. It has a maximum representable momentum  $k_{max} = \pi / \Delta x$ , (the Nyquist frequency) which is entirely defined by the coordinate grid, and must be large enough in extent to support the entire momentum representation of the wave packet. (In atomic units, momentum  $p = \hbar k = k$  ). If the wave packet has momentum components larger than  $k_{max}$ , those components will be “aliased” back into the zone with  $|k| < k_{max}$ . Thus, during the propagation, the momentum representation should also be monitored to make sure that it does not approach the momentum grid boundary.

The Fourier transform implementation itself is unique in that it introduces extremely small amounts of numerical error. Due to the fact that a uniform spatial grid is used, the sines and cosines are orthogonal on the discrete grid [63:512], and thus the discrete Fourier transform (DFT) performed on a uniform grid is an exact representation of the original function (on the uniform grid). The operation of the forward and inverse FFT can be performed millions of times in double precision and only change the very last digits stored in the floating point representation, due to computer roundoff error only.

To compute the correlation function, the overlap integral between the evolving reactant Møller state and the product Møller state is computed, using the trapezoid rule [64], which has an accuracy  $O(\Delta x^2)$ . Since the integrand approaches zero at the endpoints, the trapezoid rule is simply evaluated by summing the values of the integrand at all points for which it is tabulated. This is the simplest and fastest reasonable numerical quadrature technique for this problem.

### Accuracy of Computation of S-Matrix Elements

The evolving Møller state will eventually completely exit the interaction region, since it has no bound state components. Once it leaves the interaction region and also passes the region of the fixed Møller state, the correlation function will decay to zero. At this point, the evaluation of the correlation function can be terminated. Then, the Fourier transform of the correlation function is computed and used in Eq. ( 7 ) to obtain the S-matrix elements. If the evaluation of the correlation function is terminated before it stabilizes to (numerical) zero, the Fourier transform will be corrupted with oscillatory behavior superimposed on the true answer. This can be seen if one computes a “running” S-matrix that is evaluated over time as the correlation function is computed.

The process of dividing by the momentum space expansion coefficients  $\eta(k)$  is numerically risky for values of  $k$  where  $\eta$  is small. In the energy ranges where the expansion coefficients are small, the Fourier transform of the correlation function is usually small, but contains noise. The expansion coefficients decay exponentially, and thus the division, and the S-matrix elements, blow up outside the range over which the expansion coefficients are significantly nonzero. Thus the answer becomes clearly invalid outside a certain energy range, since the absolute value squared of S-matrix elements, which represent probabilities, must be less than one. This limitation in the valid energy range is reasonable - we should only get useful information about S-matrix elements for the energy range that we include in our wave packets that explore the interaction potential. This problem is minimized by choosing the initial wave packets to have



expansion coefficients that are significant in the entire range of interest, but it can never completely be eliminated. Another related problem is that the expansion coefficients  $\eta(k)$  may be slightly inaccurate because the initial wave packets, which are Gaussians in coordinate space, are never truly in the asymptotic limit, nor are they entirely separated from the absorbing boundary conditions. This can cause the effective wave packet that samples the potential to have slightly different expansion coefficients than those used in its initial definition. This problem is reduced only by using larger and larger grids to place the initial state closer and closer to the “true” asymptotic limit.

#### Validation of S-matrix Elements

S-matrix elements should have absolute values squared that are less than one, as discussed earlier. They should also be zero at energies for which the specific transition is energetically impossible (below threshold). One way to test the numerical parameters in the S-matrix calculations is to artificially uncouple the potential surfaces, by setting the off-diagonal terms in the diabatic potential to zero, and compute S-matrix elements for reflection where the reactants and products are on the same surface. The resulting S-matrix elements should be exactly one for all energies. The energy range over which this test numerical answer is one gives an indication of the energy range over which the true S-matrix elements should be valid, which should correspond to the numerically significant range of the momentum expansion coefficients. In Section V this test is done for the parameters used in our calculation.

One possible qualitative test of the validity of the S-matrix elements of a certain small energy range is to propagate a wave packet defined only over a narrow energy range (so that it is very broad in coordinate space), and examine the “amount” of the wave function that couples to the product state in question, computed by integrating the wave packet. This value is then compared to the value of the S-matrix computed by the channel packet method at the corresponding energy. This qualitative test is only good for S-matrix elements that are smooth, broad functions of energy, when one wants to get a general idea if the code is approximately correct. This was done in the two surface case, as an initial test of the computer code.

A strong test for validity is the fact that the sum over all possible final states of the probabilities for transition from a given initial state should be unity, which follows from the unitarity of the S-matrix [11]. Thus, when the transition probabilities (absolute value squared of S-matrix elements) are computed from the initial state to all the other states in the basis, they are added together, and the range over which this sum is unity is a good indicator of the validity of the S-matrices over that range. The results of this test will be presented in Section V.

### Graphical Visualization

Code to implement the channel packet method to obtain scattering matrix elements was written in Fortran 90, and run on a Silicon Graphics O<sub>2</sub> computer. An

important part of the implementation is the ability to check the initial conditions and monitor the progress of the calculation, using a suitable graphics display. Since a wave packet propagation may take hours of computer time, it is extremely useful to be able to evaluate the initial state visually to ensure it is correct before beginning the run. Simple mistakes such as preparing the wave packets in the wrong location (e.g. off the grid) or with the wrong energy components become immediately obvious upon visual inspection. As the wave packets evolve, they are displayed on the computer screen, together with the correlation function and current state of the S-matrix elements. During the calculation, one can examine these to ensure that the calculation is still running as planned, or to check if it is already complete. The code uses OpenGL for its graphics, combined with the GL Utilities Toolkit (GLUT). OpenGL is a platform independent 3D graphics application programming interface based on the Silicon Graphics-specific IRIS GL. When combined with GLUT, which provides basic windowing ability, it allows the entire program to be platform independent, and not tied to the Silicon Graphics computer. By use of modular programming, a non-graphics version can be made that does not require the OpenGL library, and can be run in batch mode.

The main program for two dimensional calculations is controlled by a data file of parameters that specify exactly how the initial wave packets are defined, or loaded from files, and how they are to be propagated to create Møller states or evaluate the correlation function. The potential energy surfaces are generated by a Fortran subroutine provided as part of the HIBRIDON™ software package written by M. Alexander, who graciously provided us with the subroutine. HIBRIDON™ is a package of programs for the time-

independent quantum treatment of inelastic collisions and photodissociation written by M.H. Alexander, D.E. Manolopoulos, H.-J. Werner, and B. Follmeg, with contributions by P.F. Vohralik, D. Lemoine, G. Corey, R. Gordon, B. Johnson, T. Orlikowski, A. Berning, A. Degli-Esposti, C. Rist, P. Dagdigian, B. Pouilly, G. van der Sanden, M. Yang, F. de Weerd, and S. Gregurick.

The fundamental graphics subroutine controls the plotting of a function of two variables as a grid of points, lines, or a smoothly lit surface, which can be scaled and rotated to examine it from all angles. This plotting subroutine calls commands in the OpenGL API (Application Programming Interface) to define the vertices of the grid, and the lines or polygons between the vertices in the case of a wire mesh or smooth surface. Separate routines control color and lighting parameters, as well as the geometrical viewing parameters that allow the function plot to be rotated to any angle. The user can select any function (including the potential surfaces, wavefunctions, correlation function, and S-matrix) that is displayed, and through a keyboard and menu interface, the user can control its display characteristics. Each plotted variable has a separate set of display characteristics stored in a data structure, which can be saved to disk to record a specific graphics "state" that is most convenient for the particular application. Through the use of the GLUT API, the graphical version also allows interactive control over the process. GLUT handles the window-system dependent tasks such as opening the window and receiving input via mouse clicks and pop-up menus. With the menu, the user can save and load wavefunctions, correlation functions, and S-matrices, and control the specifics of the evaluation of the correlation function. After the calculation is complete the

graphics system can be used as a visualization tool to examine the results. For intensive calculations, the graphics can be used first to check the initial parameters, and then turned off, so that processing time is not allocated to unseen graphics.

In the calculations where the basis size can be 14 (or larger), the radial dependence of the wavefunction is a 14 element column vector containing 14 “single-surface” wavefunctions. Rather than display all of these separately, it is advantageous to display them as one “two-dimensional” wavefunction where one coordinate is  $R$  and the other coordinate is the “basis coordinate”. With this approach, the entire wavefunction can be examined to ensure that it does not encounter the edge of the radial coordinate or momentum grids, and that it is properly absorbed by the ABC. One can also examine how much coupling has taken place to the other surfaces.

## V. Results and Discussion

### Truncation of Basis

In Section III, the Hamiltonian was represented in matrix form using a basis of BF functions. The full basis is infinite in size and must be truncated to treat the problem numerically. Prior to truncating the basis, one can take advantage of the fact that the Hamiltonian is block diagonal. Thus one can select specific values of  $J$  and  $M$  for the problem, and treat only that specific block (which is still infinite in size).

The Hamiltonian is also approximately block diagonal in the total body frame projection quantum number  $P = k + \omega$ . Off diagonal terms in  $P$  arise from matrix elements of the  $\hat{L}^2$  term. An approximation that we will make is to neglect these terms. This approximation has been discussed often and takes many names, including the centrifugal sudden (CS) approximation, helicity decoupling approximation, or  $J_z$ -conserving coupled states (also CS) approximation [11,45-47]. If the magnitude of the rotational constant  $B(R)$  of the A-BC system is small, due to a large reduced mass combined with a sufficiently large value of  $R$  at closest approach, and the total  $J$  is small, this may be a good approximation. For the B + H<sub>2</sub> problem, the distance  $R$  stays at values  $\gtrsim 5$  atomic units, so the magnitude of  $B$  stays small relative to the other terms in the Hamiltonian.

Additionally, as stated in Section III, rotational transitions take place separately within the sets of odd and even values of  $j$ , the rotational quantum number for the  $H_2$  molecule. Hence the Hamiltonian separates into two blocks labeled by the sign of  $(-1)^j$ , and we can choose one to work in. One must finally truncate the basis by choosing a value  $j_{max}$  that is the highest value of  $j$  that will be included in the basis. The choice of  $j_{max}$  may be aided by energy arguments; however, it is sometimes necessary to include channels of higher  $j$  that are not energetically accessible as product states but that may be temporarily accessible during the interaction. For completeness, we include the fact that the continuous infinite variable  $R$  is replaced by its finite discretization, discussed in Section IV.

### Para Basis Sets

For this problem, then, the choice must be made for the values of  $J, P, j_{max}$ , and whether  $j$  will stay even or odd. A straightforward choice for an initial treatment is to choose the lowest possible value of  $J$ , which is  $1/2$ , and choose  $P$  arbitrarily to be  $+1/2$ . The Hamiltonian matrix is independent of the total space-fixed projection  $M$ , which we can leave unspecified. We will choose to study transitions starting from the ground state, so  $j_{initial}$  will be zero, and hence  $j$  will stay even. (The  $H_2$  will stay *para*, labeled p- $H_2$ ) We study several choices of  $j_{max}$ , and hope that as  $j_{max}$  increases beyond the energetically accessible value, the scattering results converge with the corresponding increased basis size.

Thus our basis sets will be labeled by the available values of  $j$ , assuming the other choices above. The simplest basis is thus denoted by  $(0)$ , while larger bases will be labeled  $(0, 2)$ ,  $(0, 2, 4)$ , or  $(0, 2, 4, \dots, j_{max})$ . The number of basis vectors in this specific basis set will be  $3 \times j_{max} + 2$ . The reason for this is that given the full set of six spin-orbit states  $|j_a \omega\rangle$  of boron, each will have a specific value of  $\omega$ , which must be paired with exactly one available value of  $k$  to give the value  $P = k + \omega = 1/2$ . This is done for each even value of  $j$  except for  $j = 0$ , in which case there are only two legal basis vectors:

$$\begin{vmatrix} j & j_a \\ k & \omega \end{vmatrix} \in \left\{ \begin{vmatrix} 0 & 1/2 \\ 0 & 1/2 \end{vmatrix}, \begin{vmatrix} 0 & 3/2 \\ 0 & 1/2 \end{vmatrix} \right\} \quad (39)$$

For  $j = 2$ , there are six basis vectors:

$$\begin{vmatrix} j & j_a \\ k & \omega \end{vmatrix} \in \left\{ \begin{vmatrix} 2 & 3/2 \\ 2 & -3/2 \end{vmatrix}, \begin{vmatrix} 2 & 3/2 \\ 1 & -1/2 \end{vmatrix}, \begin{vmatrix} 2 & 1/2 \\ 1 & -1/2 \end{vmatrix}, \begin{vmatrix} 2 & 1/2 \\ 0 & 1/2 \end{vmatrix}, \begin{vmatrix} 2 & 3/2 \\ 0 & 1/2 \end{vmatrix}, \begin{vmatrix} 2 & 3/2 \\ -1 & 3/2 \end{vmatrix} \right\} \quad (40)$$

So the  $(0, 2)$  basis contains eight basis vectors, combining the  $j = 0$  and  $j = 2$  basis vectors listed above. There are again six basis vectors for higher values of even  $j$ , which can be seen to be exactly the same as those in Eq. (40) but with the upper left "2" replaced by the specific value of  $j$ .



If we consider matrix elements off-diagonal in  $P$ , and thus include all possible values of  $P$  in the basis set, it will be significantly larger. Table 4 summarizes the size of various bases containing even  $j$ , which we denote “ $para$ ”, with and without making the CS approximation ( $P$  conservation), with  $J = 1/2$ .

Table 4. Size of  $para$  bases with  $J = 1/2$

<u>Basis set</u>	<u>CS Basis Size</u>	<u>Non-CS basis size</u>
( 0 )	2	6
( 0, 2 )	8	36
( 0, 2, 4 )	14	90
( 0, 2, 4, 6 )	20	168
( 0, 2, ..., $j_{max}$ )	$2 + 3 \times j_{max}$	$6 \times \sum_{j \in basis} (2j + 1)$

In this thesis we will present results for the ( 0 ) , ( 0, 2 ) , and ( 0, 2, 4 ) bases, using the CS approximation. A block schematic of the Hamiltonian in matrix form is shown in Figure 6. The darkest shaded area represents the ( 0 ) basis; this together with the medium shaded area represents the ( 0, 2 ) basis (  $8 \times 8$  ). The entire shaded grid represents the ( 0, 2, 4 ) basis (  $14 \times 14$  ). Off-diagonal terms exist throughout the entire matrix.

	$\begin{matrix}  0 & j_a\rangle \\  0 & 1/2\rangle \end{matrix}$	$\begin{matrix}  2 & j_a\rangle \\  k & \omega\rangle \end{matrix}$	$\begin{matrix}  4 & j_a\rangle \\  k & \omega\rangle \end{matrix}$
$\begin{matrix} \langle 0 & j'_a   \\ \langle 0 & 1/2   \end{matrix}$	$\begin{matrix} j=j'=0 \\ \\ 2 \times 2 \end{matrix}$		
$\begin{matrix} \langle 2 & j'_a   \\ \langle k' & \omega'   \end{matrix}$		$\begin{matrix} j=j'=2 \\ \\ 6 \times 6 \end{matrix}$	
$\begin{matrix} \langle 4 & j'_a   \\ \langle k' & \omega'   \end{matrix}$			$\begin{matrix} j=j'=4 \\ \\ 6 \times 6 \end{matrix}$

Figure 6. Block schematic of the Hamiltonian matrix

The effective potential (potential energy + angular kinetic energy) matrix in the ( 0, 2, 4 ) basis has  $14^2 = 196$  elements (though it is symmetric). To present the potential surfaces in the clearest fashion, Figure 7 shows the diagonal elements of the matrix in the diabatic representation. Figure 8 shows the first row of the potential matrix in the diabatic representation. Figure 9 shows the adiabatic potential surfaces ( the diagonal and only non-zero elements in the adiabatic representation).

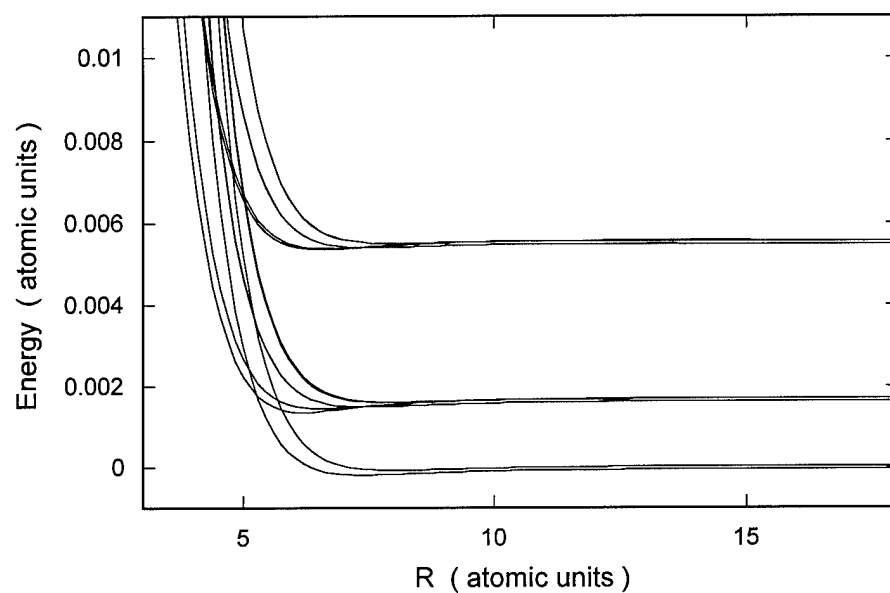


Figure 7. Diagonal elements of potential matrix in diabatic representation

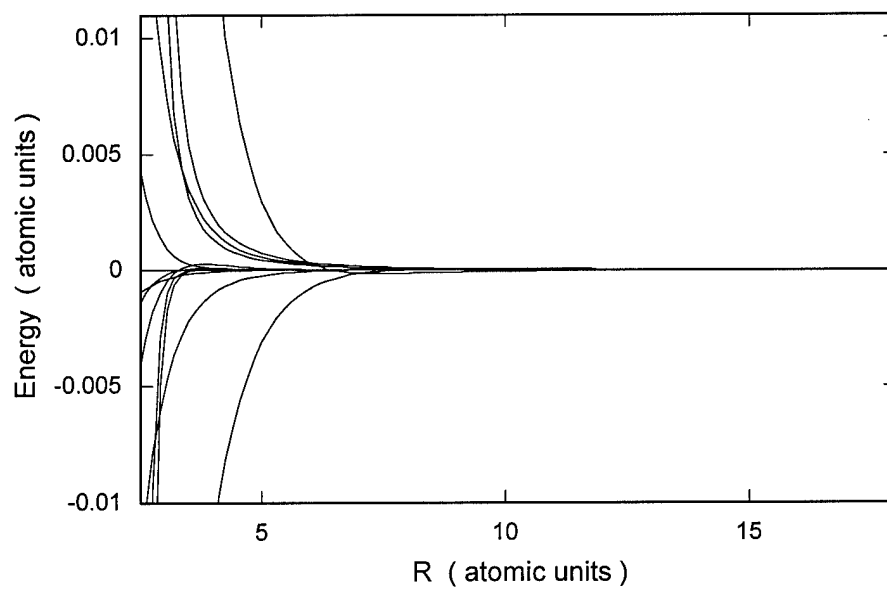


Figure 8. First row of potential matrix in diabatic representation

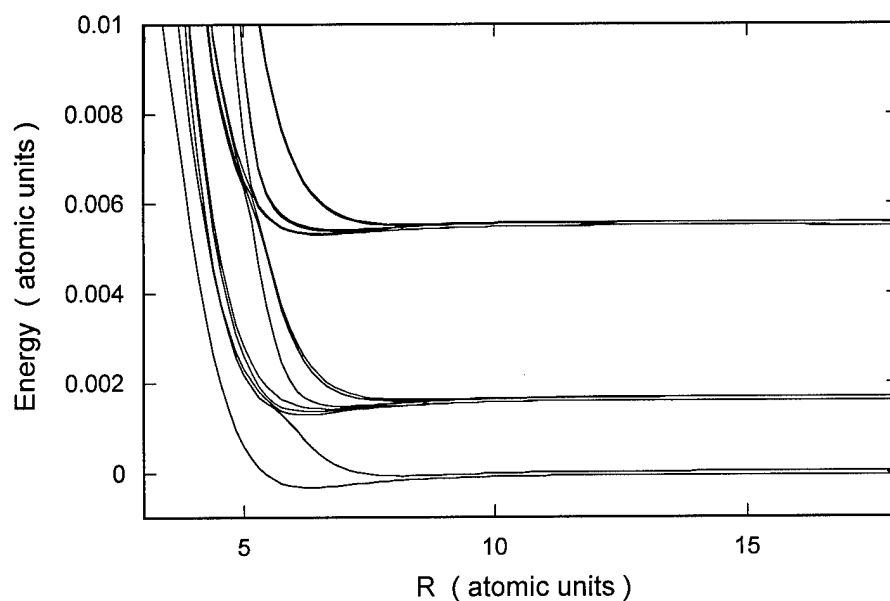


Figure 9. Adiabatic potential surfaces

### The “One-Dimensional” Problem

The even  $j$  rotational levels of  $\text{H}_2$  label *para*-hydrogen ( $p\text{-H}_2$ ), with nuclear spin wavefunction anti-symmetrized and spatial wavefunction symmetrized, forming a singlet state. The odd rotational levels are *ortho*-hydrogen, the triplet state. At room temperature, hydrogen is found in a ratio of approximately 3:1 *ortho* to *para*. However, as the temperature is lowered below 20 K or so, the hydrogen molecules freeze into their lowest state and tend to stay *para*, with frozen hydrogen being mostly *para*.

If one assumes that a p-H<sub>2</sub> molecule in its ground ( $j = 0$ ) rotational state stays in the ground state during the collision with a boron, the (0) basis set in Eq. (39) may be used. The  $2 \times 2$  matrix of the potential  $\hat{V}_{el} + \hat{V}_{so}$  in this basis is

$$\begin{array}{cc} j_a = 1/2 & j_a = 3/2 \\ j_a = 1/2 & \begin{pmatrix} V_0(R) + B(R) - \xi & -2^{1/2} V_2(R) \\ -2^{1/2} V_2(R) & V_0(R) + V_2(R) + 7B(R) + \xi/2 \end{pmatrix} \end{array} \quad (41)$$

where the values  $J = 1/2$ ,  $P = 1/2$  are used together with the value of  $j_a$  in Eq. (18) to compute the coefficient of  $B(R)$ . The functions  $V_0(R)$  and  $V_2(R)$  are given in Ref. [14] from combinations in the expansions in Eq. (30):

$$\begin{aligned} V_0(R) &= [ 2V_{l=0}^s(R) + V_{l=0}^{zz}(R) ] / 3 \\ V_2(R) &= [ -V_{l=0}^s(R) + V_{l=0}^{zz}(R) ] / 3 \end{aligned} \quad (42)$$

From Eq. (31) one can note that in terms of the body-fixed potential expansion coefficients,  $V_0(R) = V_{000}(R)$  and  $5V_2(R) = V_{020}(R)$ . The radial kinetic energy operator is

$$-\frac{\hbar^2}{2\mu_{A,BC}} \frac{1}{R} \frac{\partial^2}{\partial R^2} R \times \underline{1}, \text{ where } \underline{1} \text{ is a } 2 \times 2 \text{ unit matrix. Elements of the } 2 \times 2 \text{ matrix in}$$

Eq. (41) are shown in Figure 10, together with the adiabatic surfaces obtained from the matrix diagonalization. The adiabatic surfaces are the largest and smallest in the interaction region. The off-diagonal coupling term approaches negative infinity as  $R$  decreases.

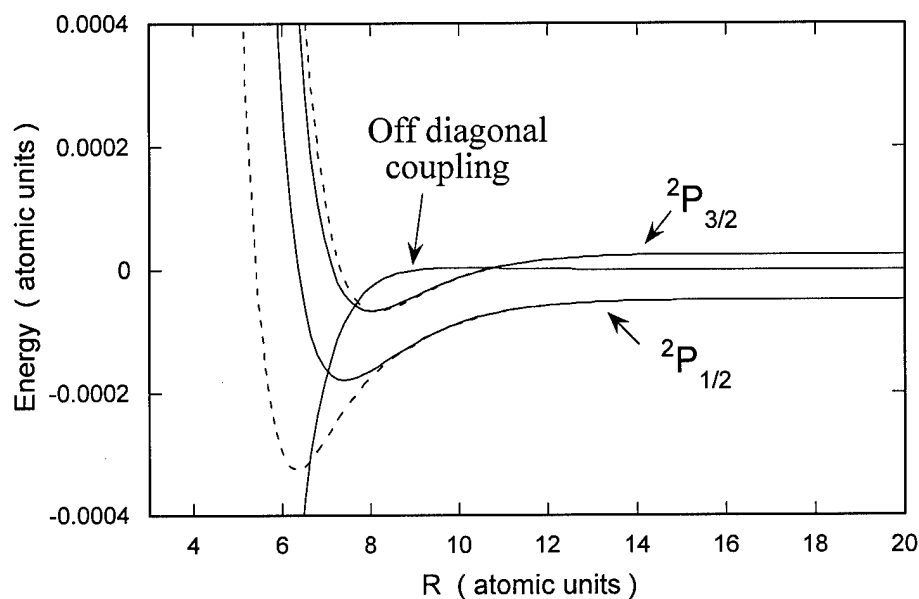


Figure 10. Diabatic (solid) and adiabatic (dashed) potential surfaces for ( 0 ) basis

In the  $2 \times 2$  ( $j = j' = 0$ ) case, the p-H<sub>2</sub> can be considered equivalent to a spherical atom colliding with the boron, and the mathematics reduces to that of atom-atom interactions, which are somewhat simpler. The three basic adiabatic potential energy surfaces reduce to two, due to the extra symmetry. These nominally correspond to the p orbital of the B atom pointing along, or perpendicular to, the direction of approach. These surfaces are one dimensional due to the spherical symmetry and correspond to averages of the isotropic terms in the full potentials. The SF basis found in Ref. [33] for atom-diatom interactions becomes simpler in the atom-atom case. In Ref. [14], Alexander uses this idea to evaluate the  $2 \times 2$  matrix in the SF frame that results when  $j$  is constrained to stay zero. This is done using simpler formulas [65-66]. The resulting matrix is the same as we find in the body-fixed case except for a sign on the

off diagonal terms, and slightly different forms of the multipliers in front of the  $B(R)$  terms. This difference may be explained by our use of the CS approximation. Numerically, we will see that the difference in the form of the angular effective potential has little effect on the S-matrix elements; we present the results for all the basis sets using the BF frame for consistency.

### Application of Channel Packet Method to "1D" Problem

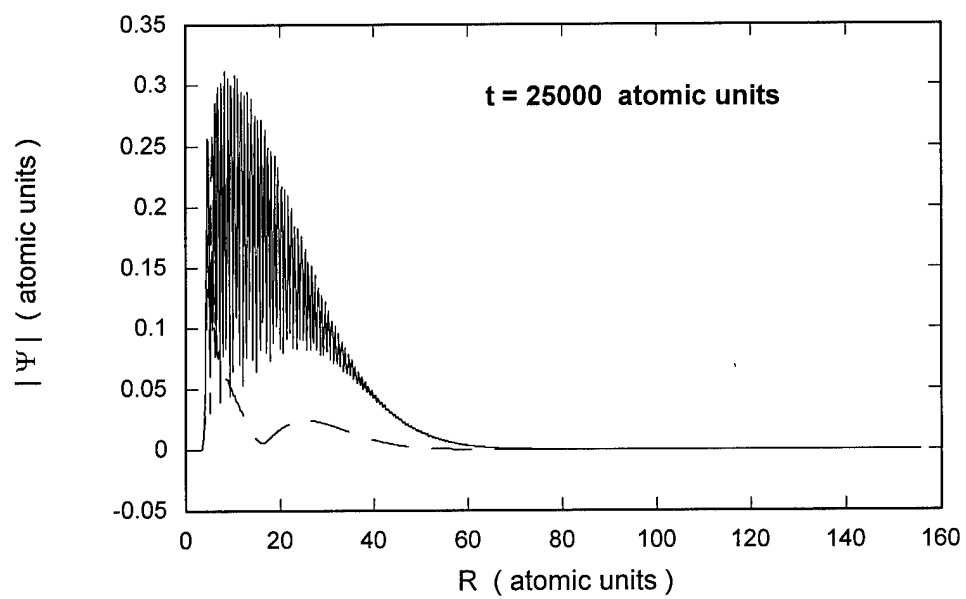
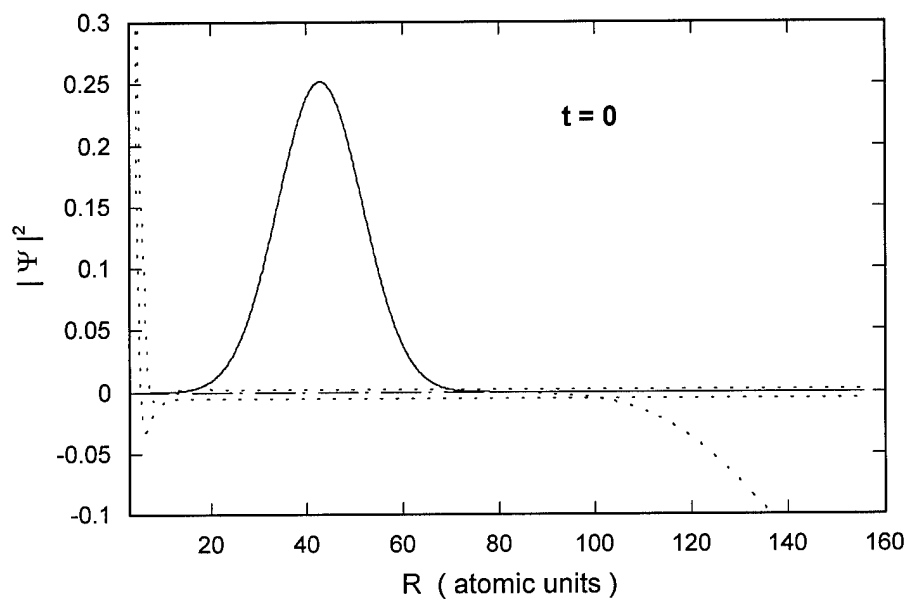
To compute S-matrix elements for the  $B(^2P_{1/2}) \rightarrow B(^2P_{3/2})$  transition in the  $(0)$  basis, we prepare the reactant Møller state, using Eq. ( 5 ), from an initial state  $(t = 0)$  on the lower  $(j_a = 1/2, j = 0, \text{ labeled } ^2P_{1/2})$  surface and the product Møller state from an initial state on the upper  $(^2P_{3/2})$  surface. The initial states are Gaussian wave packets entering (reactants) or leaving (products) the interaction region. Table 5 lists the parameters used to define the initial states. The initial momentum and momentum uncertainty of the wave packet are chosen so that the wave packet possesses a broad negative (positive) range of plane wave components for the reactants (products), but with no appreciable positive momentum (for the reactants) or negative momentum (for the products). As stated in Section II, this is required for Eq. ( 7 ) to be applicable. The energy range is also chosen so that no plane wave components penetrate the barrier for small  $R$  in the potential.

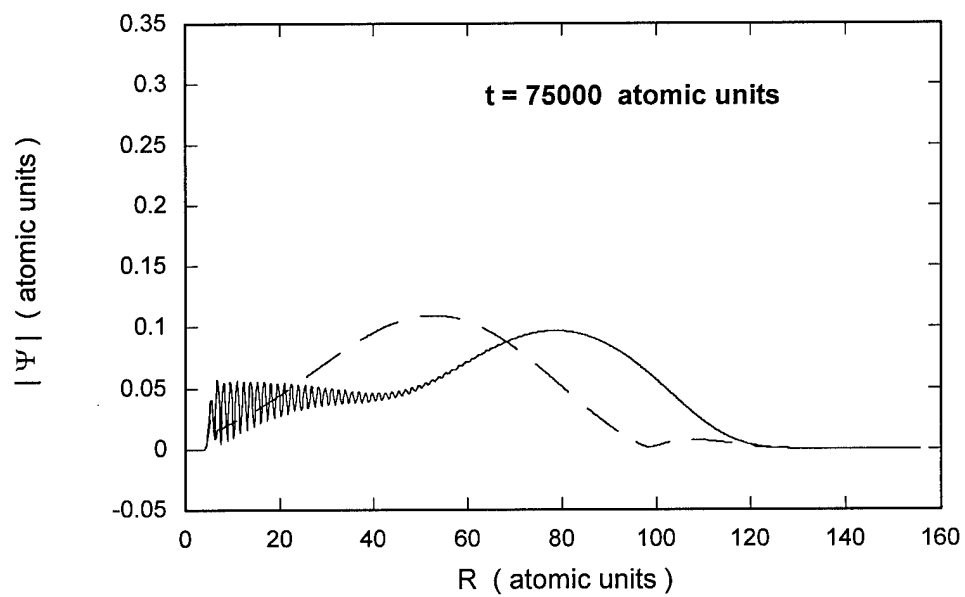
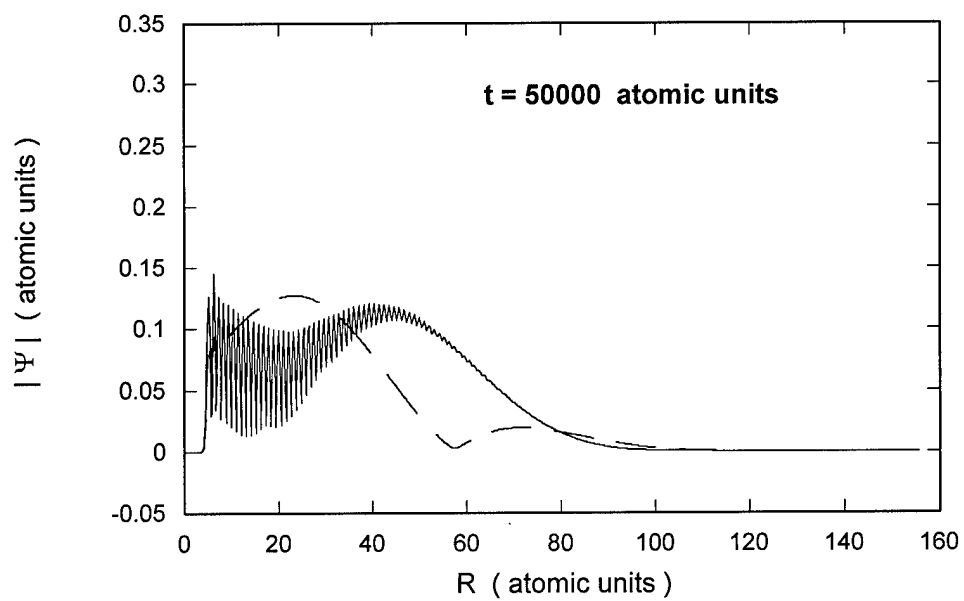
Table 5. Channel Packet Parameters

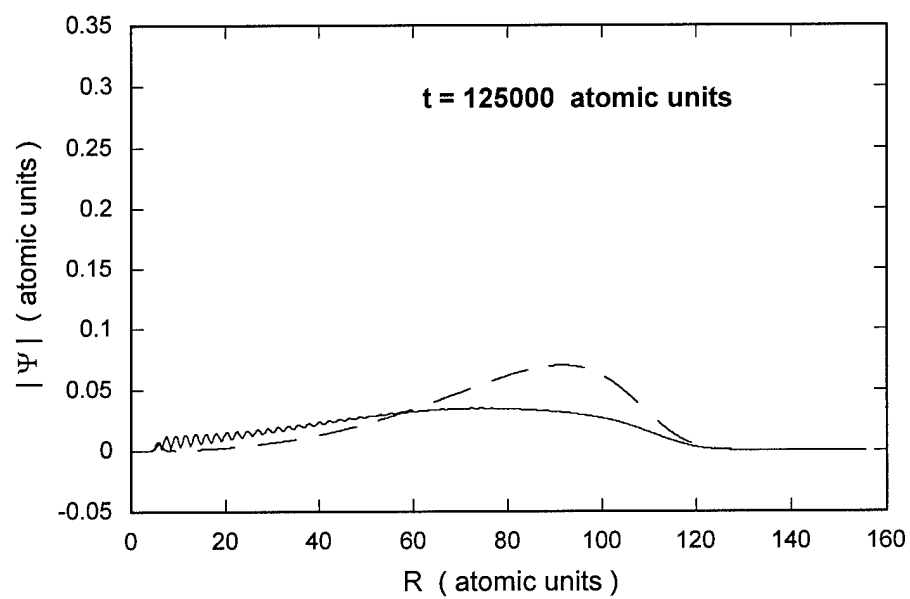
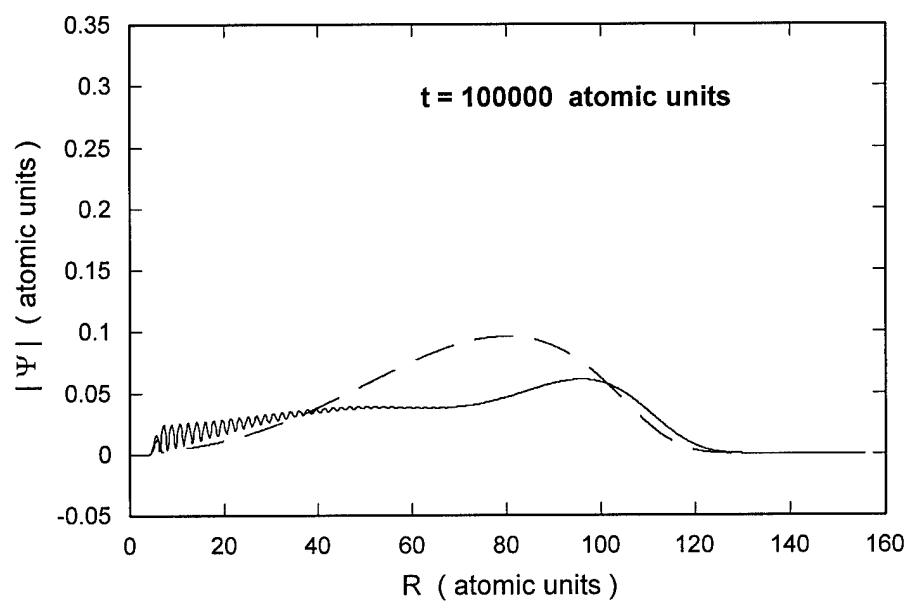
<u>Parameter</u>	<u>Value (atomic units)</u>
Reactant initial average momentum	-4.0
Product initial average momentum	+4.0
Reactant, product initial position	75.0
Reactant, product initial position uncertainty	0.65
Correlation function time range	[ 0 , $6.25 \times 10^6$ ]
Coordinate grid spacing $\Delta x$	0.15
Time step $\Delta t$	25.0
ABC parameter $A$	0.0015
ABC parameter $B$	30.0

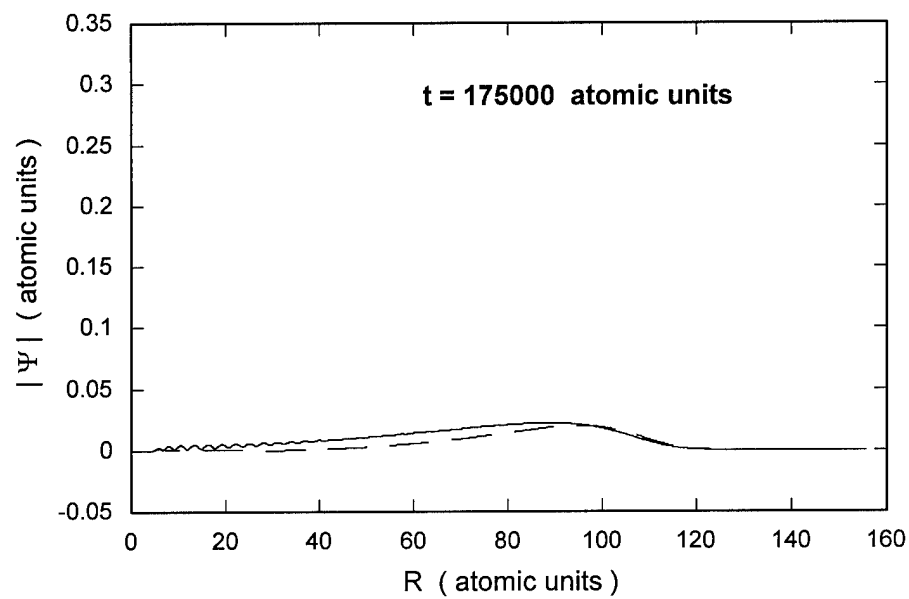
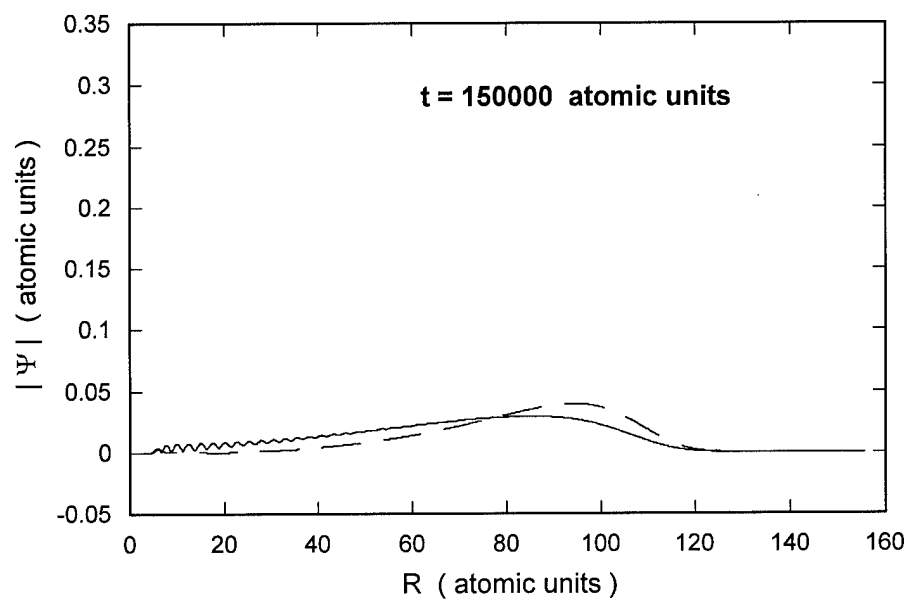
The first frame of Figure 11 shows the reactant Møller state at  $t = 0$ , on the lower surface, together with the adiabatic surfaces and absorbing boundary conditions (dotted). The remaining frames of Figure 11 show the time sequence of the propagation of the reactant Møller state, at intervals of 25,000 atomic units. The wavefunction on the lower surface is shown with a solid line, while the wavefunction on the upper surface is shown with a dashed line.

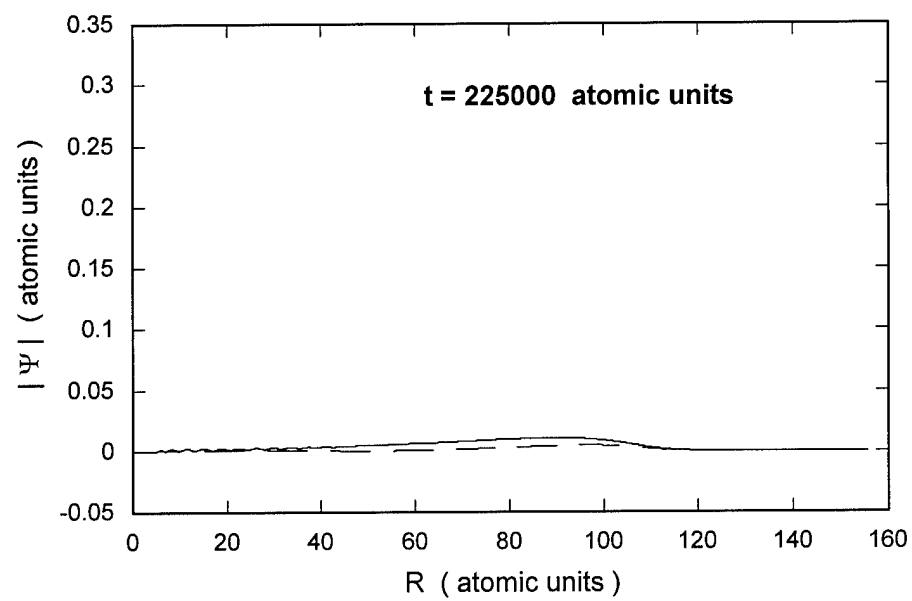
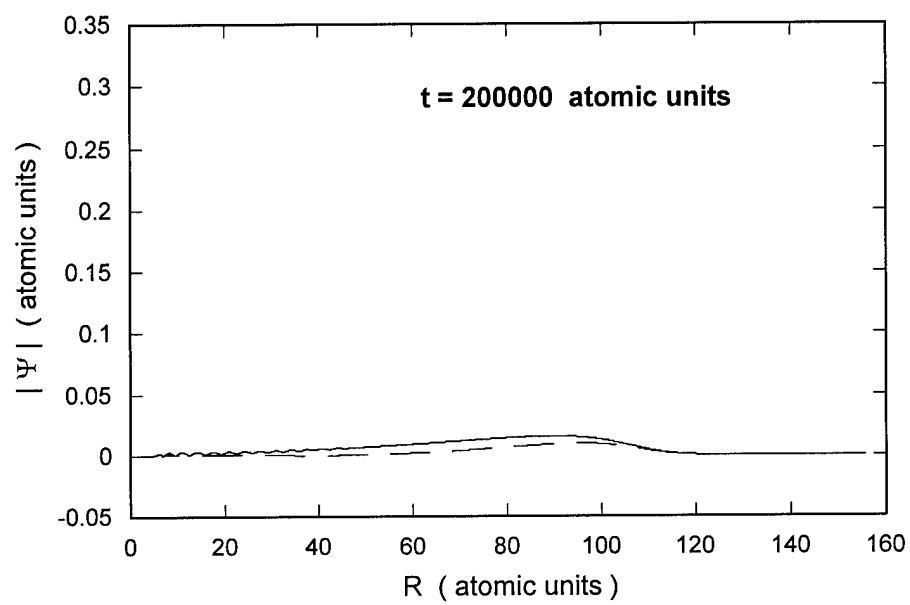


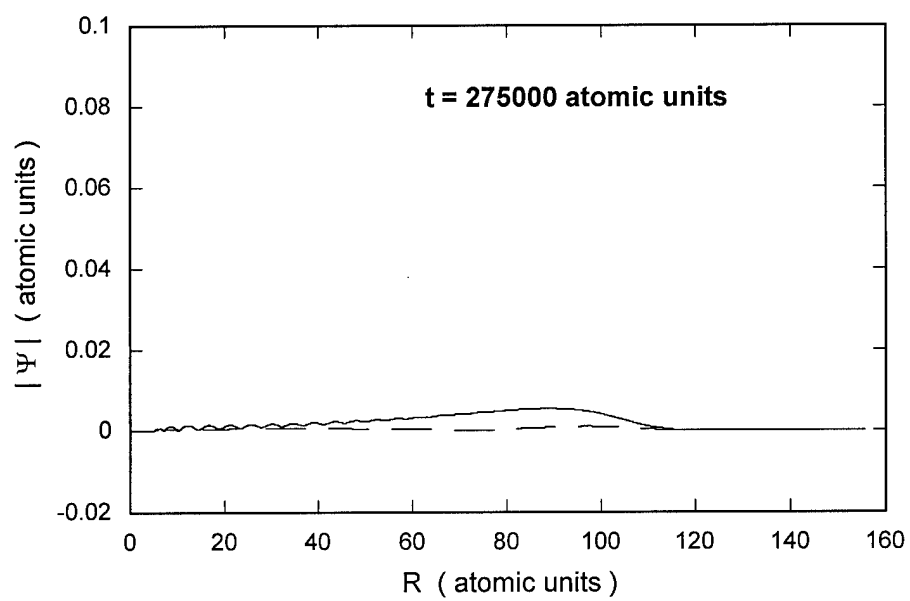
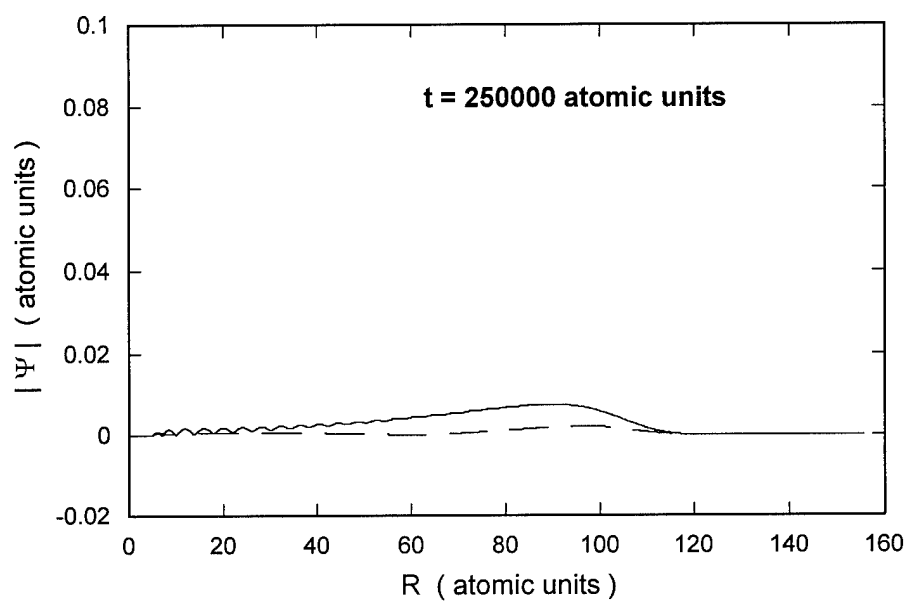












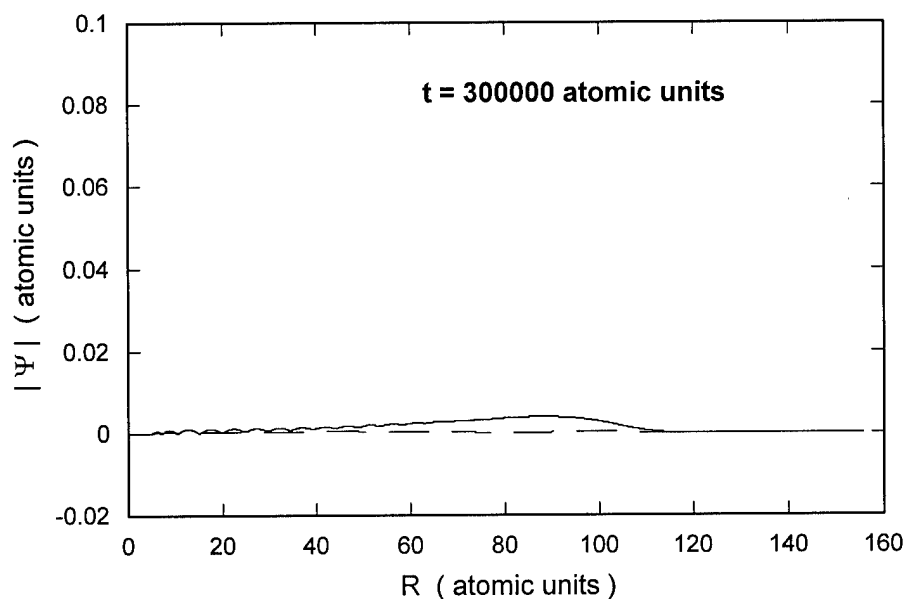


Figure 11. Propagation of reactant Møller state in  $(0)$  basis from  $t = 0$  to  $t = 300,000$  atomic units

The correlation function  $C_{3/2, 1/2}(t)$  in Eq. (6), shown in Figure 12, is computed by holding the product Møller state fixed and propagating the reactant Møller state from  $t = 0$  forward to  $t = 375,000$  atomic units. The numerical limits approximate the true time interval from  $-\infty$  to  $+\infty$ , and are chosen to include the range over which the correlation function is numerically nonzero. (In the  $(0)$  basis the correlation function has already decayed to zero by this time; propagation will only need to proceed to the full  $6.25 \times 10^6$  atomic units when the larger bases are used.) When the reactant Møller state reaches the interaction region, some of it begins to couple onto the other surface, reflect off the barrier, and overlap the product Møller state, resulting in a nonzero correlation. The

absorbing boundary conditions prevent the evolving Møller state from reflecting from the grid boundary after it has passed through the fixed product Møller state. The value of the correlation function is not affected by the attenuation of the evolving reactant Møller state in the area of the ABC, where it does not overlap the fixed product Møller state.

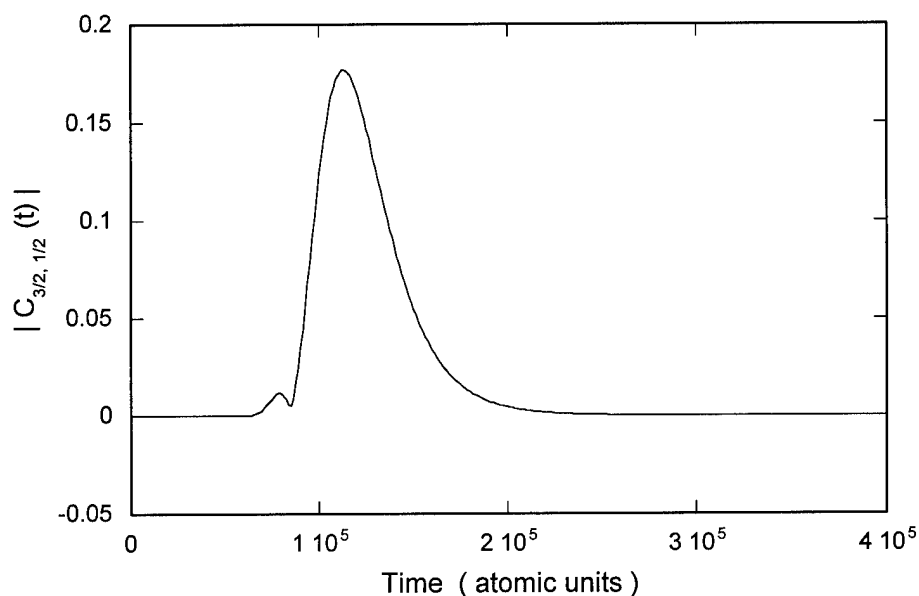


Figure 12. Correlation function  $C_{3/2,1/2}(t)$

The Fourier transform of the correlation function, shown in Figure 13, is used in Eq. ( 7 ) to compute S-matrix elements. Also required are the momentum space expansion coefficients  $\eta$ , which are evaluated implicitly as a function of energy using Eq. ( 8 ), and shown in Figure 14.



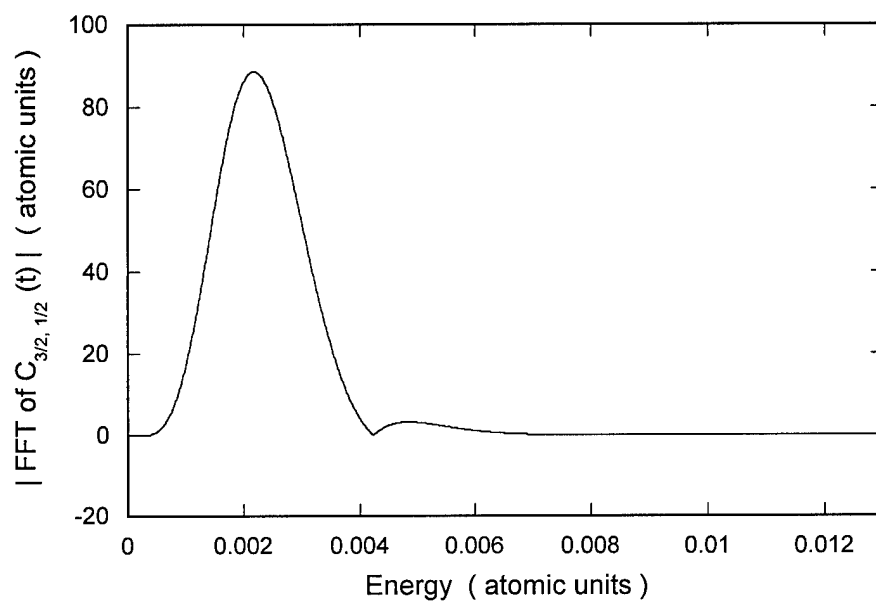


Figure 13. Fourier transform of  $C_{3/2,1/2}(t)$

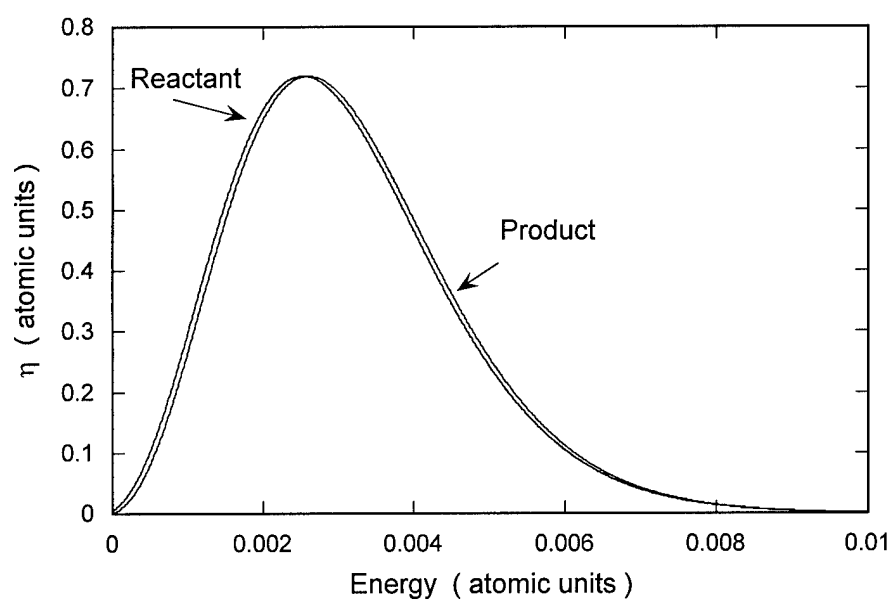


Figure 14. Expansion coefficients  $\eta$  of initial reactant and product wave packets

The absolute value squared  $|S|^2$  gives the probability  $P^{3/2, 1/2}$  for the  $^2P_{1/2} \rightarrow ^2P_{3/2}$  transition, and is shown in Figure 15. The transition probability exhibits an oscillatory dependence on energy. This is similar to the results of a previous study of transition probabilities between two surfaces using a close coupled method [13], in which there is evidence of an oscillatory dependence in the result as a function of the (discrete) energies presented. The low energy portion roughly matches the shape of the results of Flower and Launay for fine structure transitions in collisions of  $C^+ + H_2$  [4], who constrained p- $H_2$  to the  $j = 0, 2$  rotational levels in the calculation. In the higher energy range, higher rotational levels will be open to excitation, which requires the use of the larger  $(0, 2)$  and  $(0, 2, 4)$  basis sets.

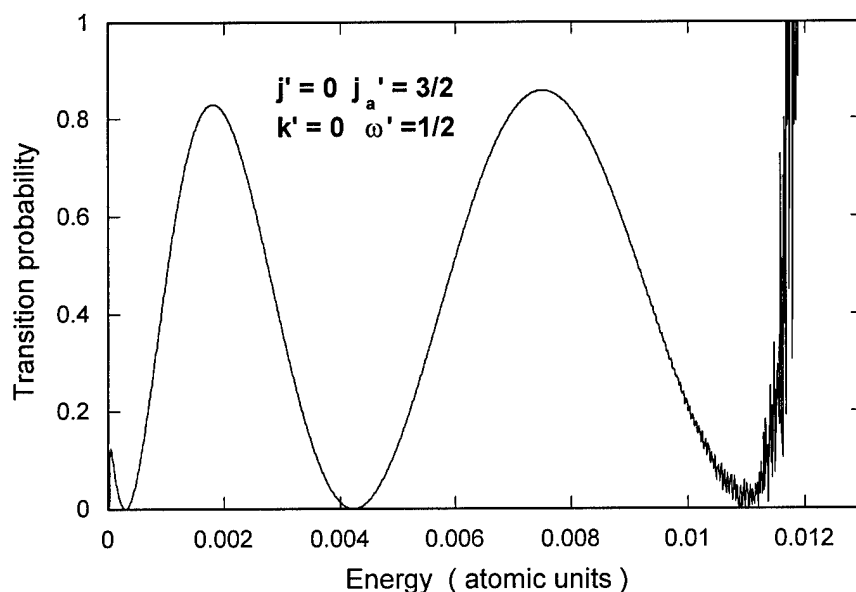


Figure 15. Probability  $P^{3/2, 1/2}$  of transition

To compute the probability for no transition from the lower state ( $^2P_{1/2} \rightarrow ^2P_{1/2}$ ) the product Møller state is prepared on the lower surface rather than the upper surface. Over the numerically valid energy range where the initial reactant and product wave packets have nonzero expansion coefficients  $\eta(k[E])$ , the sum of the transition probabilities for the reactions starting on the upper surface is close to unity. The significant spikes at the ends mark the end of the energy range for which the expansion coefficients are significantly nonzero. There is a small overall error due to the fact that the initial states can never be truly numerically placed in the asymptotic limit, which slightly modifies the true values of the expansion coefficients.

The threshold energy for a transition from the lower state to the upper state depends on the energy gap between the states and the behavior of the coupling. The B spin-orbit splitting is small ( $7.31 \times 10^{-5}$  atomic units) on the energy scale shown, and the numerical results are in question in this region. For the reverse transition, the reactants are prepared on the upper ( $^2P_{3/2}$ ) surface and the products on the lower ( $^2P_{3/2}$ ) surface. The probability  $P^{1/2, 3/2}$  obtained in this calculation is not identical to  $P^{3/2, 1/2}$ , that of the reverse reaction, due to the small excitation threshold.

As mentioned in Section IV, a test for the validity of the S-matrix element calculation is to examine the case of "uncoupled" surfaces where the off-diagonal terms in the diabatic potential are set to zero. In this case, the probability obtained from the S-matrix elements for reflection from a given surface to itself should be unity, over the valid energy range, (the range over which the  $\eta$  coefficients are numerically significant).

Figure 16 shows this for initial states on the lower surface. Here the valid energy range extends up to energies of about 0.01 atomic units.

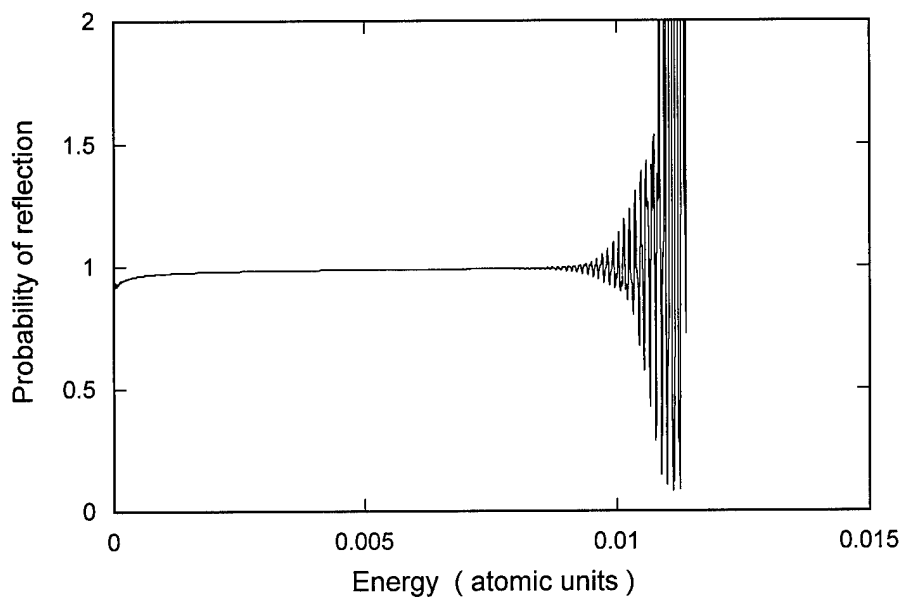


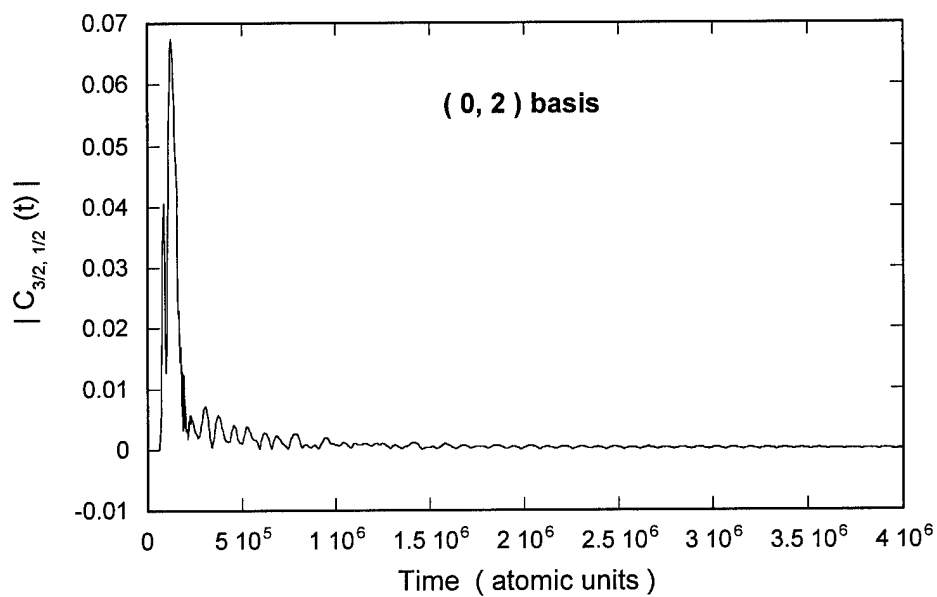
Figure 16. Probability of reflection  $P^{1/2,1/2}$  in the uncoupled case

#### Application to Larger Basis Sets

The ( 0, 2 ) and ( 0, 2, 4 ) basis sets in the CS approximation have sizes of 8 and 14 basis vectors respectively ( Table 4 ). The reactant wave packet is propagated in the same manner as in the previous discussion, with the same initial parameters ( Table 5 ), but the wavefunction is now an 8 or 14 element column vector, and the possibility of coupling to the higher rotational states is included. The correlation functions are

evaluated between the evolving reactant Møller state on the lowest surface and all 8 or 14 possible fixed product Møller states.

A significant difference that is initially observed between these cases and the  $(0)$  basis is that the correlation functions  $C_{3/2, 1/2}$  and  $C_{1/2, 1/2}$  computed in these bases are significantly longer lived than those computed in the  $(0)$  basis, and require evaluation to  $6.25 \times 10^6$  atomic units. Shown in Figure 17 are the correlation functions  $C_{3/2, 1/2}$  where the basis is  $(0, 2)$  and  $(0, 2, 4)$  (compare to Figure 12).



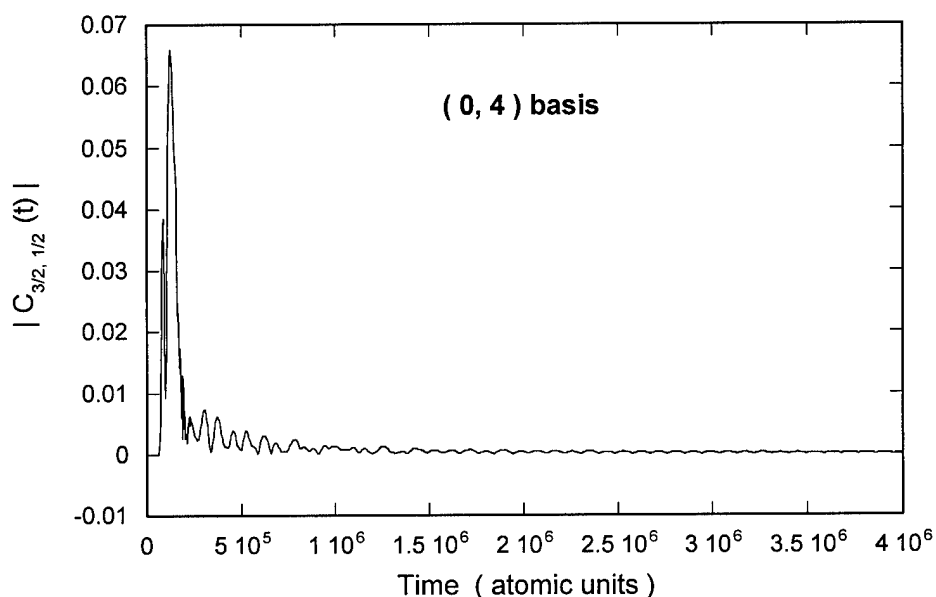
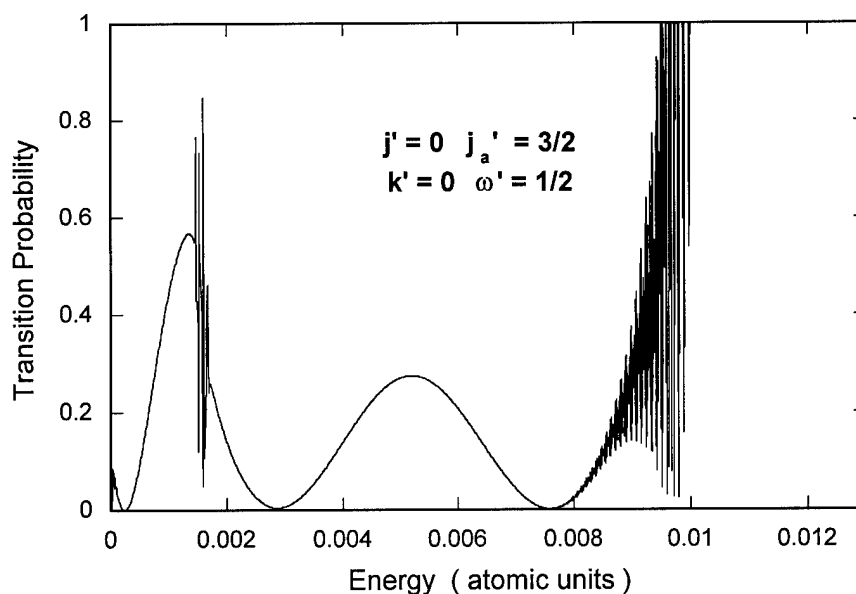


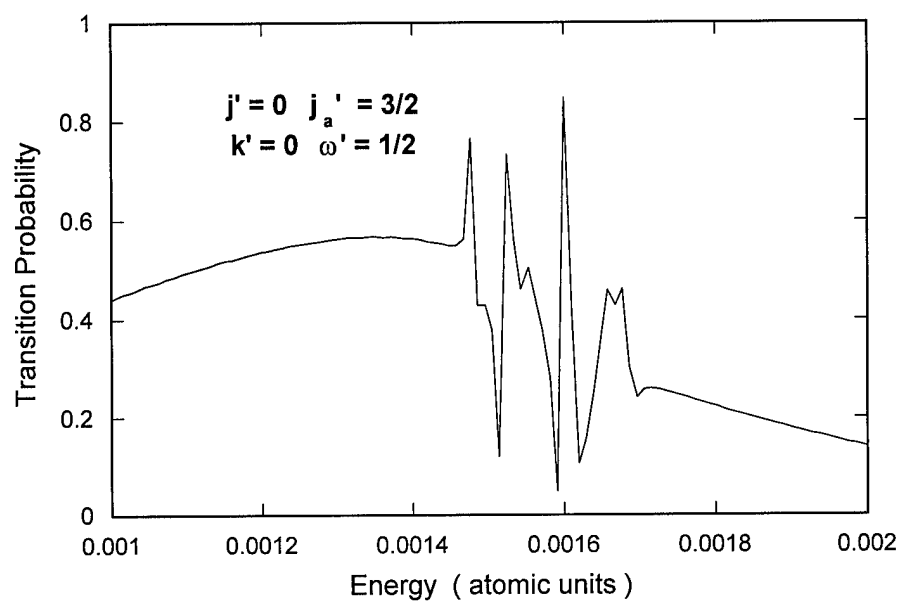
Figure 17. Correlation function  $C_{3/2, 1/2}(t)$  in the  $(0, 2)$  and  $(0, 2, 4)$  bases

The long-lived quality of these correlation functions contributes to very sharp features in their Fourier transforms, and thus in the corresponding S-matrix elements, shown in Figure 18. These features are noticeable primarily in the energy range just below the threshold for the  $j = 0 \rightarrow j = 2$  rotational transition. The reason the correlation functions last for much longer is that wave packet components that have almost enough energy to make the  $0 \rightarrow 2$  or  $0 \rightarrow 4$  transition in the asymptotic limit will actually have sufficient energy in the interaction region, where the gap is smaller due to the potential anisotropy. Hence quasi-bound states can be formed in the wells of the rotationally excited potential

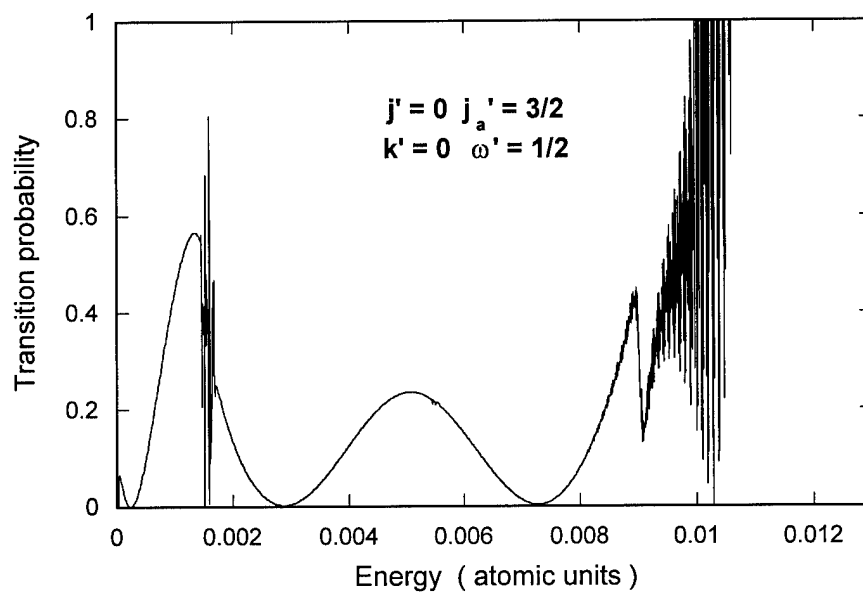
energy surfaces. These states are never fully bound; there is always enough energy to escape the well, but it may take a very long time to couple back to the lower surface. During this long calculation, it is essential that the absorbing boundary conditions cause absolutely negligible reflection or the long tail of the correlation function will be corrupted by contributions from reflections by ABC. To test for this, the calculation was done several times, with different values for the ABC parameters. The sharp features remained the same; additionally, the fact that the sharp features add to unity over most of their range provides confirmation that ABC reflections are negligible.



(a) ( 0, 2 ) basis

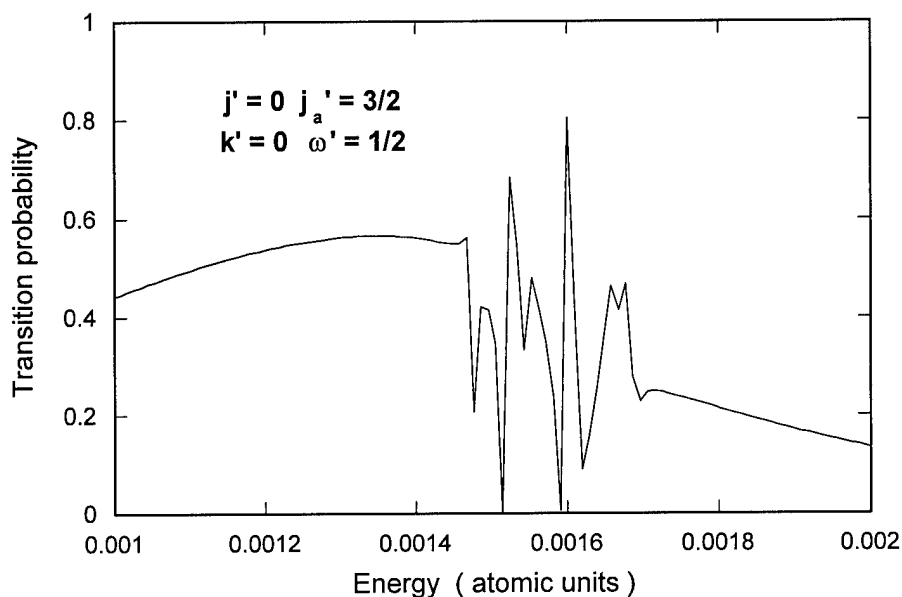


(b)  $(0, 2)$  basis magnified to show sharp features



(c)  $(0, 2, 4)$  basis





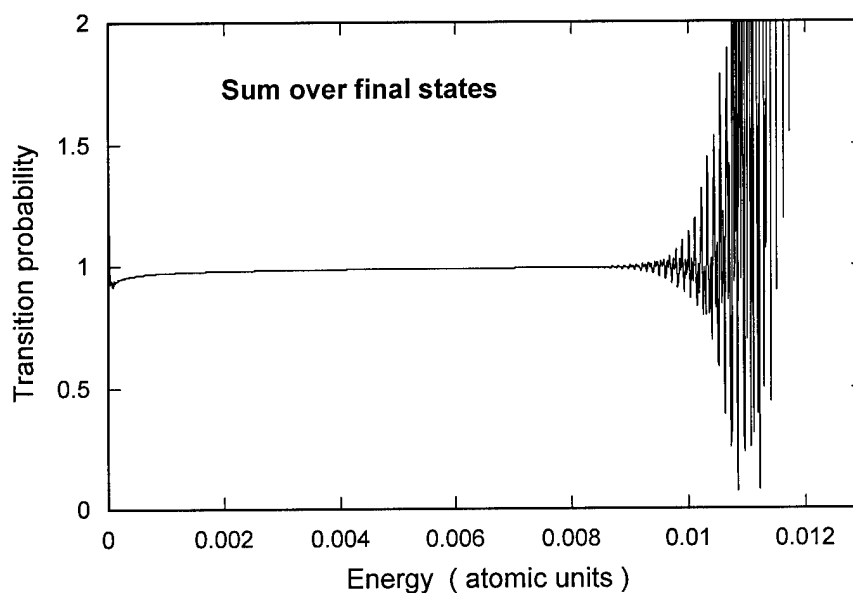
(d)  $(0, 2, 4)$  basis magnified to show sharp features

Figure 18. Probabilities of transition  $P^{3/2, 1/2}$  for the  $(0, 2)$  and  $(0, 2, 4)$  bases

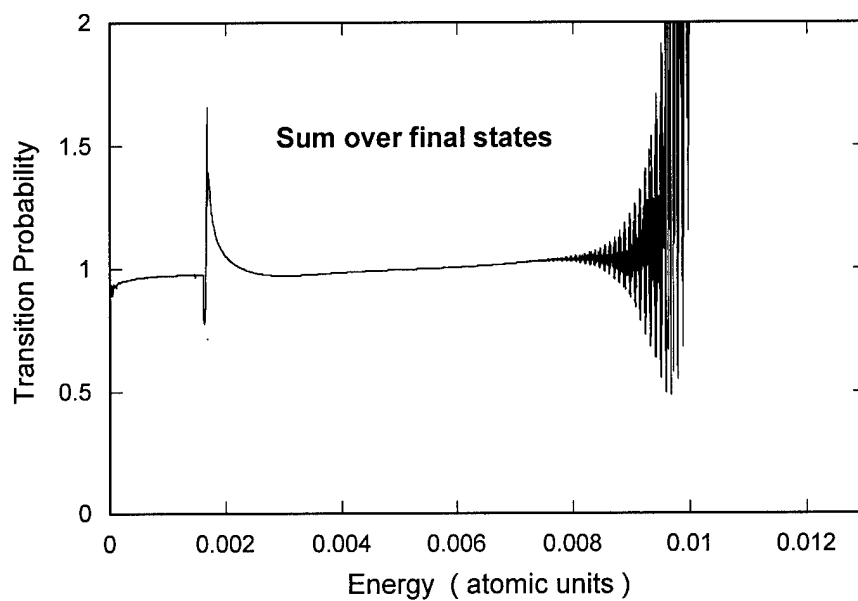
We tabulate the transition probabilities for the reactants starting in the ground state ( $B^2P_{1/2}$  and  $j = 0$ ) to the available product states, for each of the  $(0)$ ,  $(0, 2)$ , and  $(0, 2, 4)$  bases. Thus there are 2, 8, and 14 transition probabilities respectively. In Figure 19, we show the sum over all possible final state transition probabilities starting from the given initial state (the ground asymptotic state). Shown in Figure 20 are the expansion coefficients  $\eta$  of the initial reactant and product wave packets where the reactants are prepared in the ground state and the products are prepared in the third basis state in Eq. (40):  $(j = 2, j_a = 3/2, k = 2, \omega = -3/2)$ . The deviations from unity arise in the regions in which at least one of the  $\eta$  expansion coefficients that contributes to an

S-matrix element in the sum is small, and from the fact that the expansion coefficients may not truly represent the wave packet if it is defined too close to the interaction region. This latter problem can only be reduced by using larger and larger grids. The transition probabilities for final states with  $j = 2$  and  $j = 4$  are small and smaller, respectively, indicating that the results are converging with respect to increasing basis size.

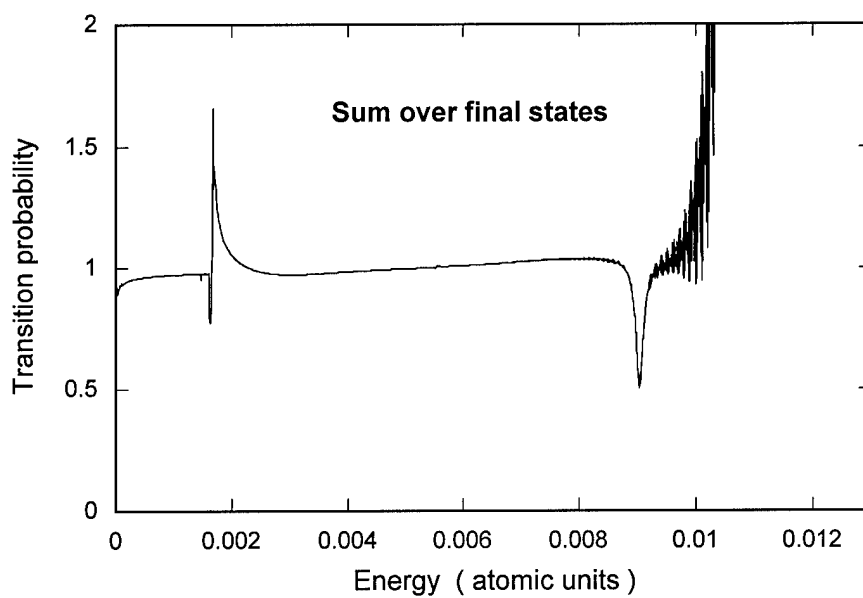
The complete set of transition probabilities from the ground state to the available product states for the three bases are shown in Figure 21, Figure 22, and Figure 23 in the Appendix. The low energy portions for the results in the  $(0, 2)$  and  $(0, 2, 4)$  basis, below the  $j = 0 \rightarrow j = 2$  transition threshold, are similar to the results calculated using the  $(0)$  basis set, but the sharp features are different.



(a)  $(0)$  basis



(b) ( 0, 2 ) basis



(c) ( 0, 2, 4 ) basis

Figure 19. Sum over final transition probabilities for all bases

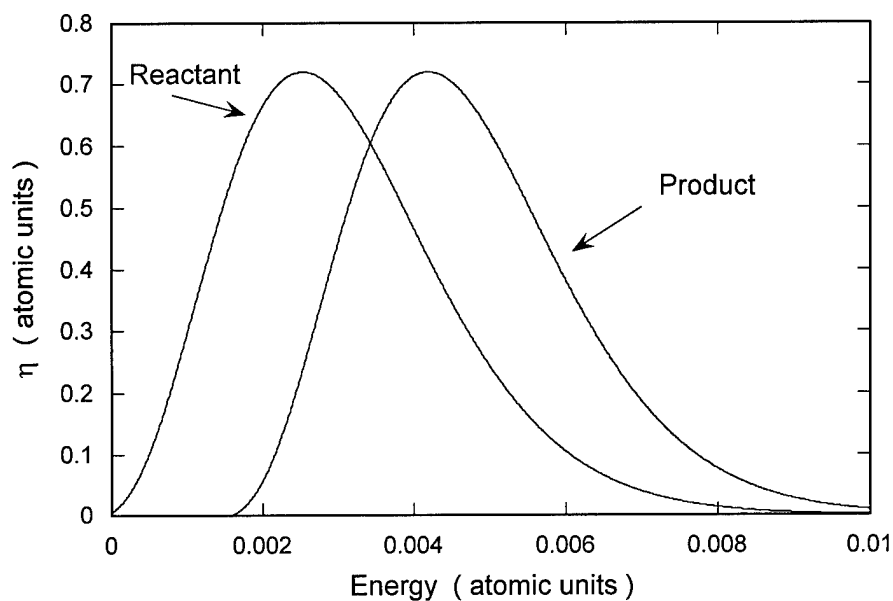


Figure 20. Expansion coefficients  $\eta$  of initial wave packets (product has  $j = 2$ )

### Conclusion

A new application of the time dependent channel packet method to problems involving coupled electronic surfaces has been used to obtain S-matrix elements for the fine structure transition that occurs in collisions of B and  $H_2$ , including the possibility of rotational excitation within the even (*para*) rotational states. The CPM gives us S-matrix elements as a function of the entire energy range of the initial channel packets. The probability of reaction generally has an oscillatory dependence on energy, and for low energy, is similar in form to that of a previous study of  $C^+ + H_2$  [4]. Sharp features show

up in the S-matrix elements when higher rotational states are considered, due to the availability of temporary potential energy for rotational excitation. S-matrix elements for transitions from the ground state to all final states in bases with  $j_{max} = 0, 2, \text{ and } 4$  were tabulated.

Recommendations for future work include a more complete study of S-matrix elements given the framework above, such as considering transitions within the odd (*ortho*) rotational quantum numbers, transitions from initial states other than the ground state, and transitions where the total angular momentum  $J$  is not constrained to  $1/2$ . A complete calculation of the S-matrix elements over the full distribution of states is required to obtain experimentally useful information such as cross sections and reaction rates.

Additionally, one could lift the restriction that  $P$  is conserved, thus ceasing to use the centrifugal sudden approximation, which would dramatically increase the basis size. A further step would be to allow for vibrational motion of the hydrogen molecule, thus adding the extra degree of freedom  $r$  back into the problem. From this point, one could consider the full *reactive* problem  $B + H_2 \leftrightarrow BH + H$ , with the added difficulty of the extra arrangement channels permitted by the reaction. This requires a full treatment of the potential energy surfaces for the reactive problem, as well as significantly more processing power to handle the extra degree of freedom.

## Appendix

This appendix contains the full tabulation of probabilities of transition from the ground state using the three different bases. The ground state has  $j = 0, j_a = 1/2, k = 0$ , and  $\omega = 1/2$ . The probabilities in the  $(0)$  basis, the  $(0, 2)$  basis, and the  $(0, 2, 4)$  basis are displayed in Figure 21, Figure 22, and Figure 23 respectively.

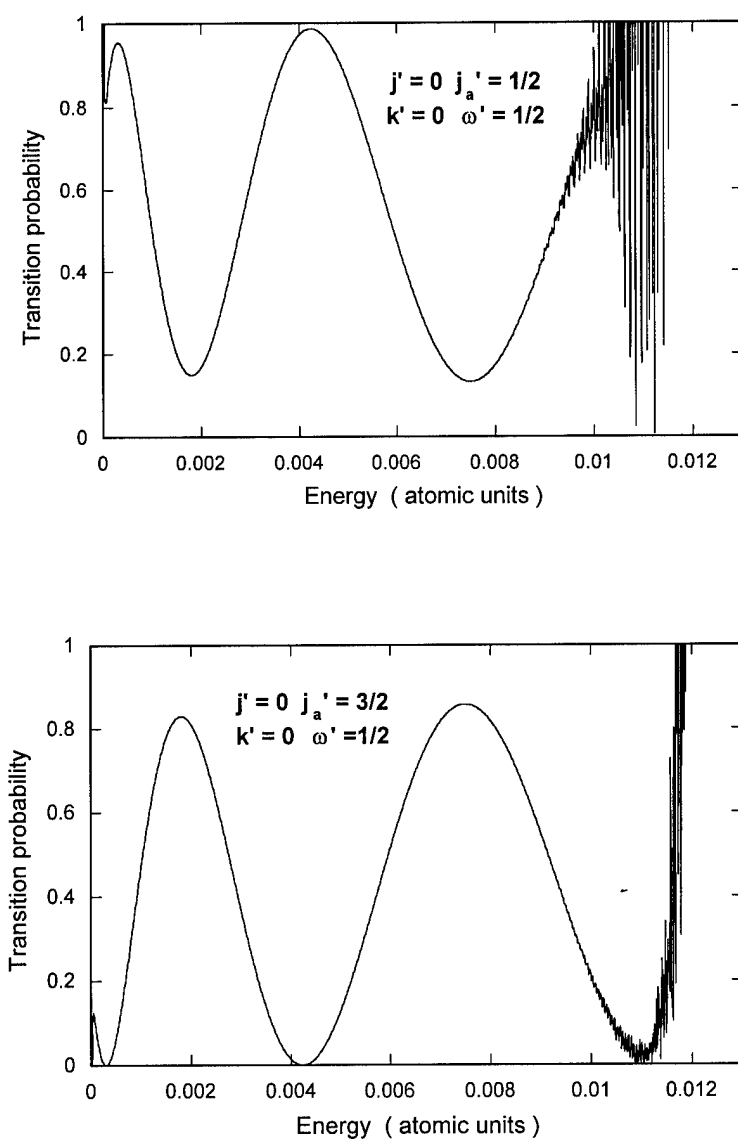
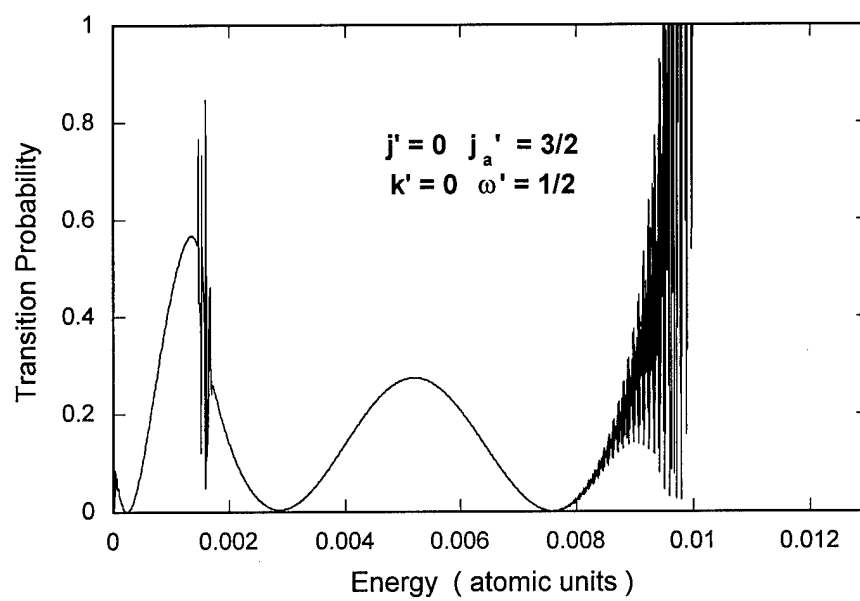
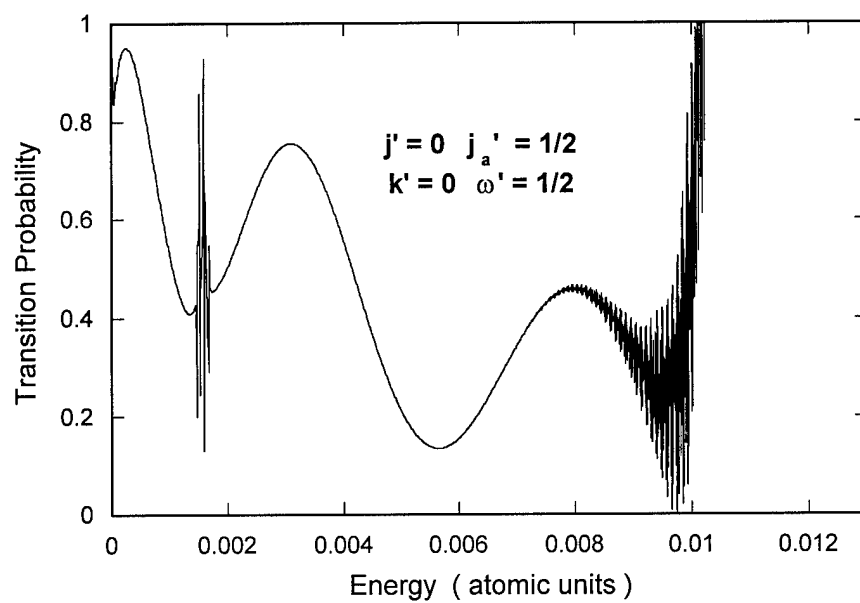
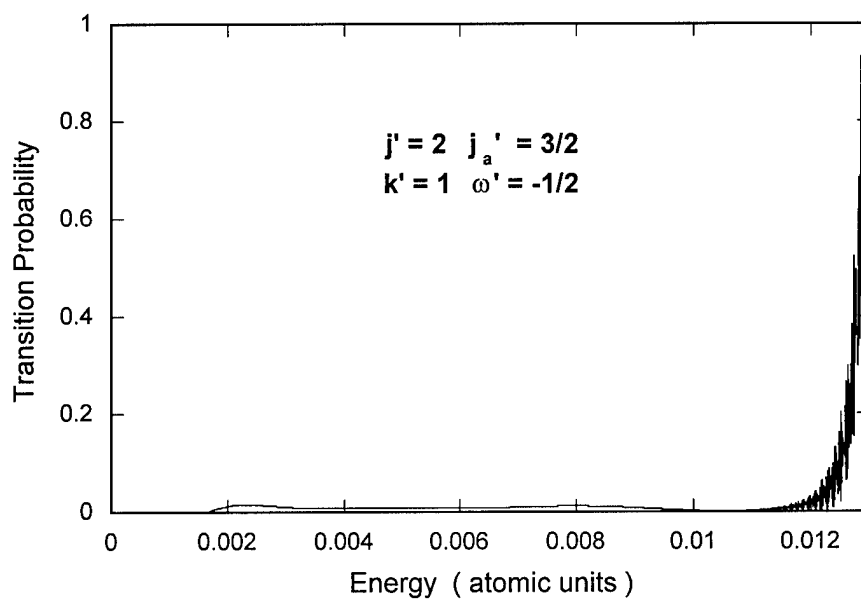
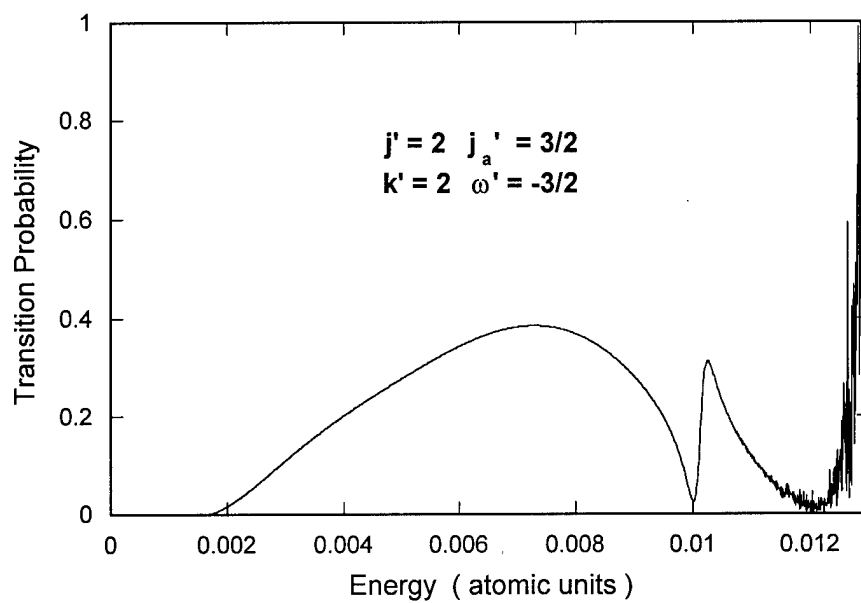
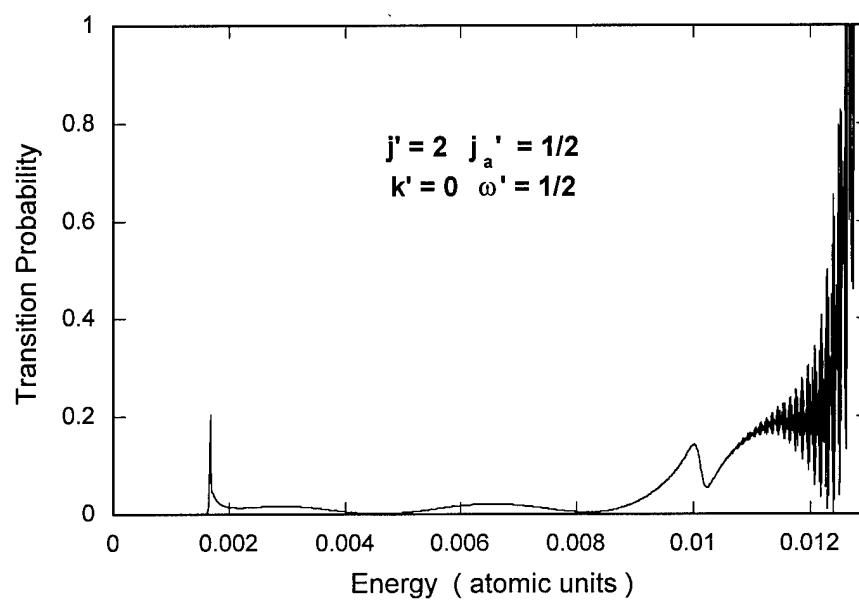
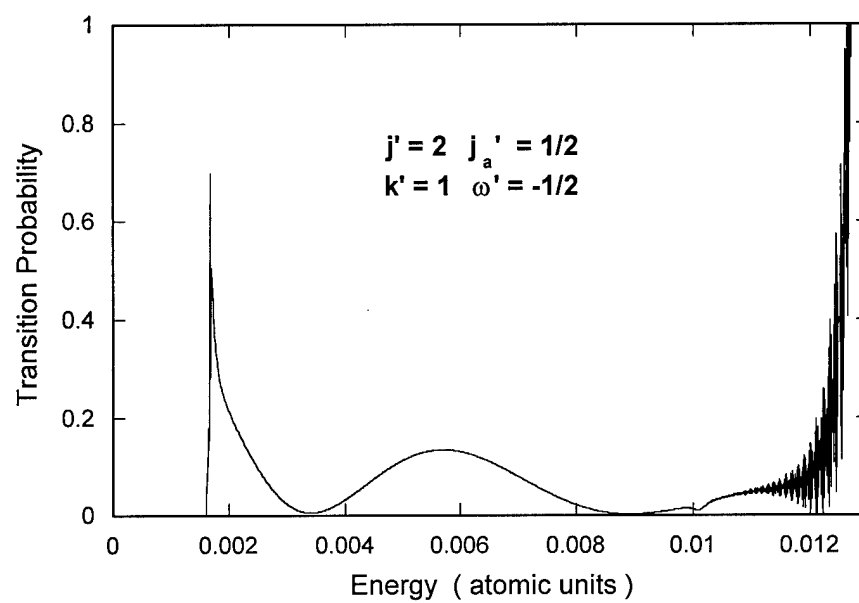


Figure 21. Probabilities of transition from the ground state in the  $(0)$  basis









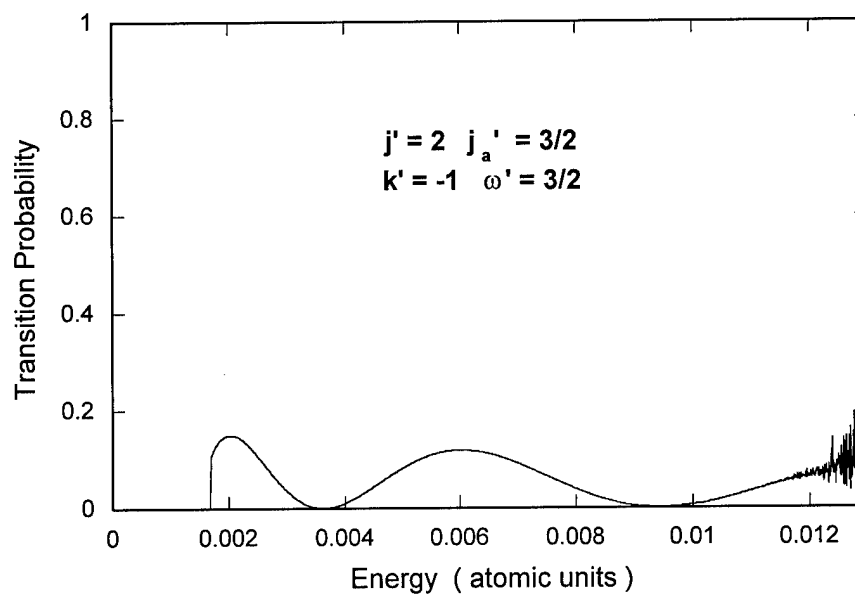
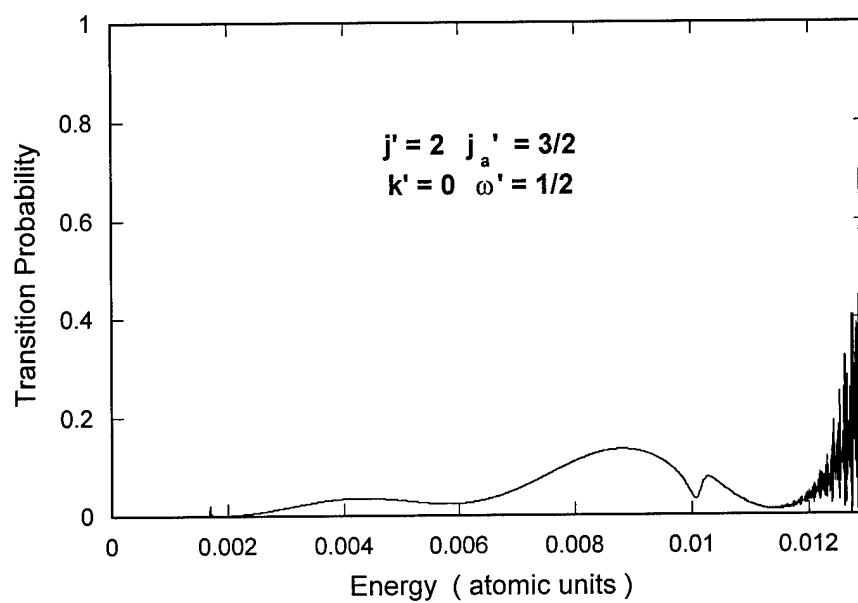
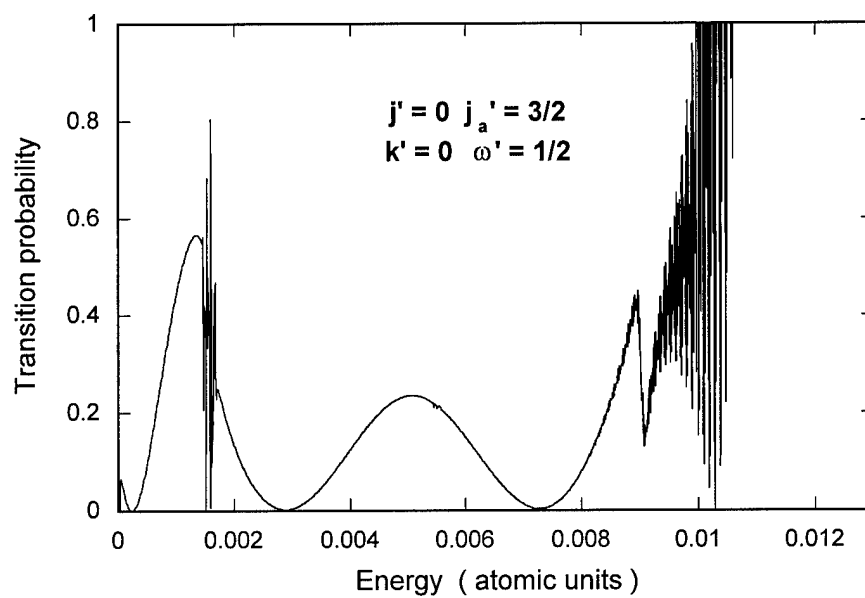
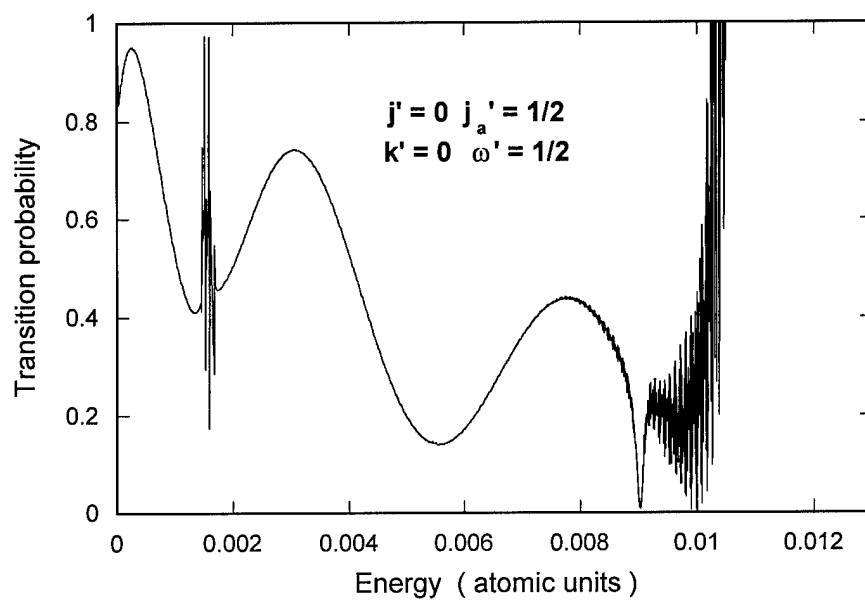
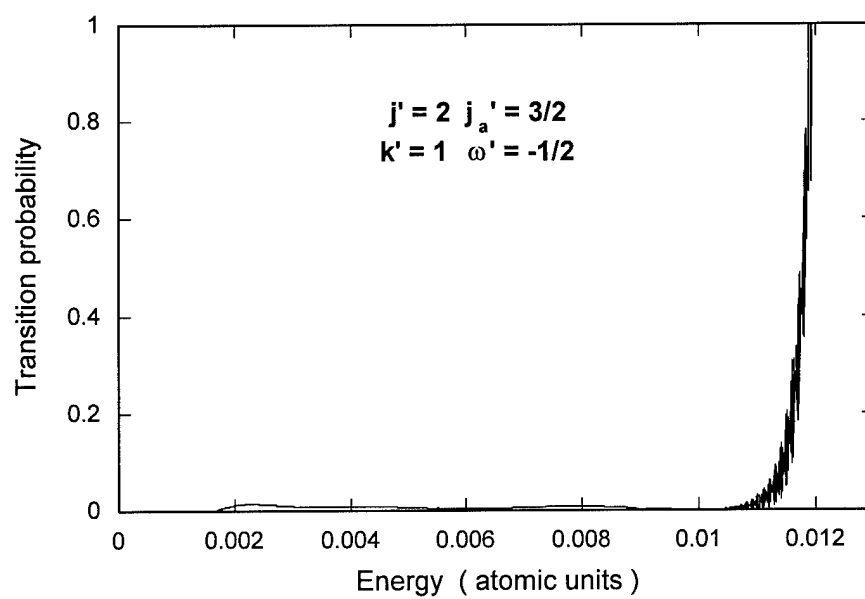
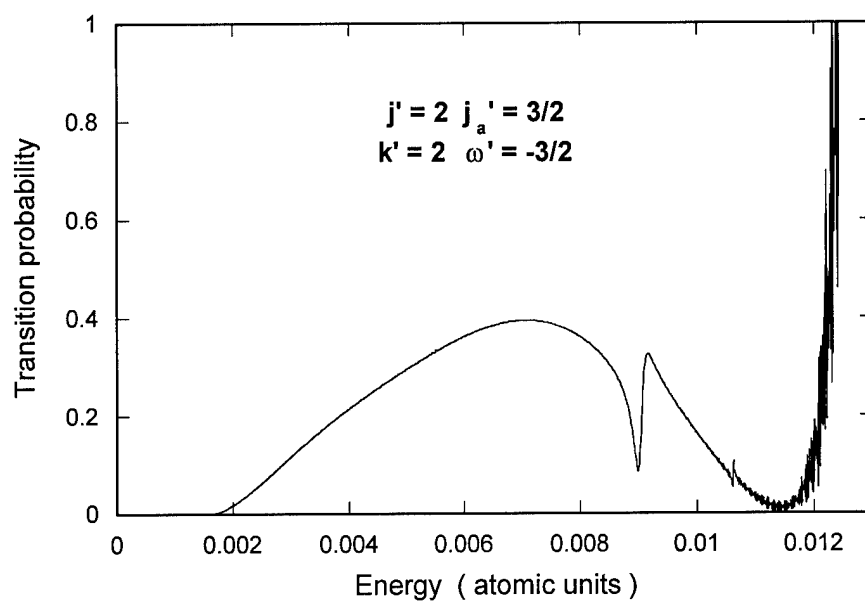
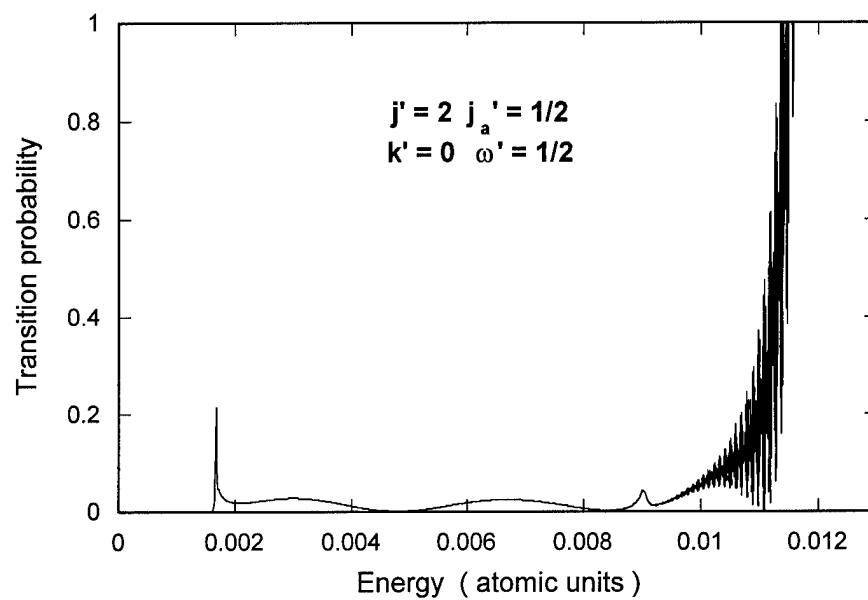
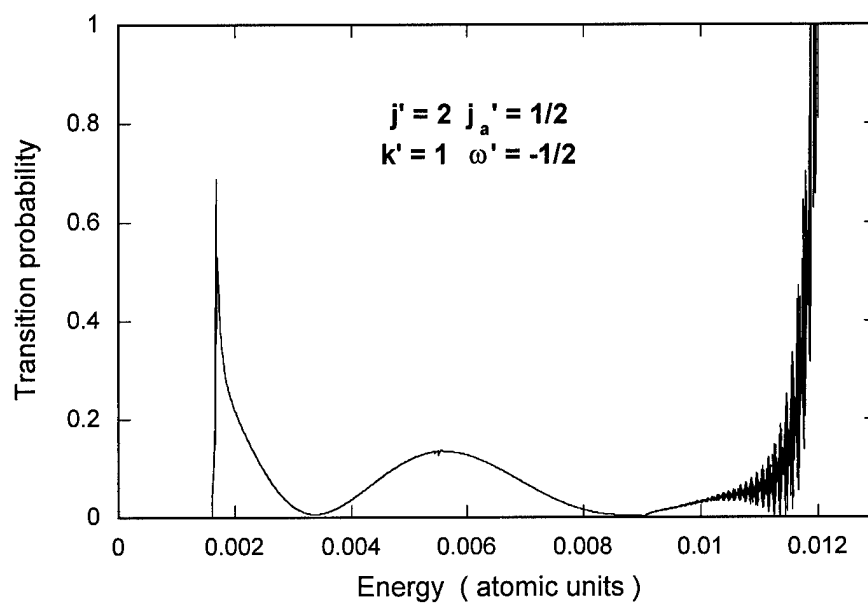
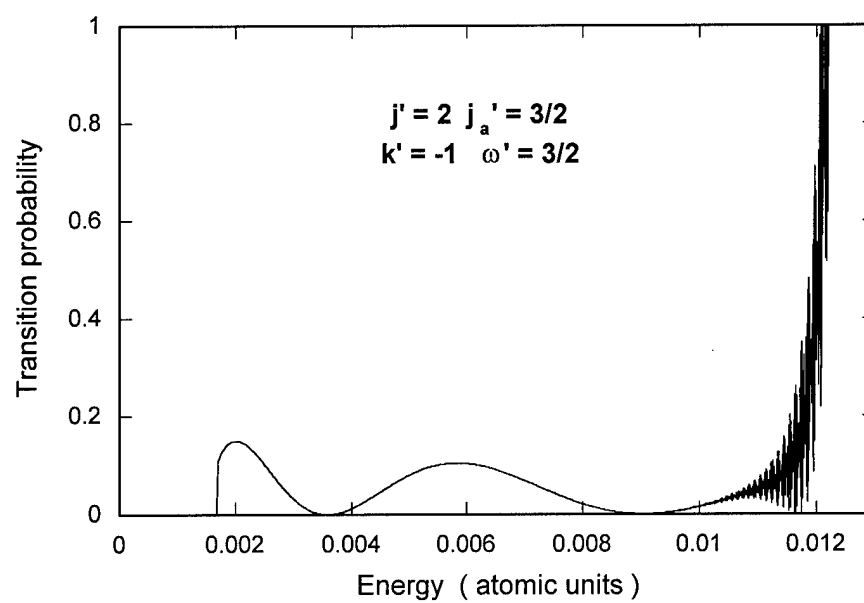
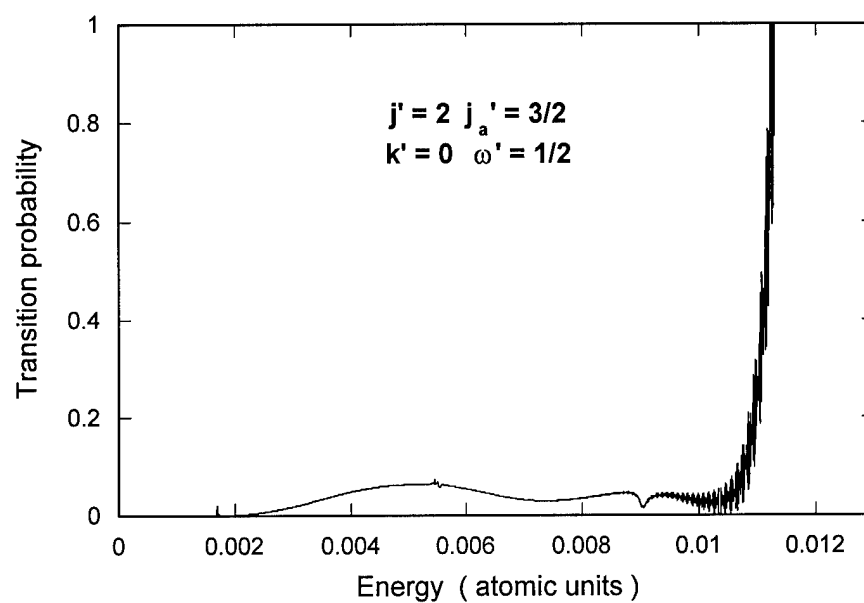


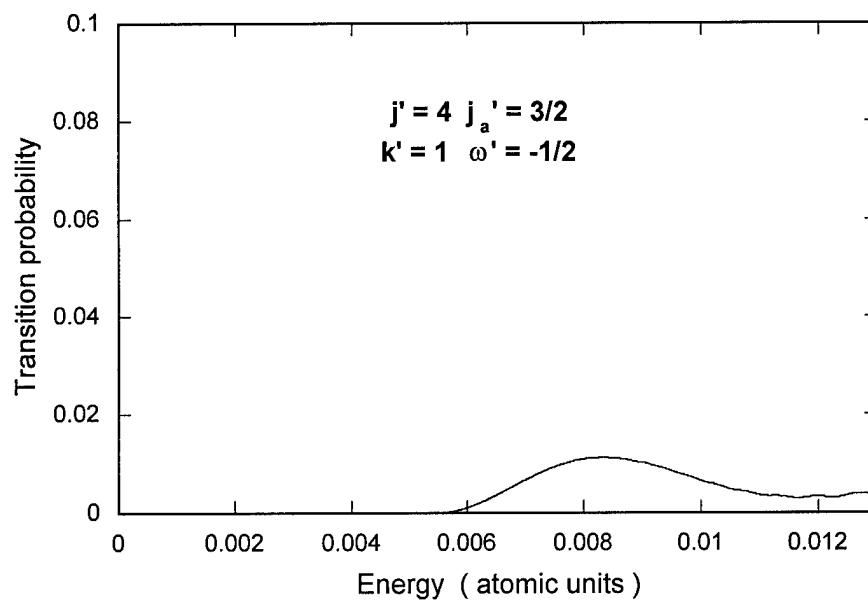
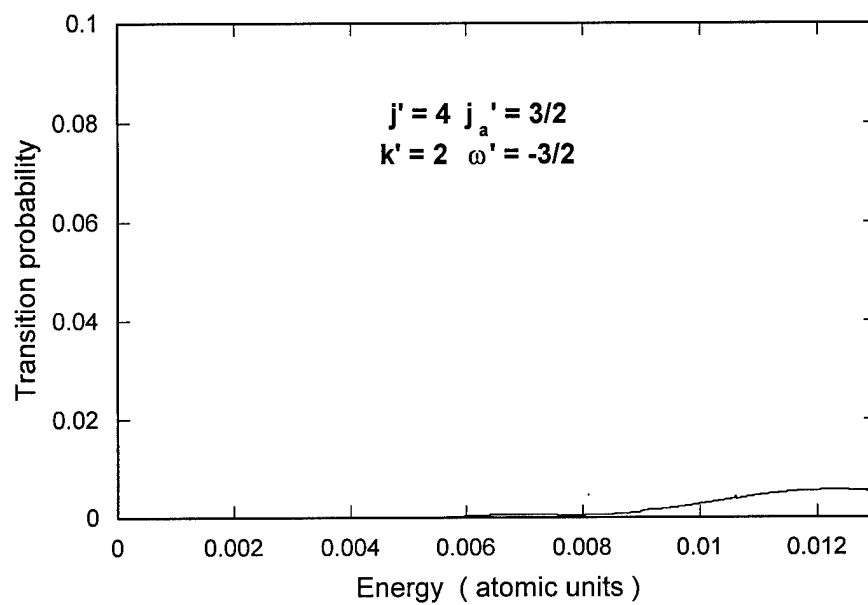
Figure 22. Probabilities of transition from the ground state in the ( 0, 2 ) basis

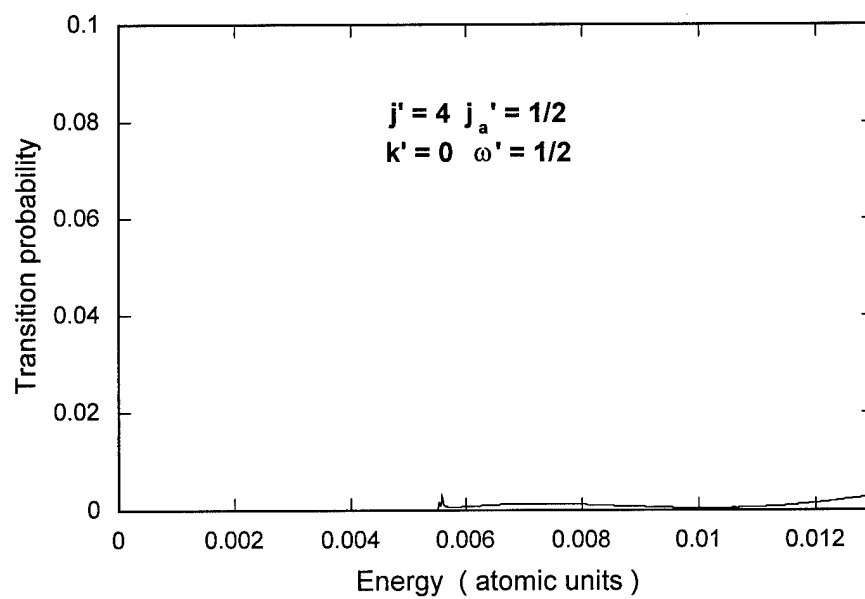
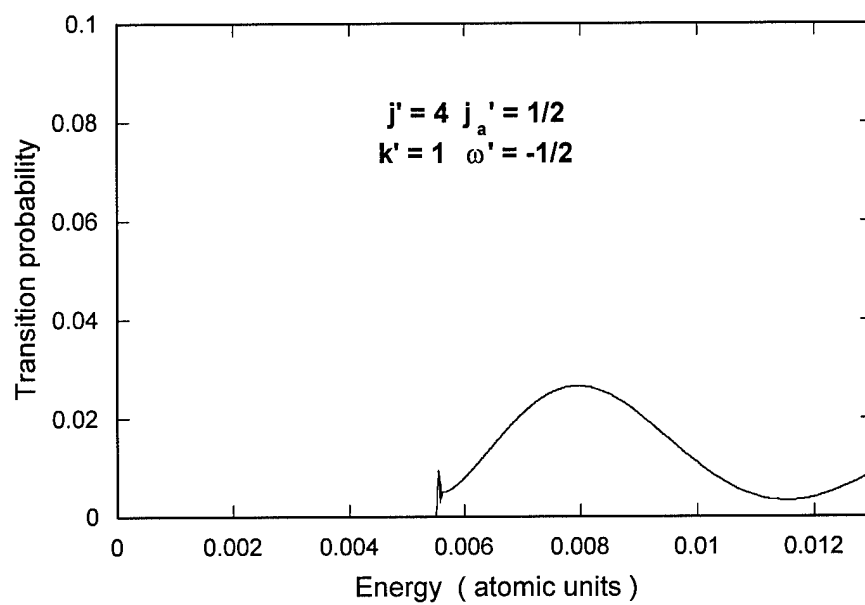














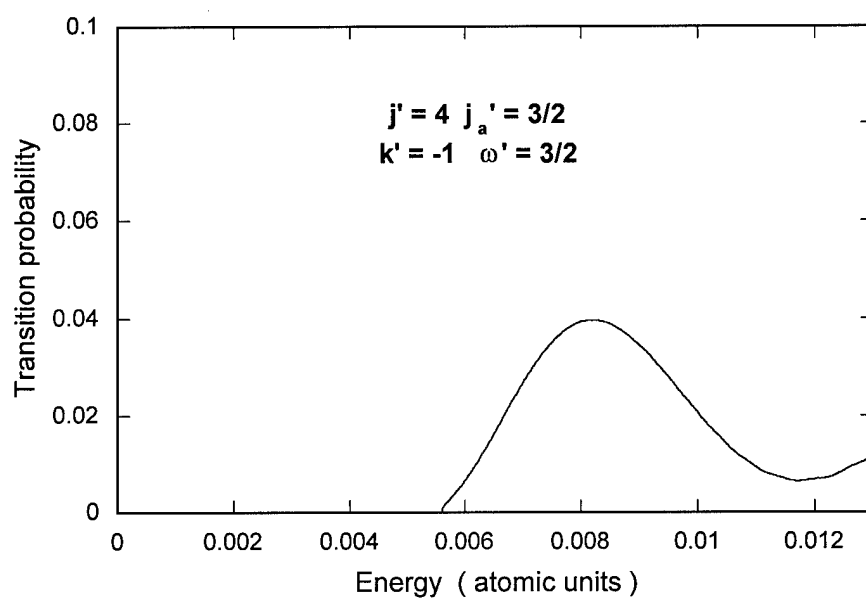
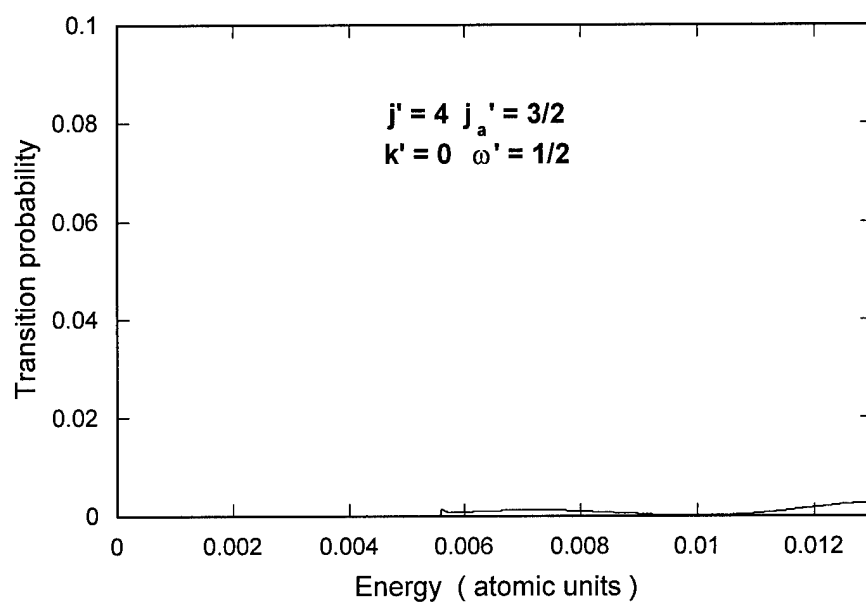


Figure 23. Probabilities of transition from the ground state in the ( 0, 2, 4 ) basis

## Bibliography

1. Fajardo, Mario E., Simon Tam, Timmie L. Thompson, and Michelle E. Cordonnier. "Spectroscopy and reactive dynamics of atoms trapped in molecular hydrogen matrices," *Chemical Physics*, 189: 351-365 (1994)
2. Chu, Shih-I and A. Dalgarno. "Fine structure transitions of  $C^+$  in collisions with  $H_2$ ," *The Journal of Chemical Physics*, 62: 4009-4015 (May 1975)
3. Flower, D.R. and J.M. Launay. "Excitation of the fine-structure transition of  $C^+$  in collisions with molecular hydrogen," *The Journal of Physics B*, 10: L229-L233 (1977)
4. Flower, D.R. and Launay, Jean-Michel. "Molecular collision processes II. Excitation of the fine structure transition of  $C^+$  in collisions with  $H_2$ ," *The Journal of Physics B*, 10: 3673-3081 (1977)
5. Reid, R.H.G. "Transitions among the  $3p^2P$  states of sodium induced by collisions with helium," *The Journal of Physics B*, 6: 2018-2038 (October 1973)
6. Nikitin, E.E. "Nonadiabatic Transitions between Fine-Structure Components of Alkali Atoms upon Collision with Inert-Gas Atoms," *The Journal of Chemical Physics*, 43: 744-750 (July 1965)
7. Rebentrost, Frank and William A. Lester, Jr. "Nonadiabatic effects in the collision of F ( $^2P$ ) with  $H_2$  ( $^1\Sigma_g^+$ ): I. SCF interaction potentials for the  $1^2A'$ ,  $2^2A'$ , and  $^2A'$  states in the reactant region," *The Journal of Chemical Physics*, 63: 3737-3740 (November 1975)
8. Rebentrost, Frank and William A. Lester, Jr. "Nonadiabatic effects in the collision of F ( $^2P$ ) with  $H_2$  ( $^1\Sigma_g^+$ ): II. Born-Oppenheimer and angular momentum coupling in adiabatic and diabatic representations," *The Journal of Chemical Physics*, 64: 3879-3884 (May 1976)
9. Rebentrost, Frank and William A. Lester, Jr. "Resonant electronic-to-rotational energy transfer: Quenching of F ( $^2P_{1/2}$ ) by  $H_2$  ( $j=0$ )," *The Journal of Chemical Physics*, 64: 4223-4224 (May 1976)
10. Rebentrost, Frank and William A. Lester, Jr. "Nonadiabatic effects in the collision of F ( $^2P$ ) with  $H_2$  ( $^1\Sigma_g^+$ ): III. Scattering theory and coupled-channel computations," *The Journal of Chemical Physics*, 67: 3367-3375 (October 1977)
11. Bernstein, Richard B. *Atom-Molecule Collision Theory*. New York: Plenum Press, 1979.

12. Levine, Raphael D. and Richard B. Bernstein. *Molecular Reaction Dynamics and Chemical Reactivity*. New York: Oxford University Press, Inc., 1987.
13. Faist, M.B. and R.B. Bernstein. "Computational study of elastic and electronically inelastic scattering of Br by ground state I atoms: Role of potential curve crossing," *The Journal of Chemical Physics*, 64: 2971-2984 (April 1976)
14. Alexander, Millard H. "Adiabatic and approximate diabatic potential surfaces for the B...H<sub>2</sub> van der Waals molecule," *The Journal of Chemical Physics*, 99: 6014-6026 (October 1993)
15. Alexander, Millard H. and Moonbong Yang. "Theoretical investigation of weakly-bound complexes of B with H<sub>2</sub>," *The Journal of Chemical Physics*, 103: 7956-7965 (November 1995)
16. Taylor, J.R. *Scattering Theory: the quantum theory of nonrelativistic collisions*. New York: Krieger, 1987.
17. Weeks, David E. and David J. Tannor. "A time-dependent formulation of the scattering matrix using Møller operators," *Chemical Physics Letters*, 207: 301-308 (May 1993)
18. Tannor, David J. and David E. Weeks. "Wave packet correlation function formulation of scattering theory: The quantum analog of classical S-matrix theory," *The Journal of Chemical Physics*, 98: 3884-3893 (March 1993)
19. Weeks, David E. and David J. Tannor. "A time-dependent formulation of the scattering matrix form the collinear reaction H + H<sub>2</sub> (  $\nu$  )  $\rightarrow$  H<sub>2</sub> (  $\nu'$  ) + H," *Chemical Physics Letters*, 224: 451-458 (July 1994)
20. Jäckle, A. and H.D. Meyer. "Reactive scattering using the multiconfiguration time-dependent Hartree approximation: General aspects and application to the collinear H + H<sub>2</sub>  $\rightarrow$  H<sub>2</sub> + H reaction," *The Journal of Chemical Physics*, 102: 5605-5615 (April 1995)
21. Calfas, R.S. and David E. Weeks. "A new application of absorbing boundary conditions for computing collinear quantum reactive scattering matrix elements," *Chemical Physics Letters*, 263: 292-296 (December 1996)
22. Weeks, David E. and Roy S. Calfas, Air Force Technical Report, in press.
23. Dai, Jiqiong and John Z.H. Zhang. "Time-dependent Wave Packet Approach to State-to-State Reactive Scattering and Application to H + O<sub>2</sub> Reaction," *The Journal of Physical Chemistry*, 100: 6898-6903 (April 1996)
24. S. Garashchuk and D.J. Tannor. *Chemical Physics Letters*, 262: 477 (1996)

25. Bransden, B.H. and C.J. Joachain. *Physics of atoms and molecules*. New York: Longman, 1984, p. 671
26. Lefebvre-Brion, H. and R.W. Field. *Perturbations in the Spectra of Diatomic Molecules*. Orlando: Academic Press, 1986.
27. Moore, C.E. "Atomic Energy Levels," NSRDS-NBS 35. Washington DC: U.S. GPO, 1971.
28. Smith, Felix T. "Diabatic and Adiabatic Representations for Atomic Collision Problems," *Physical Review*, 179: 111-123 (March 1969)
29. Mead, C.Alden and D.G. Truhlar. "Conditions for the definition of a strictly diabatic electronic basis for molecular systems," *The Journal of Chemical Physics*, 77: 6090-6098 (December 1982)
30. Ruedenberg, Klaus and Gregory J. Atchity. "A quantum chemical determination of diabatic states," *The Journal of Chemical Physics*, 99: 3799-3803 (September 1993)
31. Manaa, M. Riad and David R. Yarkony. "Nonadiabatic perturbations and fine structure splittings in the  $1,2\ ^3P_g$  states of  $B_2$ : An analysis based on adiabatic and rigorous diabatic states," *The Journal of Chemical Physics*, 100: 8204-8211 (June 1994)
32. Gordon, Mark S., Vassiliki-Alexandra Glezakou, and David R. Yarkony. "Systematic location of intersecting seams of conical intersections in triatomic molecules: The  $1^2A' - 2^2A'$  conical intersections in  $BH_2$ ," *The Journal of Chemical Physics*, 108: 5657-3803 (April 1998)
33. Dubernet, Marie-Lise and Jeremy M. Hutson. "Atom-molecule van der Waals complexes containing open-shell atoms: I. General theory and bending levels," *The Journal of Chemical Physics*, 101: 1939-1958 (August 1994)
34. Mowrey, R.C., Y. Sun, and D.J. Kouri. "A numerically exact full wave packet approach to molecule-surface scattering," *The Journal of Chemical Physics*, 91: 6519-6524 (November 1989)
35. Juvet, Christophe and J. Alberto Beswick. "Fine-structure electronic predissociation in van der Waals molecules: I. Theory," *The Journal of Chemical Physics*, 86: 5500-5508 (May 1997)
36. Hickman, A.P. "Model fore fine-structure transitions in collisions of K ( $4^2P$ ) and Rb ( $5^2P$ ) with  $H_2$  and  $N_2$ ," *The Journal of Physics B*, 15: 3005-3024 (1982)

37. Arthurs, A.M. and Dalgarno, A. "The theory of scattering by a rigid rotator," *Proceedings of the Royal Society of London*, 256: 540-551 (1960)
38. Launay, Jean-Michel. "Molecular collision processes I. Body-fixed theory of collisions between two systems with arbitrary angular momenta," *The Journal of Physics B*, 10: 3665-3672 (1977)
39. Lawley, K.P. and John Ross. "Semiclassical Theory of Rotational Excitation of a Diatomic Molecule by an Atom," *The Journal of Chemical Physics*, 43: 2930-2942 (November 1965)
40. Aquilanti, Vincenzo and Gaia Grossi. "Angular momentum coupling schemes in the quantum mechanical treatment of P-state atom collisions," *The Journal of Chemical Physics*, 73: 1165-1172 (August 1980)
41. Aquilanti, Vincenzo, P. Casavecchia, G. Grossi, and A. Laganà. "Decoupling approximations in the quantum mechanical treatment of P-state atom collisions," *The Journal of Chemical Physics*, 73: 1173-1180 (August 1980)
42. Sun, Yan and Donald J. Kouri. "Wave packet study of gas phase atom-rigid rotor scattering," *The Journal of Chemical Physics*, 89: 2958-2964 (September 1988)
43. Sun, Yan, S. Judson, and Donald J. Kouri. "Body frame close coupling wave packet approach to gas phase atom-rigid rotor inelastic collisions," *The Journal of Chemical Physics*, 90: 241-250 (January 1989)
44. Sun, Yan, R.C. Mowrey, and Donald J. Kouri. "Spherical wave close coupling wave packet formalism for gas phase nonreactive atom-diatom collisions," *The Journal of Chemical Physics*, 87: 329-349 (July 1987)
45. Pack, Russel T. "Space-fixed vs body-fixed axes in atom-diatomic molecule scattering. Sudden approximations," *The Journal of Chemical Physics*, 60: 633-639 (January 1974)
46. McGuire, Paul and Donald J. Kouri. "Quantum mechanical close coupling approach to molecular collisions.  $j_z$  - conserving coupled states approximation," *The Journal of Chemical Physics*, 60: 2488-2499 (March 1974)
47. Launay, Jean-Michel. "Body-fixed formulation of rotational excitation: exact and centrifugal decoupling results for CO-He," *The Journal of Physics B*, 9: 1823-1838 (1976)
48. Neuhauser, Daniel, Michael Baer, Richard S. Judson, and Donald J. Kouri. "The application of time-dependent wavepacket methods to reactive scattering," *Computer Physics Communications*, 63: 460-481 (1991)

49. Zhang, Dong H. and John Z.H. Zhang. "Full-dimensional time-dependent treatment for diatom-diatom reactions: The  $\text{H}_2 + \text{OH}$  reaction," *The Journal of Chemical Physics*, 101: 1146-1156 (July 1994)
50. Zhang, John Z.H., Jiqiong Dai, and Wei Zhu. "Development of Accurate Quantum Dynamical Methods for Tetraatomic Reactions," *The Journal of Physical Chemistry A*, 101: 2746-2754 (1997)
51. Herzberg, Gerhard. *Atomic Spectra and Atomic Structure*. New York: Dover Publications, Inc., 1944.
52. Tennyson, Jonathan and Brian T. Sutcliffe. "The *ab initio* calculation of the vibrational-rotational spectrum of triatomic systems in the close-coupling approach, with KCN and  $\text{H}_2\text{NE}$  as examples," *The Journal of Chemical Physics*, 1982: 4061-4072 (October 1982)
53. Friesner, Richard A., Joseph A. Bentley, Michel Menou, and Claude Leforestier. "Adiabatic pseudospectral methods for multidimensional vibrational potentials," *The Journal of Chemical Physics*, 99: 324-335 (July 1993)
54. Gazdy, Bela and Joel M. Bowman, " $L^2$  approach to the calculation of bound states and resonances in HCO: A case study," in *Advances in Molecular Vibrations and Collision Dynamics 1B*: 105-137. JAI press, Inc., 1991.
55. Harter, William G. *Principles of Symmetry, Dynamics, and Spectroscopy*. New York: John Wiley & Sons, Inc., 1993.
56. Brink, D.M., and G.R. Satchler. *Angular Momentum*. Oxford: Clarendon Press, 1962.
57. Manolopoulos, D.E. "An improved log derivative method for inelastic scattering," *The Journal of Chemical Physics*, 85: 6425-6429 (December 1986)
58. Alexander, M.H. and D.E. Manolopoulos. "A stable linear reference potential algorithm for solution of the close-coupled equations in molecular scattering theory," *The Journal of Chemical Physics*, 86: 2044-2050 (February 1987)
59. Merzbacher, Eugene. *Quantum Mechanics*. New York: John Wiley and Sons, Inc., 1997.
60. Leforestier, C., R. H. Bisseling, C. Cerjan, M.D. Feit, R. Friesner, A. Guldberg, A. Hammerisch, G. Jolicard, W. Karrlein, H.D. Meyer, N. Lipkin, O. Roncero and R. Kosloff. "A Comparison of Different Propagation Schemes for the Time Dependent Schrödinger Equation," *The Journal of Computational Physics*, 94: 59-80 (1991)

61. Alvarellos, J. and H. Metiu. "The evolution of the wave function in a curve crossing problem computed by a fast Fourier transform method," *The Journal of Chemical Physics*, 88: 4957-4966 (April 1988)
62. Calfas, Roy S. *Reactive Quantum Scattering in Two Dimensions*. Air Force Institute of Technology (AU), Wright-Patterson AFB OH, 1997. Dissertation AFIT/DSP/ENP/97-02
63. Hamming, R.W. *Numerical Methods for Scientists and Engineers*. New York: Dover Publications, Inc., 1973.
64. Burden, Richard L., and J. Douglas Faires. *Numerical Analysis*. Pacific Grove: Brooks/Cole Publishing Company, 1997.
65. Mies, F.H. "Molecular Theory of Atomic Collisions: Fine-Structure Transitions," *Physical Review A*, 7: 942-956 (March 1973)
66. Mies, F.H. "Molecular Theory of Atomic Collisions: Calculated Cross Sections for  $H^+ + F(^2P)$ ," *Physical Review A*, 7: 957-967 (March 1973)

### **Vita**

Second Lieutenant Thomas A. Niday was born on 27 December 1975 in Chicago, Illinois. He graduated from Moorpark High School in Moorpark, California in June 1993. His undergraduate study was at the California Institute of Technology in Pasadena, California, where he majored in Physics and Applied Mathematics, and graduated with honors in June 1993.

He was commissioned through the AFROTC Detachment 060 at the University of Southern California. His first assignment has been at the Air Force Institute of Technology, where he entered in June 1997 as a Masters student in the Department of Engineering Physics.

Permanent Address: 13835 Donnybrook Lane  
Moorpark, CA 93021



REPORT DOCUMENTATION PAGE			Form Approved OMB No. 0704-0188	
Public reporting burden for this collection of information is estimated to average 1 hour per response, including the time for reviewing instructions, searching existing data sources, gathering and maintaining the data needed, and completing and reviewing the collection of information. Send comments regarding this burden estimate or any other aspect of this collection of information, including suggestions for reducing this burden, to Washington Headquarters Services, Directorate for Information Operations and Reports, 1215 Jefferson Davis Highway, Suite 1204, Arlington, VA 22202-4302, and to the Office of Management and Budget, Paperwork Reduction Project (0704-0188), Washington, DC 20503.				
1. AGENCY USE ONLY (Leave blank)	2. REPORT DATE March 1999	3. REPORT TYPE AND DATES COVERED Master's Thesis		
4. TITLE AND SUBTITLE INELASTIC SCATTERING MATRIX ELEMENTS FOR THE COLLISION B(2P1/2) + H2 ( J ) -> B(2P3/2) + H2 (J')		5. FUNDING NUMBERS		
6. AUTHOR(S) THOMAS A. NIDAY				
7. PERFORMING ORGANIZATION NAME(S) AND ADDRESS(ES) Dr. David E. Weeks AIR FORCE INSTITUTE OF TECHNOLOGY 2950 P STREET WPAFB OH 45433-7765		8. PERFORMING ORGANIZATION REPORT NUMBER  AFIT/GAP/ENP/99M-06		
9. SPONSORING/MONITORING AGENCY NAME(S) AND ADDRESS(ES) Dr. Michael Berman AFOSR/NL 110 Duncan Ave, Suite B115 Bolling AFB DC 20332-8050 (202) 767-4963		10. SPONSORING/MONITORING AGENCY REPORT NUMBER		
11. SUPPLEMENTARY NOTES David E. Weeks, Associate Professor of Engineering Physics, ENP				
12a. DISTRIBUTION AVAILABILITY STATEMENT Approved for public release; distribution unlimited.			12b. DISTRIBUTION CODE	
13. ABSTRACT (Maximum 200 words) Initial efforts to characterize the scattering dynamics of B + H2 focus on computing scattering matrix elements for the fine structure transition B (2P1/2) -> B (2P3/2) in collisions with H2, allowing for rotational excitation. Using a new application of the time dependent Channel Packet Method (CPM), reactant and product wave packets are prepared in the asymptotic limit on the B (2P1/2) and B (2P3/2) surfaces. They are propagated using the split operator method together with a unitary transformation between the diabatic and adiabatic representations. Scattering matrix elements are computed from the Fourier transform of the correlation function between the evolving wave packets. These computations directly support the Air Force Office of Scientific Research (AFOSR) Molecular Dynamics program and the Air Force Research Laboratory (AFRL) High Energy Density Matter (HEDM) program. In particular, the CPM is well suited to handle non-adiabatic molecular reaction dynamics on multiple potential energy surfaces, as encountered in the dynamics of a wide variety of molecular systems, including B + H2. Further motivation for investigating the specific dynamics of B + H2 stems from the potential application of solid molecular hydrogen, doped with boron atoms, as a high energy rocket propellant.				
14. SUBJECT TERMS Molecular Dynamics, Inelastic Scattering, Fine Structure Transitions, Channel Packet Method, Time Dependent Scattering, S-Matrix Theory			15. NUMBER OF PAGES 114	
			16. PRICE CODE	
17. SECURITY CLASSIFICATION OF REPORT UNCLASSIFIED	18. SECURITY CLASSIFICATION OF THIS PAGE UNCLASSIFIED	19. SECURITY CLASSIFICATION OF ABSTRACT UNCLASSIFIED	20. LIMITATION OF ABSTRACT UL	